# Structural Insights into TRIM21 Ubiquitination Mechanisms

**Leo Kiss**

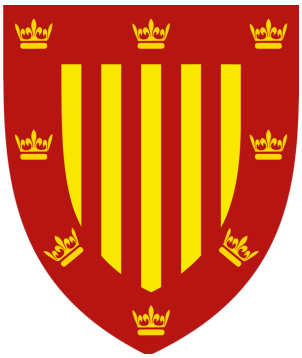

Peterhouse

University of Cambridge

MRC Laboratory of Molecular Biology

This dissertation is submitted for the degree of

*Doctor of Philosophy*

September 2021

# Declaration

This thesis is the result of my own work and includes nothing which is the outcome of work done in collaboration except as declared in the Preface and specified in the text.

I further state that no substantial part of my thesis has already been submitted, or, is being concurrently submitted for any such degree, diploma or other qualification at the University of Cambridge or any other University or similar institution except as declared in the Preface and specified in the text.

It does not exceed the prescribed word limit for the Biology Degree Committee of 60,000 words.

Leo Kiss

Peterhouse

University of Cambridge

September 2021

# Summary

## Structural insights into TRIM21 Ubiquitination Mechanisms

By Leo Kiss

The attachment of ubiquitin (Ub) to proteins is one of the most abundant and versatile of all posttranslational modifications and affects outcomes in essentially all physiological processes. During ubiquitination, RING E3 ligases direct E2 Ub-conjugating enzymes to substrates to catalyze their ubiquitination.

The cytosolic antibody receptor TRIM21 possesses unique ubiquitination activity that drives broad-spectrum anti-pathogen targeting and underpins the protein depletion technology Trim-Away. Understanding how TRIM21 functions as an E3 ligase mechanistically is required to explain how it achieves such broad-specificity and targets unrelated viruses and proteins for degradation. Moreover, it is required to further evolve TRIM21-based technologies such as Trim-Away.

The aim of my PhD was to understand how TRIM21 acts as an E3 ubiquitin ligase. In particular, I wanted to determine how TRIM21 selectively recruits only a subset of E2 enzymes and how it utilizes these for ubiquitin chain formation. Previous work suggested that TRIM21 requires the E2 enzymes Ube2W and Ube2N/Ube2V2 to build K63-linked ubiquitin chains and drive anti-viral function.

My work reveals how TRIM21 facilitates ubiquitin transfer and differentiates Ube2N from other closely related enzymes. A tri-ionic motif allows TRIM21 to wrap an Ube2N~Ub around its RING domain, promoting ubiquitin discharge. The tri-ionic motif is exclusively required for Ube2N but not other E2 enzymes and provides a generic E2-specific recruitment mechanism for RING E3s.

In addition, I have determined how TRIM21 forms a K63-linked ubiquitin chain on itself. By analyzing a catalytically trapped structure showing the initiation of TRIM21 RING-anchored ubiquitin chain elongation, I have uncovered the chemical mechanism of ubiquitin conjugation. Moreover, this mechanism enables TRIM21 to perform targeted protein degradation in cells.

My Thesis explains how TRIM21 catalyses formation of the K63-ubiquitin chains required for its function. More broadly, these findings help to illuminate the mechanism of other K63-specific RING E3s ligases.

# Acknowledgements

First, I would like to thank my two PhD supervisors David Neuhaus and Leo James for welcoming me to their labs. Thank you two for being so patient, supportive and for guiding me through my PhD. David's knowledge, care and calm together with Leo's excitement, drive and creativity has shaped me as a scientist and person and has enabled the work described here. I particularly enjoyed your open door policy, which enabled me to often ambush you out of nowhere to discuss the science I was puzzled about in that moment.

I would also like to thank my second supervisor David Barford and my university supervisor Katherine Stott for their time and valuable suggestions.

During my PhD, I have been lucky to work with many outstanding scientists who were helping me on my way. Jing Zeng and I worked together on understanding the tri-ionic motif for which he performed most of the cell biology experiments. Andi Boland taught me crystallography and together, we solved my first crystal structure – the first big highlight of my PhD. JiChun Yang taught me how to collect and analyze NMR data. Claire Dickson established many important protocols for TRIM21. Laura Easton always helped me with Molecular Biology. Dean Clift taught me how to work in tissue culture. Shannon Smyly's support in the lab was a huge contribution to Chapter 5. Sarah Maslen identified TRIM21 N-acetylation by MS. Nadine Renner constantly supported me with trouble shooting and data analysis. Thank you all! In addition, I also collaborated with Donna Mallery, Jonas Weidenhausen, Irmi Sinning, Stephen McLaughlin, Marina Vaysburd and Ralf Salzer. I am very grateful to all your contributions!

I would also like to thank all my other lab mates and colleagues for making my PhD such a special time: Tom Ogden, William Hawthorne, Guido Papa, Jakub Luptak, Tyler Rhinesmith, Anna Albecka-Moreau, Maria Bottermann, Alex Jonsson, Adam Fletcher, Sarah Caddy, Larissa Labzin, Marios Koliopoulos and Daniel Dunkelmann.

Most importantly, thank you Nadine Renner for being my Düdel and obviously the best collaborator both in and – more importantly – out of science! Finally, I would like to

thank my family for all the support during my PhD and particularly on the long and winding road before. Mama, Julius, Nora, Papa, Andrea and Nadine, I dedicate this Thesis to you!

# Table of contents

# Abbreviations

| | |
|---|---|
| Ab | Antibody |
| AdV | Adenovirus |
| AP-1 | Activator protein 1 |
| APC/C | Anaphase promoting complex / cyclosome |
| B | B-box |
| Bp | Base pairs |
| Cas9 | CRISPR-associated protein 9 |
| CC | coiled-coil |
| cGAS | Cyclic GMP–AMP synthase |
| COS | C-terminal subgroup one signature |
| COX-IV | Cytochrome C oxidase subunit 4 |
| CRISPR | Clustered regularly interspaced short palindromic repeats |
| CRL | Cullin RING ligase |
| crRNA | CRISPR RNA |
| DMEM | Dulbecco's modified eagle medium |
| DMSO | Dimethyl sulfoxide |
| DTT | Dithiothreitol |
| DUB | Deubiquitinase |
| ER | Endoplasmic reticulum |
| EV | Empty vector |
| E1 | E1 ubiquitin-activating enzyme |
| E2 | E2 ubiquitin conjugating enzyme |
| E3 | E3 ubiquitin ligase |
| FACS | Fluorescence-activated cell sorting |
| FBS | Foetal bovine serum |
| Fc | Fragment crystallizable region of antibody |
| FN3 | Fibronectin type 3 |
| HECT | Homologous to the E6AP carboxyl terminus |
| HEK | Human embryonic kidney cell line |

| | |
|---|---|
| HIV | Human immunodeficiency virus |
| HOIL | Heme-oxidized IRP2 ubiquitin ligase 1 |
| HOIP | HOIL-1-interacting protein |
| HRP | Horseradish peroxidase |
| IB | Immunoblot |
| Ig | Immuneglobulin |
| IKKα | Inhibitor of nuclear factor kappa B kinase alpha |
| IL | Interleukin |
| IPTG | Isopropyl B-D-1-Thiogalactopyranoside |
| IRF | Interferon regulatory factor |
| Kb | Kilobase |
| KO | Knock-out |
| LCMV | lymphocytic choriomeningitis virus |
| LDS | Lithium Dodecylsulfate |
| LUBAC | Linear ubiquitin chain assembly complex |
| mCh | mCherry |
| mEGFP | Monomeric enhanced green fluorescent protein |
| MES | 2-(N-morpholino)-Ethanesulfonic Acid |
| MLV | Murine leukemia virus |
| MOI | Multiplicity of infection |
| mRNA | messenger RNA |
| Nedd8 | neural precursor cell expressed developmentally down-regulated protein 8 |
| NF-κB | Nuclear factor kappa-light-chain-enhancer of activated B-cells |
| NHL | Ncl-1, HT2A, lin-41 |
| NLRP3 | NOD-, LRR- and pyrin domain-containing protein 3 |
| NMR | Nuclear magnetic resonance |
| N protein | Nucleocapsid protein |
| PAGE | Polyacrylamide gel electrophoresis |
| PBS | Phosphate buffered saline |
| PBS-T | Phosphate buffered saline with 0.1 % Tween |
| PCR | Polymerase chain reaction |

| | |
|---|---|
| PS | PRYSPRY |
| R | RING |
| RBR | RING – in between RING – RING |
| RNAi | RNA interference |
| PHD | Plant homeodomain |
| RNF | RING finger protein |
| RING | Really interesting new gene |
| RIPLET | RING finger protein leading to RIG-I activation |
| RPE-1 | Retinal pigmented epithelial-1 cell line |
| PROTAC | Proteolysis targeting chimeras |
| RT | Reverse transcription |
| SD | Standard deviation |
| SEM | Standard error of the mean |
| SOC | Super optimal broth with catabolite repression |
| SPR | Surface plasmon resonance |
| SUMO | Small ubiquitin-like modifier |
| T21 | TRIM21 |
| T5 | TRIM5 |
| TBE | Tris-borate-EDTA |
| TEV | Tobacco etch virus |
| TNF | Tumor necrosis factor |
| tracrRNA | Transactivating CRISPR RNA |
| TY | Tryptone yeast extract |
| TYE | Trypticase yeast extract |
| TRIM | Tripartite-motif containing Protein |
| Ub | Ubiquitin |
| Ube | Ubiquitin-conjugating enzyme |
| Ubl | Ubiquitin-like protein |
| WT | Wild type |

# Chapter 1 General Introduction

## 1.1 Ubiquitin

Posttranslational modification of proteins with the 76 amino acid small protein ubiquitin is a key regulatory mechanism in eukaryotic cells and involved in most cellular processes. In addition to being attached to target proteins, ubiquitin can be linked to itself, resulting in ubiquitin chains that can be connected via 8 different linkages (**Figure 1a**)[1,2]. Typically, these linkages are isopeptide bonds between the sidechain amine groups of lysine-residues and the C-terminal glycine of ubiquitin (G76). However, peptide bonds to protein N-termini[3-5] or ester-bonds to serine[6,7] and threonine side chains are also possible[8].

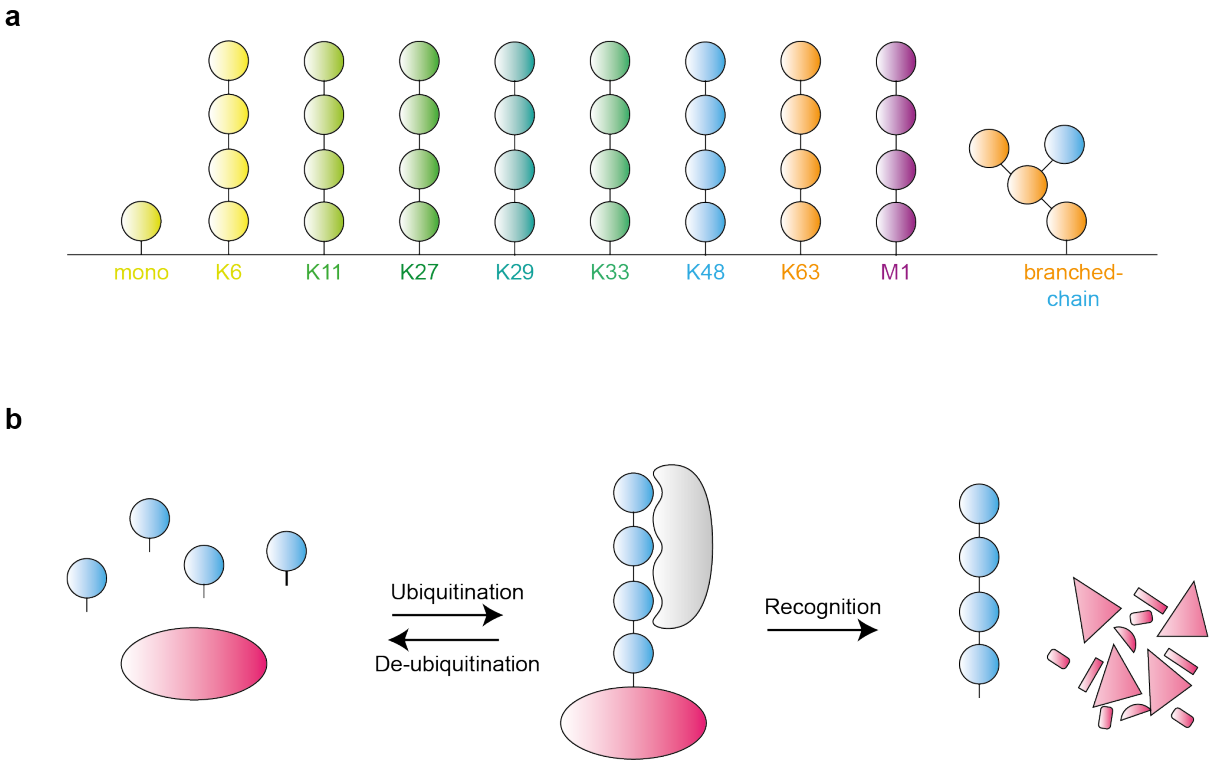


**Figure 1 The ubiquitin system. a** Cartoon depiction of the different ubiquitin linkage types. **b** Cartoon depiction of the writing (ubiquitination), erasing (de-ubiquitination) and reading (recognition) of ubiquitin signals. In this instance, the pathway illustrated is that of proteolysis of the modified protein.

Among the many functions of ubiquitin chains, the most prominent is the induction of proteasomal degradation of proteins, which is achieved via the synthesis of lysine 48 (K48) linked ubiquitin chains (**Figure 1b**)[9]. Ubiquitin chains that are linked via K63 are

not thought to mediate protein degradation but rather to have roles in processes such as immune activation[10-13], endocytosis or DNA repair[1,2,14].

### 1.1.1 The ubiquitination cascade

To target ubiquitin to target proteins or to itself, the ubiquitin transfer reaction is performed by three enzymes that work sequentially (**Figure 2**). Initially, an E1 activating enzyme uses the energy of ATP hydrolysis to form a thioester linkage to the C-terminal glycine of ubiquitin. In a subsequent reaction, this activated ubiquitin is transferred to an E2 conjugating enzyme in a transthiolation reaction. Finally, an E3 ubiquitin ligase mediates the transfer of ubiquitin from the E2 enzyme to the substrate. Humans have two E1 enzymes, ~40 E2 enzymes[8] and more than 600 E3 enzymes[15,16]; the latter can be categorised as RING, HECT and RBR type E3 ubiquitin ligases[16-18].

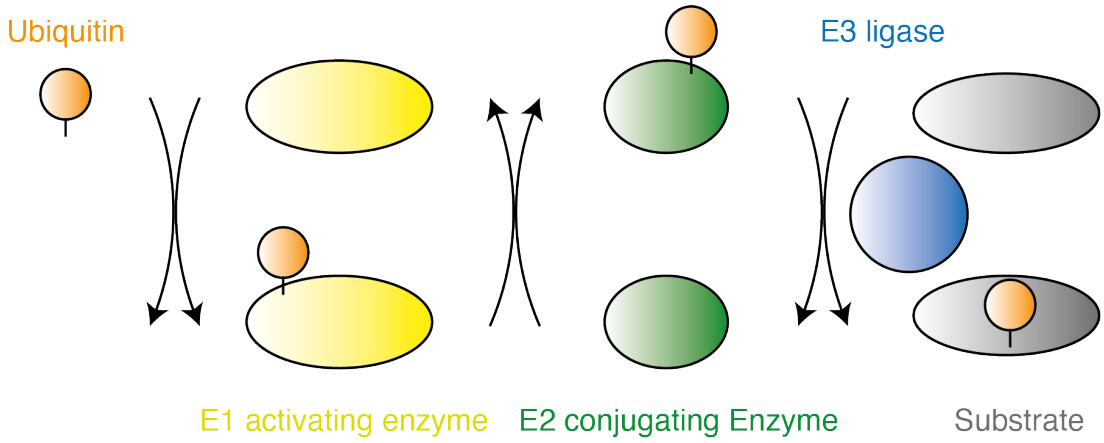


**Figure 2 The ubiquitination cascade.** Cartoon depiction of the three enzyme cascade that is required to perform ubiquitination.

### 1.1.2 Ubiquitin transfer and conjugation specificity

The types of E3 ligases differ in their structure and the mechanism by which ubiquitin is transferred from the E2 enzyme to the substrate. RING type E3 ubiquitin ligases stabilize a so-called closed conformation of the ubiquitin-charged E2 enzyme (E2~Ub) that positions the bound donor ubiquitin C-terminus bound in the E2 active site optimally for nucleophilic attack (**Figure 3a**)[19-21]. In contrast, HECT and RBR type E3s first form a thioester intermediate, before passing the ubiquitin on to the substrate (**Figure 3b**)[17,18,22]. While in humans there are 14 RBR-[23] and 28 HECT-type E3

ubiquitin ligases[24], most of the more than 600 E3 ubiquitin ligases are of the RING type[15,16]. Notably, RING E3s act by enhancing the intrinsic ubiquitination activity of E2 enzymes; thus, in these cases, the E2 also encodes specificity of ubiquitination[8,25].

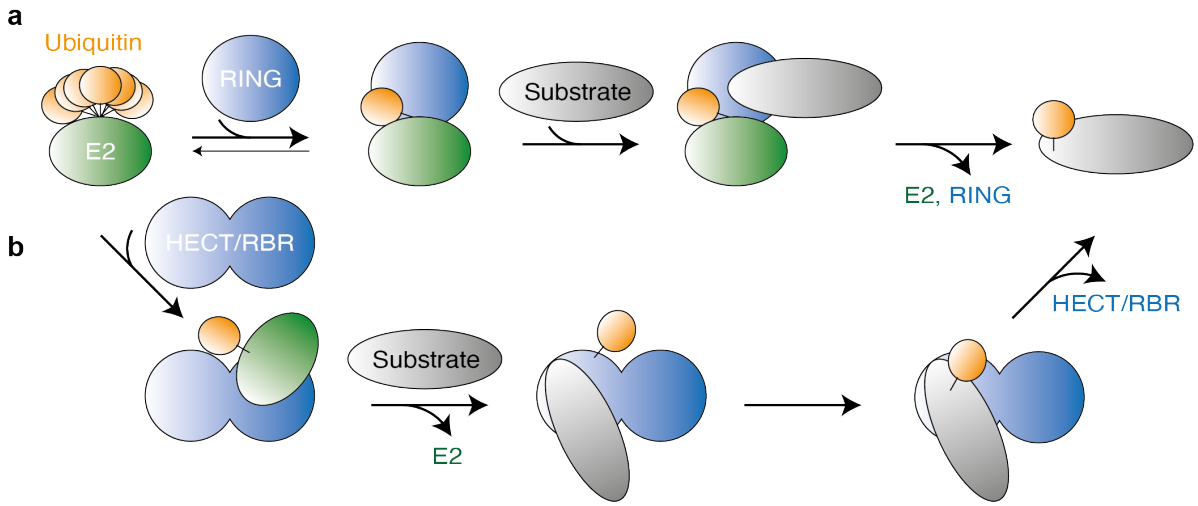


**Figure 3 The mechanism of ubiquitination E3 ligases. a** Cartoon depiction of the activation mechanism performed by RING E3 ligases. Without RINGs, the E2 and Ub components are mobile relative to each other, this arrangement also being referred to as the open conformation that is associated with inactivity. Presence of the RING shifts this equilibrium to a more structurally restricted state, called the closed conformation, in which the ubiquitin is optimally positioned for chemical attack by a lysine nucleophile provided by a substrate. **b** Cartoon depiction of ubiquitination mechanism employed by HECT and RBR E3 ligases. The interaction of these ligases with E2~Ub results in a trans-thiolation reaction with the active site cysteine of the E3. Ubiquitin transfer occurs from the E3 active site cysteine to the target lysine sidechain.

E2 conjugating enzymes can be divided into two major groups: initiators, which transfer the first ubiquitin and elongators, which elongate a ubiquitin chain. In addition, some E2 enzymes can act as both. A division of labour, where an E3 uses different E2 enzymes for initiation and elongation, is not uncommon and has been observed for instance for APC/C[26], TRIM21 (see below)[27,28] and the protein quality control RING E3 Doa10[6]. Initiator E2s that target specific chemistries (e.g. lysine side chains, N-termini or serine side chains) therefore determine whether an E3 substrate could be modified. Similarly, switching between two different elongating E2s could result in either a K48- or K63-linked ubiquitin chain on the substrate[29], further underlining the importance of precise E2 selection.

For substrate modification, an E3 ligase requires a RING domain for ubiquitination and a second domain for substrate recruitment (unless the RING itself can fulfil both criteria). However, no structural detail of these processes with ubiquitin was available

at the onset of this work. In contrast, structures of the ubiquitin-like proteins SUMO and Nedd8 have been solved in the process of their transfer to a substrate[30,31]. Both cases represent very specialized reactions, and therefore cannot be extrapolated to ubiquitination. Moreover, with >600 E3 ligases and thousands of different targets, many structures will be required to start understanding the specificity in substrate ubiquitination.

Ubiquitin chain specificity is another trait that is carried by either HECT/RBR E3 ligase or the E2 enzyme. A crystal structure and NMR models of the K63-specific E2 enzyme heterodimer Ube2N/Ube2V2 show that Ube2V2 orients the acceptor ubiquitin so that its K63 points towards the active site[32,33]. The E2 enzyme Ube2S uses substrate assisted-catalysis to enable K11 specificity[34]. Finally, linear (M1) linked ubiquitin chains are formed by the RBR ligase HOIP, which positions two ubiquitin molecules in a linear fashion, thereby generating chain specificity[35]. However, even with this wealth of information about how linkage formation specificity is achieved, it remains unclear how this is used by E3 ligases on substrates and – most importantly – inside cells.

### 1.1.3 Redirecting ubiquitination for therapeutic purposes

With ubiquitin being involved in virtually all cellular processes, this represents an obvious target for drug intervention[14]. New medicines are being developed that physically connect a disease-causing agent with an E3 ligase, resulting in ubiquitination and proteasomal degradation of this agent (**Figure 4**)[36-38]. Such drugs are called PROTACs or molecular glues. In general, molecular glues are small molecules that enable neo-complex formation between proteins, that would otherwise not interact with each other[39]. In recent years it was revealed that Thalidomide and its analogues act as molecular glues resulting in degradation of a subset of zinc-finger-transcription factors[40-43]. These drugs have been used in the clinic for decades, highlighting the huge therapeutic potential of targeted protein degradation[39]. PROTACs are fusions of two chemical entities, one targeting an E3 ligase and the other a protein, which in this way is targeted for proteasomal degradation[36,44-46]. The first PROTACs are currently in clinical trials, with many more likely to follow soon[39]. Thus, in such cases understanding the molecular basis of ubiquitination is a

prerequisite for the development of novel medicines against previously ‘undruggable’ targets.

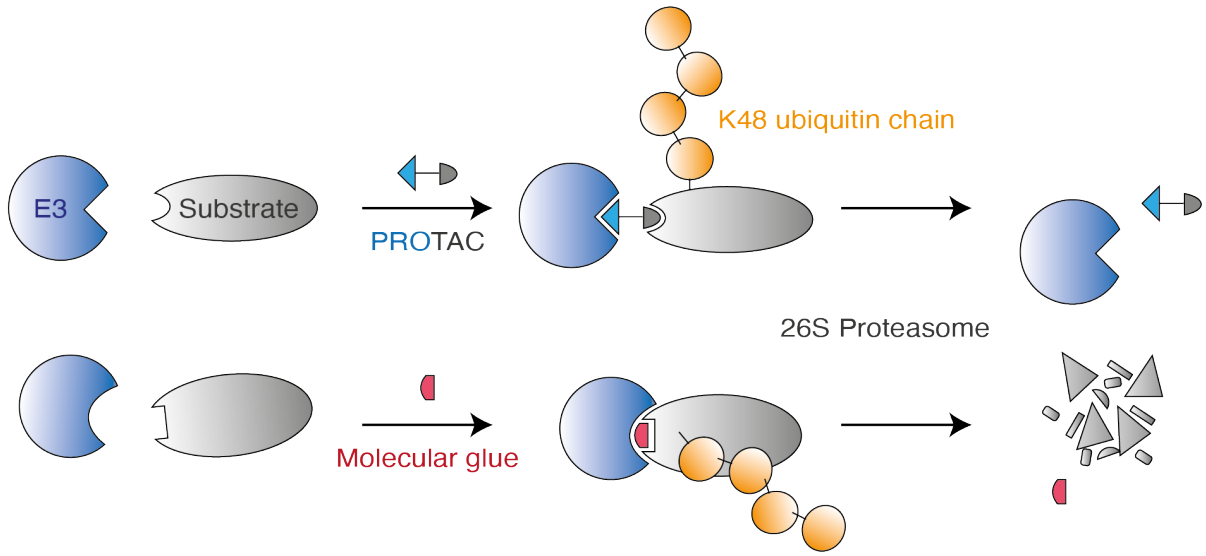


**Figure 4 Targeted protein degradation.** Schematic depiction of targeted protein degradation by PROTACs or molecular glues. In both cases, the small molecule (PROTAC or molecular glue) induces neo-complex formation between an E3 ligase and a cellular protein, which is not a usual target of this ligase. A PROTAC consists of two different chemical entities linked together, with one targeting the ligase and the other the target protein. A molecular glue does not bind the protein and ligase on their own, but can ‘glue’ them together by transforming the neo-interface. Neo-complex formation results in ubiquitination and subsequent proteasomal degradation of the substrate.

## 1.2 RING E3 ligase families

RING E3 ligases comprise of >600 members. Cullin-RING Ligases (CRLs) comprise ~250 of these and they are a product of only two RING domains (Rbx1 and Rbx2), 6 cullin proteins and a vast number of exchangeable substrate receptors[47,48]. Of the remaining RING E3 ligases, ~100 belong to the TRIM family, making it the largest family of different RING domains[49-51]. While members of this family are involved in many different pathways, many TRIM proteins have been shown to function in innate immunity[50]. Most prominently among these are the anti-viral enzymes TRIM21 and TRIM5α.

## 1.3 Introduction to TRIM21

TRIM21 (also known as Ro52) is a ubiquitously expressed cytosolic E3 ubiquitin ligase and antibody-receptor[52,53]. An increasing body of work has established TRIM21 as an antiviral effector protein that bridges innate and adaptive immunity.

### 1.3.1 History of TRIM21

Historically, TRIM21 was first described in the context of autoimmunity as an auto-antigen in lupus erythematosus patient sera[54]. Later, it was reported that patients with other autoimmune diseases also carry TRIM21 auto-antibodies[55]. There have been two studies on the effect of *TRIM21* knockout on autoimmunity in mice. While one study reported only minor effects[56], the other found a Lupus-like phenotype[57]. It was suggested that the latter knockout approach by Espinosa et al. results in the expression of a truncated TRIM21 protein, resulting in the autoimmunity phenotype[58]. Both studies agreed in showing involvement of TRIM21 in immune pathways[56,57]. TRIM21 has been reported to participate in an astonishingly wide range of unrelated cellular pathways, from the immune system to glycolysis and the cytoskeleton. However, while TRIM21 appears to be connected to many pathways, the data in each case is very limited. Thus, either TRIM21 is a universal E3 ligase involved in ubiquitous cellular processes, or alternatively it has a physical property that causes its frequent identification. Of TRIM21's many reported functions, the most comprehensively characterised is as an antibody receptor. TRIM21 binds IgG with the highest affinity reported for a mammalian Fc receptor[52,59,60]. It is this activity that likely explains why TRIM21 is often identified as an interaction partner in co-immunoprecipitation experiments: it binds all antibodies irrespective of their antigen specificity.

## 1.4 The biological function of TRIM21

### 1.4.1 Intracellular neutralization of non-enveloped viruses

Research over the past decade has established TRIM21 as an intracellular receptor for antibody-bound immune complexes. Even when coated with antibodies, viruses such as adenovirus and others still invade cells, and as a result carry antibodies into the cytoplasm (**Figure 5a**)[53]. When TRIM21 detects incoming viruses, it synthesises ubiquitin chains using its E3 ligase activity[53], resulting in destruction of the virus by the unfoldase VCP/p97[61] and the 26S proteasome[53]. Interestingly, not only the virus but also the antibody and TRIM21 are destroyed during this process[53,62]. Indeed, *TRIM21* knockout mice have increased susceptibility to fatal adenovirus infections[63]. TRIM21

is an innate immune sensor, but by recognizing antibodies, it bridges innate and adaptive immunity.

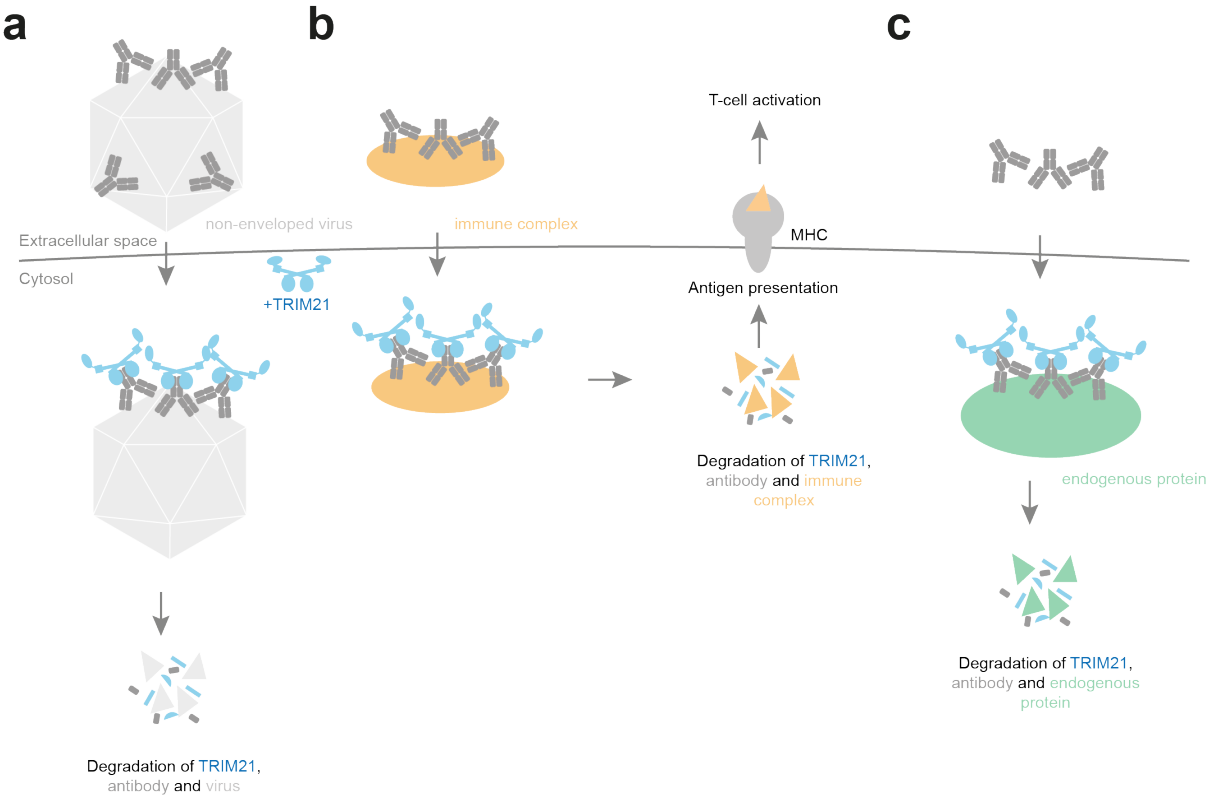


**Figure 5 Biological role of TRIM21. a** Cartoon depiction of an antibody-coated Adenovirus, infecting a cell. The antibodies are recognized by TRIM21, resulting in neutralization of the virus and destruction of its capsid, TRIM21 and the antibody. **b** Cartoon depiction of antibody-coated immune complex that is taken up by an antigen presenting cell. In the cytoplasm, the antibodies are recognized by TRIM21, resulting in degradation of this full complex. Peptides, derived from the immune complex are then presented by MHC (major histocompatibility complex) resulting in the activation of CD8+ T-killer cells. **c** Cartoon depiction of Trim-Away[62]. Delivery of antibodies against an endogenous protein into the cytoplasm results in TRIM21 recruitment and concomitant destruction of the endogenous protein, TRIM21 and antibody.

### 1.4.2 T-cell immunity against enveloped viruses

While non-enveloped viruses, such as adeno-, rhino- or rotavirus, carry capsid-bound antibodies into cells and can be directly targeted by TRIM21[53,64,65], this does not apply to enveloped viruses such as Influenza or Coronaviruses. Nonetheless, non-neutralizing antibodies against internal proteins of enveloped viruses have long been known to provide protection against infection in animal models[66-72]. Indeed, using the enveloped mouse virus LCMV, it could be shown that non-neutralizing antibodies provide protective T-cell immunity in mice and that this mechanism depends on TRIM21 (**Figure 5b**)[73]. While TRIM21's action against non-enveloped viruses applies

in all cells as TRIM21 is ubiquitously expressed, T-cells are activated by specialized antigen presenting cells. During antigen presentation, antigens like nucleocapsid (N) protein can form an immune complex with anti-N protein antibodies, whereupon they are taken up by antigen presenting cells. Immune complexes are imported into the cytoplasm as part of cross presentation, where they are thought to be detected by TRIM21 and efficiently degraded by the proteasome. Peptides generated by the proteasome can be displayed by MHC molecules, resulting in the stimulation of CD8+ T cells[73].

### 1.4.3 Activation of the immune response

TRIM21 also stimulates immune signalling pathways when it becomes activated (**Figure 6**)[28]. First, interaction with the E2 enzyme Ube2W was suggested to lead to attachment of a single ubiquitin to the N-terminus of TRIM21 itself[27]. Next, recruitment of Ube2N/Ube2V2 is thought to elongate this ubiquitin into a K63-linked ubiquitin chain[27,28]. Prior to degradation, the 26S proteasome is known to remove ubiquitin chains from its substrates using its DUB Rpn11[74]. It was therefore suggested that this process could generate free K63-linked ubiquitin chains[27]. These free K63-linked ubiquitin chains are thought to activate the immune system via the NF-κB, AP-1, IRF3, IRF5 and IRF7 pathways, culminating in the production of pro-inflammatory cytokines[28]. This involves stimulation of signalling hubs such as the TAK1 kinase complex[11-13].

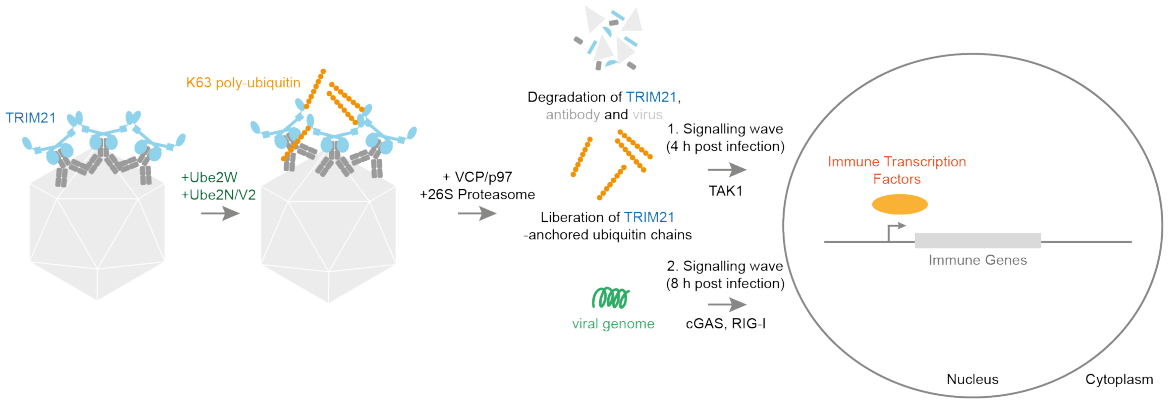


**Figure 6 Immune sensing of antibody-coated viruses by TRIM21.** Cartoon depiction of TRIM21 encountering an antibody-coated virus in the cytoplasm. Upon antibody recognition, TRIM21 interacts with the two E2 conjugating enzymes Ube2W and Ube2N/Ube2V2 to form a K63-linked ubiquitin chain on the TRIM21 N-terminus. These events lead to recruitment of VCP/p97 and the 26S proteasome, which together degrade the viral capsid. The K63-linked ubiquitin chains are liberated by the

proteasomal DUB Rpn11 (Poh1). These free K63-linked ubiquitin chains are sensed by the TAK1 kinase complex, resulting in nuclear translocation of the NF-κB transcription factor and transcription of immune genes. In addition, sensing of the viral genomes by cGAS and RIG-I results in transcription of immune genes in a second wave of immune signalling.

These signalling events occur directly upon TRIM21 sensing the incoming antibody immune complex and the resulting transcriptional activation of immune genes can be detected 4 hours post infection. However, there is a second, distinct wave of immune signalling. TRIM21-dependent degradation of adeno- and rhinovirus capsids exposes their genomes to the host cytoplasm, resulting in their sensing by cGAS and RIG-I (**Figure 6**)[65]. This second signalling wave peaks ~8 hours post infection[65]. In primary human macrophages, viral interception by TRIM21 and resulting promotion of cGAS sensing has also been shown to stimulate formation of the NLRP3 inflammasome, resulting in secretion of IL-1β and TNF[75].

It should be noted that TRIM21 itself is under the control of an interferon-inducible promotor[76,77]. Its pro-inflammatory response therefore creates a positive-feedback loop, by inducing its own expression. Thus, pathogen recognition by TRIM21 results in degradation of the pathogen and induction of two distinct immune signalling waves. By making use of multiple layers of protection, TRIM21 very efficiently targets a broad variety of pathogenic substrates that employ different approaches to avoid the host immune system. Moreover, it primes itself and its surroundings for self-defence, by inducing expression of interferon-inducible, pro-inflammatory genes.

## 1.5 The molecular structure of TRIM21

TRIM proteins have a specific domain architecture: the TRIM or RBCC motif [78]. They usually contain a RING domain, one (or two) B-boxes, a coiled-coil and a C-terminal domain. The RING is an E3 ubiquitin ligase, which together with an E2 conjugating enzyme is able to catalyse ubiquitination[16]. B-boxes are much more enigmatic and there are only two instances where their function is known, one of them being TRIM21. The TRIM coiled coil forms an antiparallel homo-dimer, resulting in positioning of the RINGs at opposing ends of the dimer[79]. The C-terminal domain of TRIM proteins is typically involved in substrate targeting and is often a PRYSPRY domain, which mediates protein:protein interactions. Other C-terminal domains found in TRIM

proteins include PHD, bromo, COS, FN3 or NHL domains[50]. TRIM21 consists of a RING, one B-box, a coiled-coil and a PRYSPRY domain (**Figure 7a,b**).

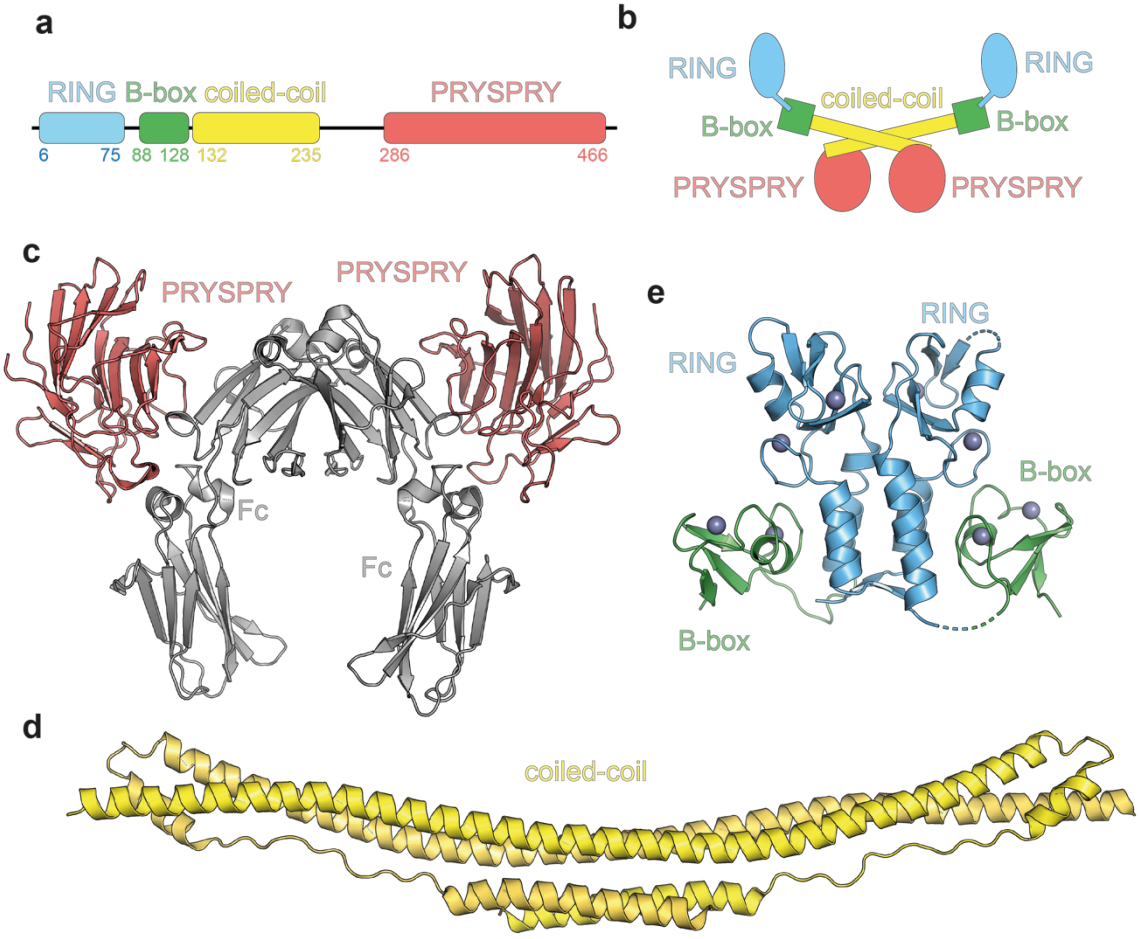


**Figure 7 Structure of TRIM21. a** Cartoon showing the domain architecture of TRIM21. **b** Cartoon showing the three-dimensional structure of TRIM21. **c** Crystal structure of the TRIM21 PRYSPRY domain in complex with Fc (PDB code: 2IWG)[52]. **d** Crystal structure of the TRIM25 coiled coil (4CFG). **e** Crystal structure of TRIM21 RING-Box showing autoinhibition of the RING domain (5OLM)[80].

### 1.5.1 PRYSPRY

TRIM21 uses its PRYSPRY domain to bind the Fc portion of IgG antibodies with a low nanomolar affinity, making it the strongest mammalian antibody receptor (**Figure 7c**)[52,59,60]. In addition to working with all IgG subclasses, TRIM21 also binds and neutralizes virus with IgM and IgA, despite their lower TRIM21 affinity[81]. Interestingly, Fc recognition by TRIM21 PRYSPRY and other Fc receptors differ. Thus, mutations can be introduced into antibodies to ablate specific Fc receptor use; for example the LALA variant (L234A/L235A) inhibits binding by FcγR receptors, while the H433A mutant inhibits TRIM21 binding[82].

### 1.5.2 Coiled-coil

The main organizer of TRIM protein architecture (**Figure 7b**) is the coiled-coil, which forms an antiparallel homo-dimer resulting in positioning of the RINGs at opposing ends, separated by ~20 nm (**Figure 7d**)[79]. RINGs are often activated by homo-dimerization[19,20,83-85] and positioning the two RINGs in an assembled TRIM protein far away from each other may be a regulatory mechanism. The unique antiparallel TRIM architecture also endows TRIM proteins with opportunities for complex higher order assembly. TRIM coiled-coils can recruit interaction partners[86], although this has not yet been reported for TRIM21.

### 1.5.3 B-box

The remaining two domains are the RING domain and the B-box. Most TRIM proteins have one or two B-boxes, with TRIM21 containing only one. The exact roles of the B-box domains remain elusive with the exception of TRIM5α and TRIM21. In the case of TRIM21, it regulates RING activity by competing for E2 binding (**Figure 7e**)[80]. Curiously, the TRIM5α B-box promotes activity by enabling higher order assembly[87,88].

### 1.5.4 RING

It is the RING domain that endows TRIM21 with its E3 ubiquitin ligase function[53]. The TRIM21 RING domains possess weak dimerization affinity in the $\mu$M regime[80]. While the coiled-coil always forms a dimer[78], RING dimerization is unlikely to occur spontaneously within the cell. Moreover, a structure of a RING-B-box construct has defined its dimerization interface, also showing the interaction between the B-Box and the E2 recruitment surface (**Figure 7e**)[80]. Previous work has suggested interactions of the TRIM21 RING with multiple E2 conjugating enzymes[27,28,89]. While some E2 enzymes, such as Ube2W and Ube2N, have been shown to be involved in TRIM21's antiviral function[27,28], others have merely been reported to interact in vitro[89]. In addition, it is unclear whether TRIM21's need for Ube2W and Ube2N in cells is based on a direct interaction, or if they play a role in another part of the pathway.

### 1.5.5 Regulation of TRIM21 RING activity

TRIM21 targets a broad range of antibody-coated pathogenic substrates for degradation. In addition, it activates pro-inflammatory pathways during infection.

These actions require TRIM21 binding to antibody and enzymatic activity by its RING E3 ligase domain[28,53]. As TRIM21 is a potent activator of pro-inflammatory function[28] it has to be tightly regulated. Constitutive ubiquitination activity could result in an autoimmune phenotype.

The structure of TRIM proteins positions the RING domains at opposite ends of the antiparallel coiled-coil (**Figure 7b**)[79]. However, RING dimerization is generally required for E3 ligase activity[19,20,83-85,90]. The structural organization of TRIM proteins inhibits RING dimerization and therefore constitutive activation of TRIM proteins. Interestingly, TRIM21 is constitutively inhibited in cells, making it a very stable protein with a long half-life[80]. TRIM21 RING activity is thus inhibited by separation of the RINGs and obstruction of E2 recruitment.

## 1.6 Translational applications of TRIM21

Protein depletion is a promising new approach for targeting disease causing agents in a therapeutic setting. PROTACs and molecular glues bind both target protein and E3 ligase, which then results in ubiquitination and proteasomal degradation of the target (**Figure 4**)[36-38]. In TRIM21-mediated degradation, the antibody plays a similar role to PROTACs or molecular glues. Thus, TRIM21 may be an ideal candidate as a PROTAC ligase.

### 1.6.1 Trim-Away

Indeed, delivery of antibody into cells by electroporation or microinjection, results in rapid depletion of the targeted protein – a method called Trim-Away (**Figure 5c**)[62,91]. This alternative to genetic knock-out or knock-down approaches by CRISPR or RNAi generates depletion phenotypes within minutes. TRIM21's ubiquitous expression enables Trim-Away in most mammalian tissues. For cells with lower TRIM21 expression levels, or depletion of very abundant proteins, additional delivery of recombinant TRIM21 protein, TRIM21 mRNA or TRIM21 overexpression enables efficient Trim-Away[62,91]. It can also be applied to zebrafish embryos[92]. For molecular biology applications, Trim-Away provides a far more convenient approach than traditional PROTACs as it does not require the bespoke design and synthesis of a small molecule that is specific to the target of interest. Instead, off-the-shelf antibodies

can be purchased commercially for a large part of the proteome or generated by simple immunization.

However, while cytosolic antibody delivery is relatively easy in the case of cells or embryos, this is not the case with complex live organisms. To harness TRIM21's degradative potential in vivo, other approaches will have to be developed. Here, a PROTAC approach where the antibody is replaced by a small molecule, would be advantageous. Another approach could be the use of Nanobody-Fc fusions, which were shown to work well for Trim-Away[62]. Protein delivery is the major barrier between Trim-Away and its application in organisms, however mRNA vector or Adenovirus-mediated gene delivery may offer solutions for Nanobody-Fc or similar protein-based constructs.

### 1.6.2 Degradation of Tau

In Tauopathies such as Alzheimer's, pathogenic Tau aggregates are formed inside cells. These aggregates are released when cells die, whereupon they can be taken up by new cells and act as seeds for further aggregation[93]. This tau propagation model of neurodegeneration is reminiscent of viral spread and indeed antibodies against Tau have been shown to prevent seeded aggregation in neuronal tissue culture in a TRIM21-dependent fashion[94]. As with in vivo Trim-Away, new methods for the delivery of antibody-like constructs into the organism will be required to bring tau-degradation from the bench to bedside. It will be interesting to see whether other amyloids can also be targeted for destruction using TRIM21.

### 1.6.3 Vaccines

TRIM21 also recognizes N-protein:antibody immune complexes, thereby inducing T-cell-immunity (**Figure 5b**)[73]. Thus, it might be advantageous not only to focus on classical vaccine candidates such as receptor binding proteins like Spike in SARS-CoV2, but also on internal viral proteins like N-proteins, so as to unleash the bodies full immunological potential. However, as TRIM21 targets Adenoviruses it can also target adenovirus vectors that are used as vaccine and gene therapy vectors[95]. It might therefore be beneficial to transiently inhibit TRIM21 activity for certain therapies.

## 1.7 Aims of this Thesis

RING E3 mechanisms have been studied extensively in recent years, yet, fundamental questions remain. This applies particularly to the TRIM family, which comprises the greatest variety of RING domains[49]. The most general determinant for catalytic function of RING E3s has been RING dimerization induced formation of the closed E2~Ub conformation[19,20]. However, how RING E3s select for a specific E2 enzyme remains largely unknown[8,25]. In cells, these interactions are highly specific and are required to form the correct ubiquitination on the right substrate. Finally, the mechanism of ubiquitin transfer from the RING:E2 complex to the substrate has yet to be understood. The work described in this Thesis tackles these questions using TRIM21 as the model E3 ligase and using a combination of structural, biochemical and cellular methods.

# Chapter 2 Materials and Methods

## 2.1 Bacterial transformation

Between 10 and 200 ng plasmid DNA were mixed with 50 μL chemically competent *Escherichia coli* DH10B, DH5α, XL-1 blue, BL21, Rosetta 2 or C41, that were thawed on ice before use. The mixture was incubated on ice for ~15 min before performing heat shock at 42 ˚C for ~45 s, followed by an incubation on ice for 10 min. Cell were then mixed with SOC media and plated on TYE agar containing the appropriate antibiotic(s) (100 μg $mL^{-1}$ Ampicillin, 34 μg $mL^{-1}$ Chloramphenicol, 50 μg $mL^{-1}$ Kanamycin). In the case of pre-cultures for protein expression, the cells were added directly into liquid 2xTY media containing the appropriate concentration of antibiotic(s). Plates and pre-cultures were generally incubated at 37 ˚C overnight (the pre-cultures shaking at 200 rpm).

## 2.2 Molecular cloning

Cloning was mostly performed using Gibson Assembly[96]. Primer design was performed using SnapGene (version 5.3.1) using primer overhangs of 15-25 bp with a melting temperature greater than 50 ˚C. Both vector backbone and insert were amplified by PCR using Q5 high-fidelity polymerase (New England Biolabs) using the PCR program shown in **Table 1**.

**Table 1 General PCR program for cloning.**

| PCR Step | Temperature (˚C) | Time |
|---|---|---|
| Initial denaturation (1x) | 98 | 30 s |
| Denaturation (35x) | 98 | 10 s |
| Annealing (35x) | 72 | 30 s |
| Extension (35x) | 72 | 30 s $kb^{-1}$ |
| Final extension (1x) | 72 | 2 min |

After PCR, the products were treated with Dpn1 (New England Biolabs) to remove template DNA and purified using QIAquick PCR purification Kit (QIAGEN). For Gibson

Assembly, ~70 ng of linearized vector were mixed with insert in a molar ratio of ~1:7 and mixed 1:1 with 2x Gibson Assembly Master Mix (New England Biolabs) on ice. Reactions were incubated at 50 ˚C for 1 h before direct transformation (of 5 µL maximal volume) into 50 µL cloning cells (*E. coli* DH10B, DH5α or XL-1 blue). On rare occasions, plasmid was linearized using restriction digestion, followed by gel purification using a DNA gel purification kit (QIAGEN).

Restriction digestion cloning was performed in rare cases. For mCherry-TRIM21-CC-PS, TRIM21$^{382-1428}$ was amplified by PCR and cut by EcoRI and NotI. A 743 bp fragment carrying mCherry was cut by AgeI and EcoRI from V60 (pmCherry-C1, Clonetech) and both fragments were ligated into pGEMHE.

Quick change mutagenesis was performed for introducing point mutations and inserting or deleting smaller sequence stretches (up to ~50 bp). Primers were designed by adding 20 – 25 up- and downstream of the mutation site and forward and reverse primer were fully complementary. Mutagenesis PCR was performed using Pfu Turbo polymerase (Agilent) using Pfu buffer and 10 mM dNTPs in a 50 µL format using exactly 200 ng of plasmid DNA and 40 nM of the forward and reverse primers each and the PCR program given in **Table 2**. After PCR, the samples were treated with Dpn1 (New England Biolabs) to remove input DNA, before 5 µL were transformed into cloning cells.

**Table 2 General PCR program for quick change mutagenesis.**

| PCR Step | Temperature (˚C) | Time |
|---|---|---|
| Initial denaturation (1x) | 94 | 5 min |
| Denaturation (35x) | 94 | 1 min |
| Annealing (35x) | 56 | 1 min |
| Extension (35x) | 72 | 1 min kb$^{-1}$ |
| Final extension (1x) | 72 | 10 min |

## 2.3 Plasmid purification

Plasmid DNA was purified from ~6 mL cultures of *E. coli* cloning cells in 2xTY or LB using the appropriate antibiotic. Cultures were grown over night at 37 ˚C and 200 rpm. Plasmid purification was performed using the QIAprep Spin Miniprep Kit (QIAGEN) following the provided protocol. Plasmids were validated by sequencing using Genewiz.

## 2.4 Plasmids

Bacterial expression constructs: Ube2V2, Ube2W and TRIM21 expression constructs but full-length TRIM21 were cloned into pOP-TG vectors and full-length TRIM21 constructs into HLTV vectors. Ube2N constructs were cloned into pOP-TS, Ube1 into pET21 and ubiquitin into pET17b. Ube2D1 was cloned into pET28a. For cloning $Ub_{4/3/2}$-TRIM21 constructs, a linear $Ub_3$ sequence was codon optimized, ordered as synthetic DNA (Integrated DNA technologies) and inserted into the $Ub^{G75/76A}$-TRIM21 construct (in pOP-TG) by Gibson Assembly. All constructs for mRNA production were cloned into pGEMHE vectors[97]. Lentiviral vectors (pNatP-TRIM21) for stable cell lines expressing TRIM21 constructs at natural levels were designed and cloned by Jingwei Zeng[77] and contained a human TRIM21 2 kb upstream promotor region. pMD2.G encoding VSV-G was purchased from A VSV-G encoding plasmid (pMD2.G) was a kind gift from Didier Trono (Addgene entry 12259) and a plasmid encoding HXB2 derived HIV-1 Gag-pol (pC/RV1) was a gift by[98]. For the NF-κB signalling assay, a plasmid (pGL4.32) containing firefly luciferase under the NF-κB response element and a constitutive Renilla luciferase control reporter (pRL-CMV) were purchased from Promega.

## 2.5 Agarose Gels

DNA samples were mixed with Purple Gel Loading Dye (New England Biolabs) to a final concentration of 1 X. Samples were loaded onto 1% agarose gels made with 1 X TBE buffer supplemented with 1:50,000 v/v ethidium bromide. Agarose gels were run in 1 X TBE buffer at 85 V for 45 min and visualised by ultra-violet transillumination or blue light transillumination for gel extraction.

## 2.6 In vitro transcription and RNA purification

For in vitro transcription of mRNA, constructs were cloned into pGEMHE vectors[97]. Plasmids were linearized using AscI (New England Biolabs). Capped (but not polyA-tailed) mRNA was synthesized with T7 polymerase using the HiScribe™ T7 ARCA mRNA Kit (New England Biolabs) according to the manufacturer's instructions.

For phenol-chloroform extraction, 1 (v/v) phenol/chloroform/isoamyl alcohol (24:25:1, pH 6.7 for RNA) was added to the samples and vortexed for 15s. Aqueous and organic phases were separated by centrifugation (16,000 xg for 1 min). Traces of phenol in the aqueous were removed by mixing with 1 (v/v) of chloroform followed by centrifugation at 16,000 x g for 1 min to separate the phases. The aqueous phase was transferred to a new clean tube while the organic phase was discarded.

For ethanol extraction, RNA was precipitated by addition of 10% (v/v) of 5 M sodium acetate (pH 5.5) and 2.5 (v/v) of ethanol. The samples were chilled for at least for 1 h at -20 °C. Nucleic acids were recovered by centrifugation at 21,000 xg at 4 °C for 15 min. Pellets were washed with 500 µl of ice cold 70% ethanol followed by centrifugation at 21,000 xg at 4 °C for 10 min. Supernatants were removed and the pellets were air-dried before resuspension in nuclease-free water. Due to nucleotide contamination, the concentration was determined by running 1 $\mu$L on a gel and calculating the concentration by relative comparison to a known standard.

## 2.7 LDS-PAGE

Protein samples in 1x LDS buffer (either containing 50 mM DTT or not) were loaded onto NuPAGE gels (10-, 12-, 15- or 17-well) after boiling for ~10 min at >95 ˚C. Gels were run in MES buffer at 180 V for 40 min (in rare cases 60 min). Proteins were visualized using Instant Blue (Abcam).

## 2.8 Protein expression and purification

TRIM21-RING (residues 1-85), Ub-TRIM21-RING, TRIM5α-RING (1-88), Ube2N, Ube2V2, Ube2W Ube2D1 constructs were expressed in *Escherichia coli* C41 DE3 or BL21 DE3 cells. Ubiquitin and Ube1 were expressed in *E. coli* Rosetta 2 DE3 cells. All

cells were grown in 2xTY media supplemented with 2 mM $MgSO_4$, 0.5 % glucose and 100 $\mu$g mL$^{-1}$ ampicillin (and 34 $\mu$g mL$^{-1}$ for Rosetta 2 cells). Cells were induced at an $OD^{600}$ of 0.7. For TRIM proteins, induction was performed with 0.5 mM IPTG and 10 $\mu$M $ZnCl_2$, for ubiquitin and Ube1 with 0.2 mM IPTG. *Chaetomium thermophilum* Naa50$^{82-289}$ containing a C-terminal His-tag was expressed using *E. coli* Rosetta 2 cells in ZY autoinduction media[99] which was grown at 37 ˚C and 220 rpm. At $OD^{600}$ of 0.7, the temperature was reduced to 18 ˚C for expression overnight.

After centrifugation, cells were resuspended in 50 mM Tris pH 8.0, 150 mM NaCl, 10 $\mu$M $ZnCl_2$, 1 mM DTT, 20 % Bugbuster (Novagen) and c0mplete protease inhibitors (Roche). Lysis was performed by sonication. TRIM proteins and Ube2V2 were expressed with N-terminal GST-tag and purified via glutathione sepharose resin (GE Healthcare) equilibrated in 50 mM Tris pH 8.0, 150 mM NaCl and 1 mM DTT. The tag was cleaved on beads overnight at 4 ˚C. In case of Ubiquitin-TRIM21 constructs, the eluate was supplemented with 10 mM imidazole and run over 0.25 mL of Ni-NTA beads to remove His-tagged TEV. Ube2N and Ube1 were expressed with an N-terminal His-tag and were purified via Ni-NTA resin. Proteins were eluted in 50 mM Tris pH 8.0, 150 mM NaCl, 1 mM DTT and 300 mM imidazole. For Ube2N, TEV-cleavage of the His-tag was performed overnight by dialyzing the sample against 50 mM Tris pH 8.0, 150 mM NaCl, 1 mM DTT and 20 mM imidazole. Afterwards, His-tagged TEV protease was removed by Ni-NTA resin. The cleavage left an N-terminal tripeptide scar (GSH) on recombinantly expressed TRIM proteins and Ube2W, an N-terminal G scar on Ube2N and an N-terminal GSQEF scar on Ube2V2. Finally, size exclusion chromatography was carried out on a HiLoad 26/60 Superdex 75 or HiLoad 16/600 Superdex 75 prep grade column (GE Healthcare) in 20 mM Tris pH 8.0, 150 mM NaCl and 1 mM DTT, except for E1 enzyme, which was purified via the S200 equivalent.

Ubiquitin purification was performed following the protocol established by the Pickart lab[100]. After cell lysis by sonication (lysis buffer: 50 mM Tris pH 7.4, 1 mg mL$^{-1}$ Lysozyme (Sigma Aldrich), 0.1 mg mL$^{-1}$ DNAse (Sigma Aldrich), a total concentration of 0.5 % perchloric acid was added to the stirring lysate at 4 ˚C. The (milky) lysate was incubated for another 30 min on a stirrer at 4 ˚C to complete precipitation. Next, the lysate was centrifuged (19,500 rpm) for 30 min at 4 ˚C. The supernatant was dyalized

overnight (3,500 MWCO) against 3 L 50 mM sodium acetate. Afterwards, Ub was purified via cation-exchange chromatography using a 20 mL SP column (GE Healthcare) using a NaCl gradient (0 – 1000 mM NaCl in 50 mM NaAc pH 4.5). Finally, size exclusion chromatography was carried out on a HiLoad 26/60 Superdex 75 prep grade column (GE Healthcare) in 20 mM Tris pH 7.4.

Full-length TRIM21 (Ub-R-B-CC-PS or Ub-R-R-B-CC-PS) proteins were expressed as His-Lipoyl-fusions in *E. coli* BL21 DE3 cells. Cells in 2xTY were grown to an OD600 of 0.8 and induced with 0.5 mM IPTG and 10 $\mu$M $ZnCl_2$. Cells were further incubated at 18 ˚C, 220 rpm overnight. After centrifugation, cells were resuspended in 100 mM Tris pH 8.0, 250 mM NaCl, 10 $\mu$M $ZnCl_2$, 1 mM DTT, 20 % Bugbuster (Novagen), 20 mM Imidazole and c0mplete protease inhibitors (Roche, Switzerland). Lysis was performed by sonication. His-affinity purification was performed as described above. Immediately afterwards, the protein was applied to an S200 26/60 column (equilibrated in 50 mM Tris pH 8.0, 200 mM NaCl, 1 mM DTT) to remove soluble aggregates. After concentration determination, the His-Lipyol tag was cleaved using TEV protease overnight. Since full-length TRIM21 is unstable without tag, the protein was not further purified but used for assays directly.

*Ct*Naa50$^{82\text{-}289}$ was purified as follows: Cells were harvested, resuspended in buffer A500 (20 mM HEPES pH 7.5, 500 mM NaCl, 20 mM imidazole) supplemented with a protease inhibitor mix (SERVA Electrophoresis GmbH, Germany) and lysed with a microfluidizer (M1-10L, Microfluidics). The lysate was cleared for 30 min at 50,000 g, 4 °C and filtered through a 0.45 $\mu$m membrane. The supernatant was applied to a 1 mL HisTrap FF column (GE Healthcare) for Ni-IMAC (immobilized metal affinity chromatography) purification. The column was washed with buffer A500 and the proteins were eluted with buffer A500 supplemented with 250 mM imidazole. CtNaa5082-289 was subsequently purified by SEC (size-exclusion chromatography) using a Superdex 75 26/60 gel filtration column (GE Healthcare) in buffer G500 (20 mM HEPES pH 7.5, 500 mM NaCl). This protein was a prepared by Jonas Weidenhausen (Irmgard Sinning lab, Heidelberg University).

Isotopically labelled proteins were expressed using *Escherichia coli* BL21 DE3 cells (TRIM proteins) or *E. coli* Rosetta 2 DE3 cells (ubiquitin) in M9 minimal media

supplemented with either $^{15}NH_4Cl$ or $^{15}NH_4Cl$ and [$^{13}C_6$]glucose (Sigma-Aldrich ISOTEC).

All proteins were flash frozen in small aliquots (30 – 100 $\mu$L) and stored at -80 ˚C. Freeze-thaw cycles were kept to a minimum to avoid compromising enzymatic activity.

## 2.9 Formation of an isopeptide-linked Ube2N~Ub

Ube2N$^{C87K/K92A}$ charging with WT ubiquitin was based on a protocol of the Hay lab[101]. The isopeptide charging reaction occurred in 50 mM Tris pH 10.0, 150 mM NaCl, 5 mM $MgCl_2$, 0.5 mM TCEP, 3 mM ATP, 0.8 mM Ube1, 100 $\mu$M Ube2N and 130 $\mu$M ubiquitin at 37 ˚C for 4 hours. After conjugation, Ube2N$^{C87K/K92A}$~Ub was purified by size exclusion chromatography (Superdex S75 26/60, GE Healthcare) that was equilibrated in 20 mM Tris pH 8.0 and 150 mM NaCl.

## 2.10 Western Blotting

Protein transfer onto nitrocellulose membrane was performed using an iBlot Gel Transfer Device (Invitrogen) using programme P1 for 7 min. Blots were blocked in either 5% (w/v) non-fat milk (Marvel) in PBS-T (PBS with 0.01% Tween 20) or 3 % BSA (Sigma Aldrich) in PBS-T. Antibodies were diluted in milk or BSA solutions given above and were incubated for at least 1 h. Washing was performed using PBS-T. Visualization was performed using either fluorescence or chemo-luminescence. For chemo-luminescence, Amersham ECL, ECL Prime or ECL Select detection reagent (GE Healthcare Life Sciences) were used. Fluorescent blot detection was performed using LI-COR Odyssey CLx imaging system. Band intensities were quantified using Image Studio Lite (LI-COR) software. If required, blot membranes were stripped using ReBlot Plus Strong Antibody Stripping Solution (Millipore).

### 2.10.1 Antibodies

Mouse 9C12 anti-adenovirus 5 hexon IgG was purified from hybridoma obtained from the Developmental Studies Hybridoma Bank, University of Iowa, IA, USA. Humanized anti-adenovirus hexon antibody 9C12 were produced by the Andersen lab for previous studies[102,103]. Primary antibodies used in immunoblots were anti-TRIM21(D-12) Santa Cruz Biotechnology (SC25351), TRIM21: rabbit anti-TRIM21 D101D (ST#9204)

(1:1,000), 1:5000, anti-TRIM21 [raised against human TRIM21 RING-B-Box-Coiled Coil[53], 1:1000], Vinculin: rabbit anti-Vinculin EPR8185 ab 217171 (1:50,000); Caveolin-1: rabbit anti-Cav1 (BD: 610059, 1:1,000), 1:500, anti-Ube2D (-UbcH5) Boston Biochem (A-615), 1:1000, anti-Ube2N Bio-Rad (AHP974), 1:1,000, anti-COX IV LI-COR Biosciences (926-42212), 1:5,000, anti-Ub-HRP Santa Cruz (sc8017-HRP P4D1), anti-β-actin-HRP Santa Cruz (sc47778), 1:20,000, goat anti-human IgG Fc broad 5211-8004 (1:2,000), anti-His antibody (Clontech, 631212, 1:5000).

Secondary antibodies were anti-mouse-HRP Sigma (A0168), 1:5,000, anti-rabbit-HRP Cell Signaling (7074), 1:5,000. All antibodies were diluted in PBS containing 5% non-fat milk and 0.01% Tween20 or 3 % BSA in 0.01 % Tween20 for ECL and LI-COR visualization, respectively. Visualization was carried out using an ECL Western Blotting Detection System (GE Healthcare) or Odyssey CLx near-infrared imaging system (LI-COR Bioscience).

## 2.11 E2 conjugating enzyme screen

The E2Select Ubiquitin Conjugating Kit (K-982, Boston Biochem, Cambridge, USA) was used as described in the product manual. The E3 concentration was 1.8 $\mu$M TRIM21-RING and for detection anti-Ub-HRP (Santa Cruz, sc8017-HRP P4D1, 1:10,000) or anti-TRIM21-RING sera (1:1,000[80]) was used.

## 2.12 E2~Ubiquitin discharge assay

Ube2N$^{K92R}$ or Ube2D1 were charged with ubiquitin by incubating 40 $\mu$M E2, 1 $\mu$M Ube1, 0.37 $\mu$M ubiquitin and 3 mM ATP in 50 mM HEPES pH 7.5, 150 mM NaCl, 20 mM $MgCl_2$ at 37 ˚C for 45 min. Afterwards, this charging mix was cooled at 4 ˚C and used within 1 h. To observe E2~Ub discharge, 2 $\mu$M E2~Ub was added to 50 mM HEPES pH 7.5, 150 mM NaCl, 20 mM $MgCl_2$, 50 mM L-lysine and 2.5 $\mu$M Ube2V2. For TRIM21 assays with Ube2N$^{K92R}$ or Ube2D1, respectively 1.5 $\mu$M and 1 $\mu$M TRIM21-RING were used respectively. For TRIM5α assays, 10 $\mu$M TRIM5α-RING was used. The reaction took place at 37 ˚C and was initiated by addition of the E3. Samples were taken at the time points indicated and the reaction was stopped by addition of LDS sample buffer at 4 ˚C. Samples were boiled for 20 s at 90 ˚C, resolved

by LDS-PAGE and observed using western blot. Anti-E2 enzyme western blots were imaged using the LiCor system and analyzed using Image Studio Lite (LiCor Biosciences).

## 2.13 Ubiquitin chain formation assay

In Chapter 3, ubiquitination reactions were performed using 0.1 mM ubiquitin, 2 mM ATP, 1 $\mu$M Ube1 and 0.5 $\mu$M Ube2N/V2 or 0.25 $\mu$M Ube2D1 in 50 mM Tris pH 8, 2.5 mM $MgCl_2$, 0.5 mM DTT. The reaction took place at 37 ˚C and was initiated by addition of E3. For TRIM21, 1.5 $\mu$M TRIM21-RING and for TRIM5α 10 $\mu$M TRIM5α-RING constructs were used. Samples were taken at the time points indicated and the reaction was stopped by addition of LDS sample buffer at 4 ˚C.

In Chapter 4, ubiquitin chain formation assays were performed in 50 mM Tris pH 7.4, 150 mM NaCl, 2.5 mM $MgCl_2$ and 0.5 mM DTT. The reaction components were 2 mM ATP, 0.25 $\mu$M Ube1, 80 $\mu$M ubiquitin, 0.5 $\mu$M Ube2N/Ube2V2 or Ube2D1 together with the indicated concentration of E3. Samples were taken at the time points indicated and the reaction was stopped by addition of LDS sample buffer at 4 ˚C. The samples were boiled at 90 ˚C for 2 min and resolved by LDS-PAGE. Ubiquitin chains were detected in the western blot.

## 2.14 Kinetics of di-ubiquitin formation

Kinetic measurements of di-ubiquitin formation were measured for Michaelis-Menten, and p$K_a$ analysis. The experiment was performed in a pulse-chase format, where the first reaction generated Ube2N~$^{His}$-Ub and was chased by $Ub^{1-74}$. Under these conditions, $Ub^{1-74}$ only acts as acceptor, as it cannot be charged onto the E1 enzyme. His-tagged ubiquitin on the other hand serves as donor. Although, theoretically His-Ub could also act as an acceptor, the high concentrations of $Ub^{1-74}$ outcompete His-Ub as an acceptor. Initially, I determined the linear range of the reaction for all different constructs, so as to later measure only one point on this trajectory as a representative for the initial velocity ($v_0$). For Michaelis-Menten kinetics I used the following times: WT, 3 min; D119A, 100 min; D119N, 30 min; N123A, 3 min; D124A. 3 min, and for p$K_a$ measurements the following: WT, 40 s; D119A, 5 min; D119N, 60 s; N123A, 40 s; D124A, 40s.

First, Ube2N-charging was performed in 50 mM Tris pH 7.0, 150 mM NaCl, 20 mM $MgCl_2$, 3 mM ATP, 60 $\mu$M His-ubiquitin, 1 $\mu$M GST-Ube1 (Boston Biochem) and 40 $\mu$M Ube2N. The reaction was incubated at 37 ˚C for 12 min and stored afterwards at 4 ˚C until use (within 1 h).

For Michaelis-Menten kinetic analysis, the reaction was conducted in 50 mM Tris pH 7.4, 150 mM NaCl with the indicated amount of $Ub^{1-74}$ (0 – 400 $\mu$M), while for p$K_a$ determination in 50 mM Tris and the indicated pH (7.0 - 10.5), 50 mM NaCl and 250 mM $Ub^{1-74}$. Apart from the buffer, the reaction mix contained 2.5 $\mu$M Ube2V2. The reaction was initiated by addition of charging mix that was diluted 1 in 20, resulting in 2 $\mu$M Ube2N in the reaction. The reaction was stopped by addition of 4x LDS loading buffer. The samples were boiled at 90 ˚C for 2 min and resolved by LDS-PAGE. Western blot was performed with anti-His antibody (Clontech, 631212, 1:5000) via the LiCor system, leading to detection of the following species: $^{His}$Ub, $^{His}$Ub-$Ub^{1-74}$, Ube2N~$^{His}$Ub, Ube2N~($^{His}$Ub)$_2$ (a side product of the charging reaction that shows ubiquitination rates similar to Ube2N~$^{His}$Ub) and E1-$^{His}$Ub. The concentration of $^{His}$Ub-$Ub^{1-74}$ was determined by dividing the value for $^{His}$Ub-$Ub^{1-74}$ by the sum of all bands detected and multiplying this by the total concentration of $^{His}$Ub in the reaction (3 $\mu$M). Experiments were performed in technical triplicates. Michaelis-Menten kinetics data were fit to Equation (1):

$$(1) \qquad V = \frac{E_t * k_{cat} * S}{K_M * S}$$

where $V$ is the measured velocity, $E_t$ the total concentration of active sites (2 $\mu$M) and S the substrate concentration. The curve was fit to determine $k_{cat}$ and $K_M$. To determine the p$K_a$, the data was fit to Equation (2):

$$(2) \qquad V = \frac{V_{HA} * 10^{-pH} + V_{A-} * 10^{-pKa}}{10^{-pKa} + 10^{-pH}}$$

as given in[104], where $V$ is the measured velocity, $V_{A-}$ the velocity for the basic species and $V_{HA}$ the velocity for the acidic species.

## 2.15 Mono-ubiquitination assay

Ube2W-dependent TRIM21-mono-ubiquitination assays were performed in 50 mM Tris pH 7.4, 150 mM NaCl, 2.5 mM $MgCl_2$ and 0.5 mM DTT. The reaction components were 2 mM ATP, 1 $\mu$M GST-Ube1, 80 $\mu$M ubiquitin, 1 $\mu$M Ube2W (unless stated differently in the Figure legend) together with 10 $\mu$M TRIM21. The reaction was initiated by addition of either E2 or E3 and performed at 37 ˚C in a thermocycler. The reaction was stopped by addition of LDS sample buffer containing 50 mM DTT at 4 ˚C and visualization was performed by Instant Blue stained LDS-PAGE only.

For antibody-induced mono-ubiquitination similar conditions were used as for the LDS-PAGE analysed mono-ubiquitination described above. However, the concentration of TRIM21 was reduced to 100 nM and GST-Ube1 to 0.25 $\mu$M. Anti-GFP antibody (9F9.F9, Abcam) was added in one molar equivalent to TRIM21. The reaction was initiated by addition of Ube2W (concentrations are given in Figure legends). The reaction was stopped by addition of LDS sample buffer at 4 ˚C. Samples were boiled at 90 ˚C for 2 min and resolved by LDS-PAGE. TRIM21 was visualized using western blot.

## 2.16 Acetylation and mono-ubiquitination assay

N-terminal acetylation of TRIM21 was mediated by the *Chaetomium thermophilum* N-acetyl transferase (NAT) Naa50ΔΔ. This NAT can efficiently acetylate N-termini starting with MA (Jonas Weidenhausen and Irmgard Sinning, unpublished Data). Acetylation reactions were performed in 50 mM Tris pH 7.4 and 150 mM NaCl for 4 h at 25 ˚C. The reactions contained 20 $\mu$M TRIM21, 1 mM Acetyl-CoA and 1 $\mu$M *Ct*Naa50ΔΔ.

After the Acetylation reaction was finished, it was mixed 1:1 with a Ube2W-ubiquitination mix containing 100 mM Tris pH 7.4, 300 mM NaCl, 5 mM $MgCl_2$ and 1 mM DTT, 4 mM ATP, 2 $\mu$M GST-Ube1, 160 $\mu$M ubiquitin and 2 $\mu$M Ube2W. The Ube2W ubiquitination reaction was performed for 1 h at 37 ˚C and stopped by addition of LDS sample buffer containing 50 mM DTT at 4 ˚C and visualization was performed by Instant Blue stained LDS-PAGE only.

## 2.17 Protein crystallization, structure solution and refinement

For the TRIM21 RING:Ube2N~Ub structure, 10 mg $mL^{-1}$ of TRIM21-RING with $Ube2N^{C87K/K92A}$~Ub in 50 mM deuterated Tris pH 7.0, 150 mM NaCl and 1 mM deuterated DTT were subjected to sparse matrix screening in sitting drops at 17 ˚C and crystals were initially obtained in the MORPHEUS I screen[105]. After crystal growth refinement, crystals grew in 0.1 M Tris/BICINE pH 8.5, 10.5 % (w/v) PEG3350/PEG 1K/MPD and 0.08 M sodium nitrate/sodium phosphate/ammonium sulphate. Crystals were flash frozen in the crystallization condition supplemented with 15 % glycerol.

Data was collected at the Diamond Light Source beamline i04, equipped with a PILATUS 6M Prosport+ detector at a wavelength of 0.97952 Å (Beamline i04). Diffraction images were processed using XDS[106] to 2.8 Å resolution ($CC_{1/2}$: 0.998 (0.735 for 2.8 - 2.9 Å)). The crystals belong to the space group P1 with two complexes per asymmetric unit (2xTRIM21-RING, 2x $Ube2N^{C87K/K92A}$~Ub; **Appendix Figure 2e**). The structure was solved by molecular replacement using PHASER-MR implemented in the Phenix suite[107]. Search models were the RING domain of TRIM21-RING-Box structure (5OLM)[80] and the Ube2N~Ub (5EYA)[85] from a complex structure with $TRIM25^{RING}$. Model building and real space refinement was carried out in COOT[108] and refinement was performed by using phenix-refine toll in PHENIX and REFMAC5 iteratively[107,109]. The isopeptide bond between Ube2N K87 and ubiquitin G76 was modelled using aceDRG[110]. Overall, 96.8 % of backbone dihedrals were in favoured Ramachandran regions with 0.51 % as Ramachandran outliers (**Appendix Table 1**). The structure is deposited in the Protein Data Bank under the accession code 6S53.

For the structure showing TRIM21 self-ubiquitination, 5 mg $mL^{-1}$ of human $Ub^{G75/76A}$-TRIM21-RING, $Ube2N^{C87K/K92A}$~Ub and Ube2V2 in 20 mM Tris pH 8.0, 150 mM NaCl and 1 mM DTT were subjected to sparse matric screening in sitting drops at 17 ˚C (500 nL protein was mixed with 500 nL reservoir solution). Crystals were obtained in Morpheus II screen[111] in 0.1 M MOPSO/bis-tris pH 6.5, 12.5 % (w/v) PEG 4K, 20 % (v/v) 1,2,6-hexanetriol, 0.03 M of each Li, Na and K.

For the Ube2N$^{C87K/K92A}$~Ub:Ube2V2 structure, 10 mg mL$^{-1}$ TRIM21-RING, Ube2N$^{C87K/K92A}$~Ub, Ube2V2 and Ub in 20 mM Tris pH 8.0, 150 mM NaCl and 1 mM DTT were subjected to sparse matrix screening in sitting drops at 17 ˚C (200 nL protein was mixed with 200 nL reservoir solution). Crystals were obtained in the Morpheus III screen[112] in 0.1 M bicine/Trizma base pH 8.5, 12.5% w/v PEG 1000, 12.5% w/v PEG 3350, 12.5% v/v MPD, 0.2 %(w/v) of each of the anesthetic alkaloids (lidocaine HCl·$H_2O$, procaine HCl, proparacaine HCl, tetracaine HCl). Crystals were flash frozen for data collection without the use of additional cryo-protectant.

Data were collected at the Diamond Light Source beamline i03, equipped with an Eiger2 XE 16M detecter of a wavelength of 0.9762 Å. For Ub$^{G75/76A}$-TRIM21-RING:Ube2N$^{C87K/K92A}$~Ub:Ube2V2. Diffraction images were processed using XDS[106] to 2.2 Å resolution. The crystals belong to space group number 5 (C2) with each of the components present as a single copy in the asymmetric unit. Analysis of the raw data revealed moderate anisotropy in the data. The structure was solved by molecular replacement using PHASER-MR implemented in the Phenix suite[107]. Search models were TRIM21-RING and Ube2N from 6S53[113], ubiquitin from 1UBQ[114] and Ube2V2 from 1J74[115]. Model building and real-space-refinement was carried out in coot[108], and refinement was performed using phenix-refine[116]. The anisotropy in the data could be observed in parts of the map that were less well resolved. While all interfaces show clear high-resolution density, particularly parts of Ube2V2 (chain A) that were next to a solvent channel proved challenging to build. The structure is deposited in the Protein Data Bank under the accession code 7BBD. The crystallographic data table is given in **Appendix Table 2**.

For Ube2N$^{C87K/K92A}$~Ub:Ube2V2, diffraction images were processed using XDS[106] to 2.54 Å resolution. The crystals belong to space group number 145 ($P3_2$) with each component present three times in the asymmetric unit, related by translational non-crystallographic symmetry. The structure was solved by PHASER-MR implemented in the Phenix suite[107]. Search models used were Ube2N from 6S53[113], ubiquitin from 1UBQ[114] and Ube2V2 from 1J74[115]. Model building and real-space-refinement was carried out in coot[108], and refinement was performed using phenix-refine[116]. The structure is deposited in the Protein Data Bank under the accession code 7BBF (**Appendix Table 2**).

The TRIM21-RING:Ube2W$^{V30K/D67K/C91K}$ complex was crystallized by Dr Claire F Dickson and data was collected by her at the European Synchrotron Radiation Facility. She solved the structure using Phaser[107] with TRIM21 RING domain(5OLM[80]) and Ube2W residues 1-118 (2MT6[117]) as search models. Model building and real-space-refinement was carried out in coot[108], and refinement was performed using phenix-refine[116]. The refinement was performed by Dr Claire F Dickson and I. Statistics are given in **Appendix Table 3**.

## 2.18 NMR spectroscopy

Two-dimensional NMR measurements ($^{15}$N-HSQC and $^{15}$N-BEST-TROSY[118]) were performed at 25 ˚C on Bruker Avance I and III 600 MHz spectrometers equipped with 5mm $^{1}$H-$^{13}$C-$^{15}$N cryogenic probes. Data was processed with the program Topspin (Bruker BioSpin GmbH) and analyzed with the program CCPN analysis v2[119]. Samples were buffer exchanged into 50 mM deuterated Tris pH 7.0, 150 mM NaCl and 1 mM deuterated DTT (Cambridge Isotopes, United Kingdom).

Chemical shift perturbations (CSPs) were calculated using equation (3):

$$\Delta\delta_{N,HN} = \sqrt{(\Delta\delta(^{1}H)^2 + (\Delta\delta(^{15}N)^2 * 0.14)} \quad (3)$$

where $\Delta\delta_{N,\,HN}$ is the CSP, $\Delta\delta(^{1}H)$ and $\Delta\delta(^{15}N)$ are the chemical shift differences between the position of proton or nitrogen signal in absence and presence of titrant.

Differential chemical shift perturbations (dCSPs) were calculated using the same formula as for CSPs, but applied to differences between chemical shifts measured for the corresponding signal at the corresponding titration point during titrations with two different titrants.

Dissociation constants ($K_D$) of the TRIM21-RING$^{M10E}$ constructs with Ube2N were determined by fitting the titration points to the following formula (from Graphpad Prism 7; GraphPad Software Inc):

(4)

$$\Delta\delta_{obs} = \frac{\Delta\delta_{max}\{([T21]_t + [2N]_t + K_D) - \sqrt{(([T21]_t + [2N]_t + K_D)^2 - 4[T21]_t[2N]_t)}\}}{2[T21]_t}$$

Where $\Delta\delta_{obs}$ is the observed CSP, $\Delta\delta_{max}$ is the maximum CSP, which is obtained during fitting, $[T21]_t$ is the total concentration of TRIM21-RING$^{M10E}$, $[2N]_t$ is the total concentration of Ube2N and $K_D$ the dissociation constant.

TRIM21 assignments were used from a previous publication[80]. TRIM21 titrations with Ube2N$^{C87K/K92A}$ were performed with 100 $\mu$M T21-RING$^{M10E}$. The Ube2D1 titration contained 200 $\mu$M T21-RING$^{M10E}$.

## 2.19 Surface Plasmon Resonance

Surface Plasmon Resonance (SPR) data were collected using a BIAcore T200 instrument (GE Healthcare Life Sciences) at a flow rate of 30 µl min$^{-1}$ in 20 mM Tris-HCl pH 8.0, 150 mM NaCl, 1 mM DTT at 25 °C. GST-tagged TRIM21-RING, or recombinant GST on the reference channel, were captured on an anti-GST antibody-coated CM5 sensor chip (GE Healthcare) prepared according to the supplied instructions. Ube2N~Ub or Ube2N in 1:2 dilution series with initial concentrations of 80 $\mu$M were injected for 60 s and dissociation monitored for 300 s. The sensor surface was regenerated after each injection with a 120 s injection of 10 mM glycine pH 2.1. Data were doubly-referenced by subtraction of the reference channel data and from injections of buffer alone. The data were fit using KaleidaGraph (Synergy Software) and Prism (GraphPad Software Inc). The rate constants of dissociation were measured by fitting dissociation data at time t ($R_{dissoc}$) using a single-exponential function:

$$R_{dissoc} = R_0 exp^{-(k_{off}t)} + RI + Dt \quad (5)$$

where $k_{off}$ is the dissociation rate constant, $R_0$ is maximum change in response each phase, $RI$ is the bulk resonance change and $D$ is a term to allow for linear drift. The responses at equilibrium ($R_{eq}$) were fitted using a single-site binding model:

$$R_{eq} = \left(\frac{CR_{max}}{C + K_D}\right) + RI \quad (6)$$

Where $K_D$ is the dissociation constant, $C$ is the analyte concentration and $R_{max}$ is the maximum change in resonance.

## 2.20 Mass spectrometry

Excised protein gel pieces were destained with 50 % v/v acetonitrile:50 mM ammonium bicarbonate. After reduction with 10 mM DTT and alkylation with 55 mM iodoacetamide, the proteins were digested overnight at 37 °C with 6 ng $\mu L^{-1}$ of Asp-N (Promega, UK). Peptides were extracted in 2 % v/v formic acid : 2 % v/v acetonitrile and subsequently analyzed by nano-scale capillary LC-MS/MS with an Ultimate U3000 HPLC (Thermo Scientific Dionex) set to a flowrate of 300 nL $min^{-1}$. Peptides were trapped on a C18 Acclaim PepMap100 5 µm, 100 µm × 20 mm nanoViper (Thermo Scientific Dionex) prior to separation on a C18 T3 1.8 µm, 75 µm × 250 mm nanoEase column (Waters). A gradient of acetonitrile eluted the peptides, and the analytical column outlet was directly interfaced using a nano-flow electrospray ionization source, with a quadrupole Orbitrap mass spectrometer (Q-Exactive HFX, ThermoScientific). For data-dependent analysis a resolution of 60,000 for the full MS spectrum was used, followed by twelve MS/MS. MS spectra were collected over a *m/z* range of 300–1,800. The resultant LC-MS/MS spectra were searched against a protein database (UniProt KB) using the Mascot search engine program. Database search parameters were restricted to a precursor ion tolerance of 5 ppm with a fragmented ion tolerance of 0.1 Da. Multiple modifications were set in the search parameters: two missed enzyme cleavages, variable modifications for methionine oxidation, cysteine carbamidomethylation, pyroglutamic acid and protein N-term acetylation. The proteomics software Scaffold 4 was used to visualize the fragmented spectra. LC-MS/MS was performed by Sarah Maslen.

## 2.21 Multiple sequence alignment

Multiple sequence alignments were performed using Clustal Omega[120] using reference sequences obtained from Uniprot[121]. The alignments were visualised and edited using Jalview V2[122].

## 2.22 Cell lines

Human embryonic kidney 293T (293T; ATCC number CRL-3216) and HeLa cells (ATCC number: CCL-2) were maintained in Dulbecco's Modified Eagle Medium

supplemented with 10 % (v/v) foetal bovine serum (Gibco), 100 U $ml^{-1}$ penicillin and 100 $\mu$g $ml^{-1}$ streptomycin. Cells were cultured at 37°C with 5 % $CO_2$ and passaged every 2-3 days. NIH3T3-*Caveolin-1-EGFP*[123] cells were cultured in DMEM medium (Gibco; 31966021) supplemented with 10% Calf Serum and penicillin-streptomycin. RPE-1 cells (ATCC) were cultured in DMEM/F-12 medium (Gibco; 10565018) supplemented with 10% Calf Serum and penicillin-streptomycin.

All cells were grown at 37°C in a 5% $CO_2$ humidified atmosphere and regularly checked to be mycoplasma-free. The sex of NIH3T3 cells is male. The sex of RPE-1, 293T and HeLa cells is female. Following electroporation, cells were grown in medium supplemented with 10% Calf Serum without antibiotics. For live imaging with the IncuCyte (Sartorius), cell culture medium was replaced with Fluorobrite (Gibco; A1896701) supplemented with 10% Calf Serum and GlutaMAX (Gibco; 35050061).

RPE-1 TRIM21 knockout cells were generated using the Alt-R CRISPR-Cas9 system from Integrated DNA technologies (IDT) with a custom-designed crRNA sequence (ATGCTCACAGGCTCCACGAA). Guide RNA in the form of crRNA-tracrRNA duplex was assembled with recombinant Cas9 protein (IDT #1081060) and electroporated into RPE-1 cells together with Alt-R Cas9 Electroporation Enhancer (IDT #1075915). Two days post-electroporation cells were plated one cell per well in 96 well plates and single cell clones screened by western blotting for TRIM21 protein. A single clone was chosen that contained no detectable TRIM21 protein and confirmed TRIM21 knockout phenotype in a Trim-Away assay.

For proteasome inhibition experiments MG132 (Sigma; C2211) was used at a final concentration of 25 $\mu$M.

## 2.23 Lentiviral vector production

Pseudotyped Lentiviral vectors were produced by co-transfection of 5 x $10^6$ WT 293T cells in 10 $cm^2$ dishes with 1 $\mu$g pCRV-GagPol, 1 $\mu$g pMD2G-VSVg and 2 $\mu$g pNatP-TRIM21 using Fugene-6 (Promega). Viral supernatants were harvested at 48 hours post transfection and filtered using 0.45 $\mu$M syringe filters.

For lentiviral transduction, 1 x $10^5$ cells were plated in 6-well plates the day before transduction. After 24 h, the media was replaced with 2 mL fresh media containing 5

– 8 $\mu$g mL-1 polybrene. The cells were infected with 70 $\mu$L virus to achieve a multiplicity of infection (MOI) of ~1. 48 h post transduction, cells were expanded into 10 cm dishes and selected using 2.5 $\mu$g mL$^{-1}$ (293T) or 1.5 $\mu$g mL$^{-1}$ (HeLa) of puromycin. Dead cells were removed by exchanging the media every 2-3 days. After 1 week, puromycin selection was stopped.

## 2.24 Generation of stable cell lines

*TRIM21* KO 293T cells (generated for a previous study[80]) were infected with lentivirus containing supernatant at an MOI ~1 in the presence of 5 µg mL$^{-1}$ polybrene and stably transduced cells were selected using puromycin at 2.5 µg ml$^{-1}$.

## 2.25 Transient siRNA knockdown

For transfection, 30 pmol of pooled small interfering (si) RNA oligonucleotides for Ube2D1, Ube2D2 and Ube2D3 (CCAAAGAUUGCUUUCACAAUU (Ube2D1), GGUGGAGUCUUCUUUCUCAUU (Ube2D2), CAGUAAUGGCAGCAUUUGU (Ube2D2 and Ube2D3, GAUCACAGUGGUCGCCUGC (Ube2D1)) were mixed with 500 $\mu$L Ptimem and 5 $\mu$L RNAi Max (Invitrogen) in one well of a six-well plate. Samples were incubated at room temperature for 20 min, then $10^5$ cells were added to each well in 2 mL complete media. Neutralization assays were carried out 48 – 72 h post-transfection. siRNA knockdown experiments were performed by Dr Donna L Mallery.

## 2.26 Transient protein expression from mRNA

To enable precise control of protein expression levels, constructs were expressed from in vitro transcribed mRNA. mRNA was delivered into cells by electroporation using the Neon Transfection system (Invitrogen). For each electroporation reaction 8 x $10^5$ RPE-1 *TRIM21*-knock out or NIH3T3-*Caveolin1-EGFP*[123] cells suspended in 10.5 $\mu$l of Resuspension Buffer R were mixed with 2 $\mu$L of the indicated mRNA in water. After electroporation, cells were transferred into antibiotic-free DMEM or DMEM/F-12 media supplemented with 10 % FBS and left to incubate for 5 h before cells were harvested. Typically, expression could be detected from 30 min after electroporation and lasted for about 24 h.

## 2.27 Trim-Away

For each electroporation reaction 8 x $10^5$ NIH3T3-*Cav1-EGFP*-knock in cells[123] suspended in 10.5 $\mu$l of Resuspension Buffer R were mixed with the indicated amount of antibody-mixture diluted in 2 $\mu$l of PBS. mRNAs were added immediately prior to electroporation, to limit degradation by potential RNAse activity. mRNA encoding Vhh-Fc (WT or PRYSPRY binding deficient H433A mutant) or anti-GFP antibody (9F9.F9, Abcam) and TRIM21 were electroporated. The cell mRNA mixtures were taken up into 10 $\mu$l Neon electroporation pipette tips (Invitrogen) and electroporated using the following settings: 1400 V, 20 ms, 2 pulses (as described in[62,91]). Electroporated cells were transferred to antibiotic-free Fluorobright media supplemented with 10 % FBS and left to incubate for 5 h in an incubator before the cells were harvested for immunoblotting. GFP-fluorescence measured using an Incucyte® (essenbioscience) and was normalized to the control (Vhh-$Fc^{H433A}$). Protein detection was performed using western blots.

## 2.28 GFP-Fc degradation assay

For GFP-Fc degradation assay, 0.4 $\mu$M mEGFP-Fc mRNA together with 1.2 $\mu$M of the indicated TRIM21 mRNA were electroporated into 8 x $10^5$ cells, as described above. Electroporated cells were transferred to antibiotic-free DMEM supplemented with 10 % FBS. For western analysis only, cells were incubated for 5 h in an incubator before harvest. For Flow cytometry analysis, half of the cells were taken and treated with 25 $\mu$M MG132 while the other half were treated with DMSO. Then cells were incubated for 5 h in an incubator before being harvested. Cells were fixed before being subjected to flow cytometry. In addition, western blots was performed to visualize protein other than GFP.

## 2.29 Flow Cytometry

Cells were fixed prior to flow cytometry. For this, cells were resuspended in FACS fixative (4 % formaldehyde, 2 mM EDTA in PBS) and incubated at room temperature for 30 min. Afterwards, cells were centrifuged and resuspended in FACS buffer (2 % FBS, 5 mM EDTA in PSB) and stored at 4 ˚C, wrapped in aluminium foil until use. Flow

cytometry was performed using an Eclipse (iCyt) A02-0058. Live cells were selected based on forward and side scattering and only the median GFP fluorescence of live cells was used for further analysis.

## 2.30 Adenovirus neutralization assay

For Adv5-GFP infections in siRNA knockdown experiments, HeLa cells were seeded at 1 x $10^5$ cells per well in 2 mL complete DMEM in six-well plates the day before infection. 5 x $10^4$ infectious units (IU) of AdV5-GFP were incubated with mouse 9C12 antibody in a 10 $\mu$L volume for 30 min at room temperature before addition to cells. Cells were incubated for 48 h before washing, trypsiniation and fixing in 4 % paraformaldehyde. GFP positive cells were enumerated by flow cytometry (FACSCalibur, BD Biosciences).

In case of virus neutralization assays of TRIM21 mutants, 293T cells were plated at a density of 5 x $10^4$ cells per well in 24-well plates and were allowed to attach overnight. For each well, 2.5 x $10^5$ IU of Adv5-GFP (ViraQuest) were mixed 1:1 with human 9C12 antibody (at the indicated concentrations), and incubated for 1 h at 20 °C before adding to cells. 10 $\mu$L of virus-antibody complex were added per well and cells were incubated for 20 h at 37 °C. Cells were then harvested by trypsiniation and evaluated for GFP expression by flow cytometry (LSRFortessa, BD Biosciences). The results were analyzed using FlowJo software (FlowJo LLC) and relative infection was calculated using the method described previously[53]. Gating was performed for GFP positive and negative cells. Cells that were not infected with GFP labelled virus were used as control (background 0.1 %). All Adenovirus neutralization experiments shown in this Thesis were performed by either Dr Jingwei Zeng or Dr Donna L Mallery.

## 2.31 NF-κB signalling assay

293T cells were plated at a density of 5 x $10^4$ cells per well in 6-well plates a day before transfection with 250 ng of pGL4.32 NF-κB luciferase (Promega) using FuGENE 6 (Promega). Cells were incubated for 6 h at 37 °C before reseeding at a density of 1 x $10^4$ per well in Corning® CellBIND® 96-well plates and allowed to adhere overnight. For each well, 6.25 x $10^6$ IU of Adv5-GFP (ViraQuest) were mixed 1:1 with 20 µg $mL^{-1}$

antibody (human 9C12) and incubated for 1 h at 20 °C to allow complex formation. 5 µL of the virus-antibody complex were added per well and allowed to incubate for 6 h at 37 °C before the cells were lysed with 100 µL per well steadylite plus luciferase reagent (Perkin Elmer). The luciferase activity was measured using a BMG PHERstar FS plate reader. NF-κB signalling experiments shown in this Thesis were performed by Dr Jingwei Zeng.

## 2.32 Statistics

Graphs were plotted using GraphPad Prism 7 and 8 software and error bars represent the standard error of the mean (SEM) unless otherwise stated in the Figure legends. Linear regression correlation analyses were performed using GraphPad Prism 8.

# Chapter 3 Specific E2 selection by TRIM21

## 3.1 Introduction

The TRIM family represents the largest family of RING E3s[49], yet their precise structural and cellular mechanism of ubiquitination remains unknown. The best studied members of this family are TRIM21 and TRIM5α, which both possess an unusual catalytic mechanism whereby they mediate target degradation by transferring ubiquitin to themselves rather than to their substrate[27,124]. TRIM21 is further distinct in that it does not engage its target directly but indirectly using antibodies (**Figure 5a**)[53], which function as natural PROTACs (**Figure 4**). These properties of indirect targeting and ubiquitination allow TRIM21 to inhibit infection by a diverse array of pathogens, including viruses, bacteria and prions, by causing their proteasomal degradation and activating immune signalling[28,53,62,94]. Moreover, they allow TRIM21 to deplete endogenous cellular proteins during application of Trim-Away[62].

The general principles of E2:E3 catalysis are well established. RING E3s typically dimerize and use one RING protomer to recruit an E2, while the second RING protomer engages its charged ubiquitin[19,20]. The key catalytic residue is thought to be provided by an arginine or lysine sidechain, called the linchpin, which interacts close to where the C-terminus of ubiquitin is conjugated to the E2 and forms contacts with both proteins[19-21]. Mutation of this linchpin residue typically reduces, although crucially does not always abolish, catalytic activity. Despite identification of these general principles, key questions of E2:E3 catalysis remain unanswered. For instance, RINGs are typically constitutively active *in vitro* but not in cells. How regulation is achieved is poorly understood, although higher order oligomerization has been linked to activation of the anti-retroviral E3 ligase TRIM5α[125,126]. A second key question is how RING E3s catalyze the formation of specific ubiquitin chain linkages. Chain specificity is mainly determined by the recruited E2[8] but E2s are structurally highly related and, despite

numerous studies, it remains unclear how RINGs recruit a specific E2 in order to catalyze synthesis of the required chain type.

In addition to its unusual properties of indirect substrate engagement and self-ubiquitination-driven target degradation, TRIM21 does not conform to many of the general rules of E2:E3s given above. It retains activity as a monomeric RING and uses a domain uniquely found in TRIMs, the B-box, to prevent constitutive ubiquitination by blocking E2 recruitment[80]. Upon its activation during engagement of antibody-coated pathogens or proteins in the cytosol, TRIM21 is thought to recruit the E2 conjugating enzymes Ube2W and Ube2N/Ube2V2 sequentially[27,28]. It uses Ube2W to modify its own N-terminus with a mono-ubiquitin[27], which, in conjunction with Ube2N/Ube2V2, it then extends into a K63-linked anchored polyubiquitin chain[27,28]. The detected antibody complex, along with TRIM21 itself, is subsequently degraded by recruitment of the AAA ATPase VCP/p97 and the 26S proteasome[53,61]. Moreover, TRIM21's ubiquitination activity induces robust immune signalling via NF-κB, AP-1 and IRF3/5/7[27,28].

### 3.1.1 Aims

In this chapter, I set out to unravel how TRIM21 recruits its canonical E2 enzyme Ube2N and catalyzes ubiquitin transfer. I describe the cellular E2-specific recruitment mechanism in RING E3s and show how it drives ubiquitination both in vitro and in cells. X-ray crystallography and NMR spectroscopy reveal a tri-ionic motif that captures Ube2N~Ub in the active closed state by providing conformation-specific anchor points. This tri-ionic motif is conserved across TRIM RING ligases and is also used by the antiretroviral TRIM5α to drive K63-ubiquitin chain synthesis. Finally, I identify structurally conserved charged anchor points across divergent RINGs suggesting that this may be a common mechanism for Ube2N-specific catalysis.

## 3.2 Results

### 3.2.1 TRIM21 catalyzes ubiquitination with redundant E2s *in vitro*

Antibody-dependent virus neutralization by TRIM21 is dependent on the E2 enzymes Ube2W and Ube2N(Ubc13)/Ube2V2 (Mms2; alternatively Ube2V1/Uev1 can replace Ube2V2)[27,28]. However, whether additional E2 enzymes are also required is unclear.

For instance, it has been suggested that an additional E2 might be required in order to build K48 chains, which are classically associated with proteasomal recruitment[27]. To address this question, a biochemical screen for catalytic activity against 26 E2 enzymes was performed (**Figure 8**, **Appendix Figure 1**). Apart from Ube2W and Ube2N, this screen revealed TRIM21 ubiquitination activity with Ube2D1 to Ube2D4 (UbcH5a/b/c/d), Ube2E1 (UbcH6) and Ube2E3 (UbcH9). In contrast to a previous report[89], activation of Ube2E1 and Ube2E3 by TRIM21 was minimal, and involved conjugation of ubiquitin to the E2 enzymes themselves rather than TRIM21 (**Appendix Figure 1**). The Ube2D E2s are known to catalyze K48-chain formation but are also highly promiscuous. To analyze their interaction with TRIM21 in more detail, an NMR titration of $^{15}$N-labelled TRIM21-RING$^{M10E}$ (here abbreviated as T21-R$^{M10E}$) with Ube2D1 was performed (**Figure 8b**). This TRIM21 mutant greatly improved spectral quality relative to WT, since it suppresses the weak dimerization of the WT RING domain, while retaining ubiquitination activity[80]. This titration revealed that Ube2D1 interacts with TRIM21 in a manner comparable to Ube2N (**Figure 8c**). Ube2D enzymes are widely used in E3 ubiquitination assays but evidence for their involvement in specific physiological functions is scarce. TRIM21 actively formed ubiquitin chains with Ube2D1 in vitro (**Appendix Figure 1d**). However, in Ube2D1/Ube2D2/Ube2D3 depleted cells, antibody-dependent virus neutralization was indistinguishable from WT, as opposed to the almost complete lack of neutralization in TRIM21 depleted cells (**Figure 8c-f**). Importantly, this suggests that TRIM21 must be capable of differentiating between E2s and that this property is not captured when using *in vitro* assays.

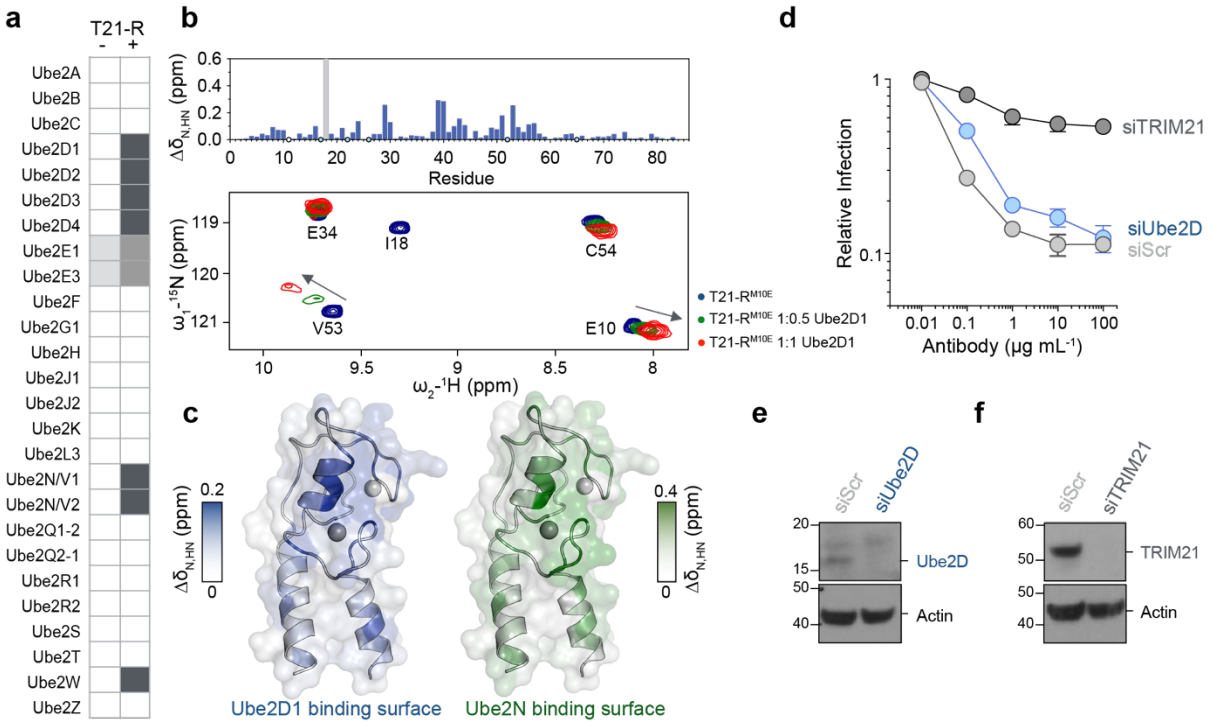


**Figure 8 TRIM21 binds and catalyzes ubiquitination with physiologically redundant E2s. a** In vitro E2 enzyme screen (no catalysis, white; catalysis, dark). Full blots are given in (**Appendix Figure 1**). **b** A part of $^{15}$N-HSQC spectra of T21-R$^{M10E}$ in absence (dark blue) and presence of 0.5 (green) or 1 (red) molar equivalents of Ube2D1. Histogram of the chemical shift perturbations is shown against sequence. Blue circles indicate proline residues, white circles missing assignments. The grey bar in the histogram represents intermediate exchange of the amide of I18, as inferred from the disappearance of the I18 signal upon addition of Ube2D1. **c** The amide chemical shift perturbation upon E2 titration is mapped onto the T21-R structure in blue for the Ube2D1 titration (shown in **b**) and green for the Ube2N titration (shown in **Figure 10**). **d** Antibody (9C12)-dependent adenovirus5 (Adv5) neutralization in HeLa cells stably transduced with small-interfering RNA (siRNA) targeted against Ube2D or TRIM21. Data represent the mean ± SEM from three independent experiments and normalized to virus only. Immunoblots of siRNA mediated protein depletion of **e** Ube2D and **f** TRIM21. SiScr, scramble control siRNA. Experiments in panels **d**, **e** and **f** were performed by Dr Donna L Mallery.

### 3.2.2 Crystal structure of TRIM21-RING with Ube2N~Ub

My attempt to unpick the basis of fine E2 specificity began with solving the complex between TRIM21-RING and a stable isopeptide-linked Ube2N~ubiquitin (Ube2N~Ub) conjugate (**Appendix Table 1**, **Appendix Figure 2**). The structure was solved to 2.8 Å resolution and contained two full complexes (2xTRIM21-RING and 2xUbe2N~Ub) in the asymmetric unit. The overall domain orientation shows Ube2N~Ub in the closed conformation primed for catalysis, bound by the two protomers in the RING dimer (**Figure 9a,b**). While Ube2N only contacts the proximal RING domain, ubiquitin is bound by both the proximal and distal RING. Typically, E2s interact with the RING via residues in helix 1 and loops 4 and 7[8]. At the E2:E3 interface are a number of

hydrophobic interactions, mediated by aromatic side chains and conserved hydrogen bonds. The generic interactions present in the structure include hydrogen bonds between Ube2N S96 sidechain and TRIM21 P52 carbonyl, as well as Ube2N R7 sidechain to TRIM21 I18 carbonyl (**Figure 9c**). The TRIM21 linchpin-residue (R55) contacts Ube2N (K94 carbonyl) and ubiquitin (Q40 sidechain and R72 carbonyl) simultaneously (**Figure 9b**). However, a particularly striking feature was the prominent involvement of three anionic residues: E12, E13 and D21 (**Figure 9**e, **Appendix Figure 2c**). Residues E12 and D21 hold Ube2N in place via a cluster of positively charged residues (R6, R7, K10 and R14) arranged on the same RING-facing surface of Ube2N helix 1, supported by interactions with backbone carbonyls (I18 and L20) (**Figure 9c,e**). The final charged residue in the motif, E13, mediates a complex hydrogen bond network with both ubiquitin via K11, and with the distal RING protomer via N71, which in turn hydrogen bonds with the carbonyl of ubiquitin K33 (**Figure 9d**). The tri-ionic motif is perfectly positioned to capture the E2~Ub specifically in its active, closed conformation, providing optimally distributed anchor points. Thus, in contrast to the generic interactions that are always found in E2:E3 complexes, here specific electrostatic interactions rather than hydrophobic contacts appear to drive binding and, more crucially, impart specificity for the closed conformation. Additional charge-charge associations also support ubiquitin interactions. H33 of the proximal RING forms a hydrogen bond with the ubiquitin carbonyl E34, while R67 of the distal RING is positioned towards the C-terminal end of helix 1 of ubiquitin, interacting with its negative dipole moment. These latter interactions can also be found in other RING E3 complexes; for instance the RING E3 TRAF6 bound by Ube2N~Ub[127], while TRIM25 uses a lysine residue to hydrogen bond with D32 of ubiquitin[84,85].

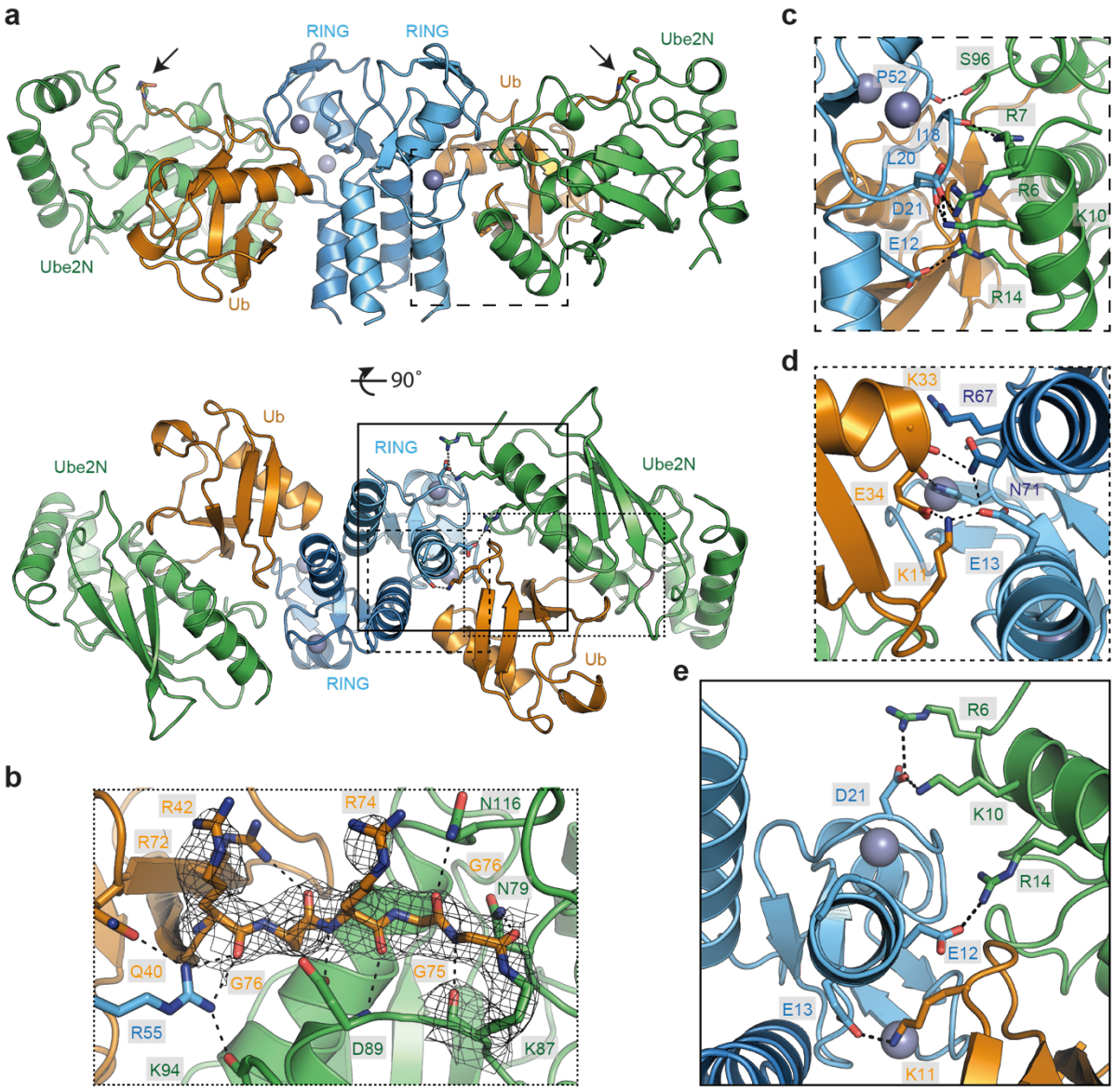


**Figure 9 X-ray structure of TRIM21-RING in complex with Ube2N~Ub. a** 2.8 Å X-ray structure of T21-R (blue) in complex with Ube2N~Ub (Ube2N in green, Ub in orange). Close-ups of the **b** the ubiquitin C-terminus (showing the $2F_O$-$F_C$ density at 2.0 sigma for selected residues), **c** the RING:E2 interface, **d** the RING:Ub interface and **e** the three ionic anchor points. $Zn^{2+}$-atoms are shown as grey spheres, the isopeptide in panel **a** is marked by an arrow and polar interactions are indicated by dashed black lines.

### 3.2.3 Formation of the closed Ube2N~Ub conformation in solution

To test whether the tri-ionic motif provides anchor points for conformation-specific capture of Ube2N~Ub, NMR titrations were performed against monomeric T21-$R^{M10E}$. The obtained amide chemical shift perturbations (CSPs) upon titration of Ube2N into $^{15}$N-labelled T21-$R^{M10E}$ (**Figure 10**, **Figure 8c**) agree well with the crystal structure described above. In the crystal structure, the TRIM21 di-glutamates form salt bridges with both Ube2N and ubiquitin (**Figure 9e**), suggesting distinctive roles for the two

residues in this process. The E13A mutation causes no significant reduction of CSP during titration of Ube2N into $^{15}$N-labelled T21-R$^{M10E/E13A}$, whereas mutation of E12 to alanine or arginine does (**Figure 10a,b**). To quantify these interactions, I used the CSPs to calculate a $K_D$ for T21-R$^{M10E}$ binding to Ube2N of 15 ± 4 $\mu$M (**Figure 10c**), similar to the $K_D$ between the RING E3 TRAF6 and Ube2N[128]. Mutation E12R led to a fourfold increase in $K_D$ to 57 ± 13 $\mu$M, indicating impaired but not abolished Ube2N recruitment.

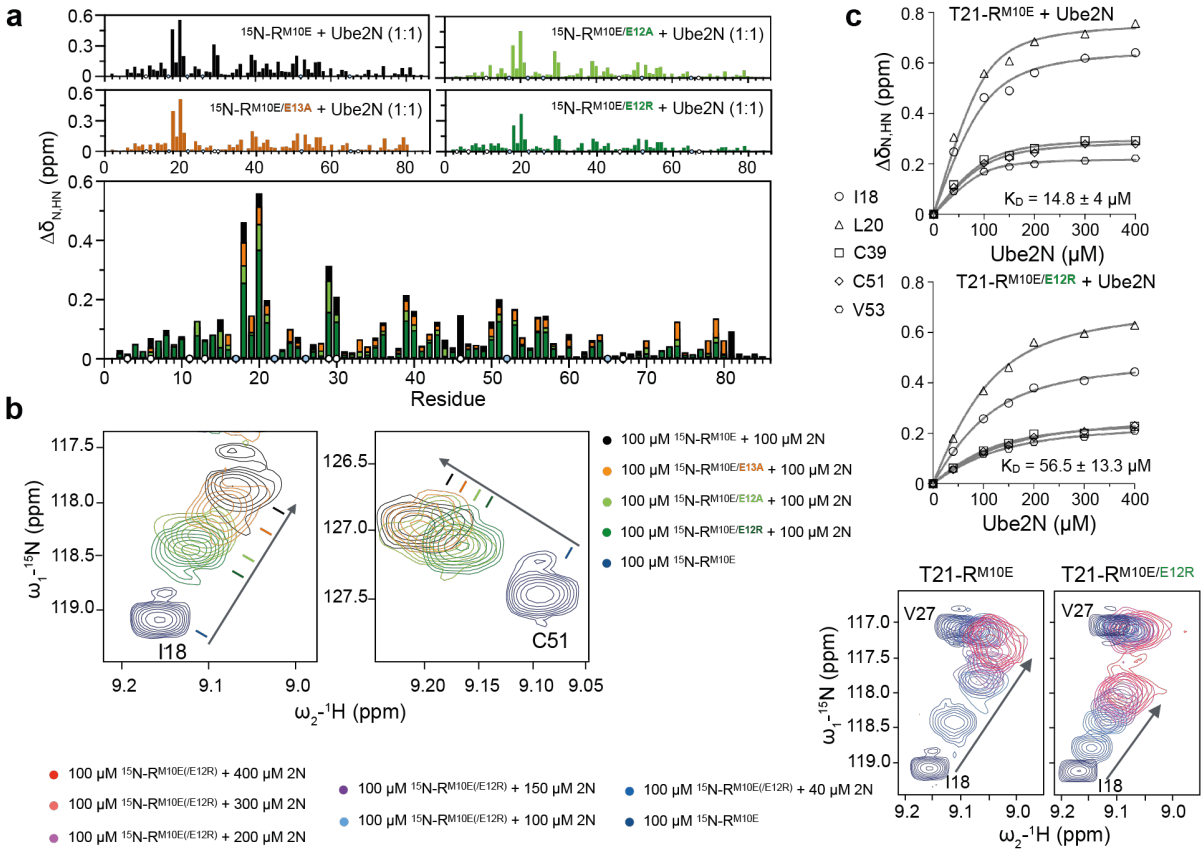


**Figure 10 The effect of the tandem glutamates in binding Ube2N. a** Histograms for the titrations of Ube2N into T21-R$^{M10E}$, showing CSP vs. sequence position. Blue circles indicate proline residues, white circles missing assignments. **b** Expansions showing peaks of selected amides (I18 and C51) of T21-R$^{M10E}$ (abbreviated R$^{M10E}$ on color key) are shown in absence of titrant, as well as different RING mutants in presence of 1 molar equivalent of Ube2N (abbreviated 2N on color key). **c** Dissociation constant fitting plots and peak of amide I18 are shown for T21-R$^{M10E}$ and T21-R$^{M10E/E12R}$ titration with Ube2N. $K_D$ values represent the mean ± SD of 5 different peaks that were fitted as described in Chapter 2.

Based on the crystal structure, Ube2N~Ub should bind TRIM21-RING with higher affinity than Ube2N, due to the additional ubiquitin interactions (**Figure 9**). Such behaviour was observed for BIRC7 and Ube2D2~Ub[20]. To investigate this, a series of binding experiments was carried out using surface plasmon resonance (SPR), which

allowed measurement of binding to the wild-type T21-R. First, a $K_D$ of 43 ± 5 $\mu$M between immobilized GST-T21-R and Ube2N was measured (**Figure 11a**), which is slightly higher than the one measured using NMR under a different experimental setup and using T21-R$^{M10E}$ (see Chapter 2). Repeating the SPR measurement using Ube2N~Ub, an increase in affinity by nearly an order of magnitude was observed to a $K_D$ of 5 ± 1 $\mu$M (**Figure 11b**). RING E3s enable catalysis by promoting the closed E2~Ub conformation[19-21]. To observe formation of the closed conformation in solution, $^{15}$N-T21-R$^{M10E}$ was titrated with Ube2N~Ub. Comparison with the titration of uncharged Ube2N revealed a small number of amide peaks with a different magnitude and direction of CSP (**Figure 11c,d**). In order to isolate the effects due to the presence of ubiquitin, differential chemical shift perturbation (dCSP, Chapter 2) were calculated between the peaks of TRIM21 in the presence of either Ube2N or Ube2N~Ub. The amides showing the strongest dCSP values are E12, V53, C54 and R55 (**Figure 11c**), in agreement with the two interfaces between ubiquitin and the proximal RING observed in the crystal structure (**Figure 9**). The distal interface cannot be observed in these experiments as monomeric TRIM21-RING$^{M10E}$ was used. To confirm formation of the closed conformation in these experiments, T21-R$^{M10E}$ was also titrated into Ube2N~$^{15}$N-Ub, which indeed showed amide CSPs on ubiquitin at interfaces present in the closed Ube2N~Ub conformation (**Appendix Figure 3d-f**).

Mutation of E13, which directly stabilizes ubiquitin in the closed conformation (**Figure 11d,e**), to alanine led to a strong reduction of dCSP on TRIM21 (**Figure 11e**). The same was observed when T21-R$^{M10E/E12A}$ was used, and in the case of T21-R$^{M10E/E12R}$ no dCSP could be observed at all. This latter result was unexpected as E12 contacts Ube2N, not ubiquitin, in the crystal structure (**Figure 9c,e**). This suggests that the interaction between TRIM21 E12 and Ube2N R14 might be important for positioning TRIM21 E13 towards ubiquitin K11, thereby explaining the effect of E12 mutation on formation of the closed conformation. In addition, these results suggest that the tri-ionic motif promotes catalysis by monomeric TRIM21 RING, as they enable a single RING to bind the closed conformation.

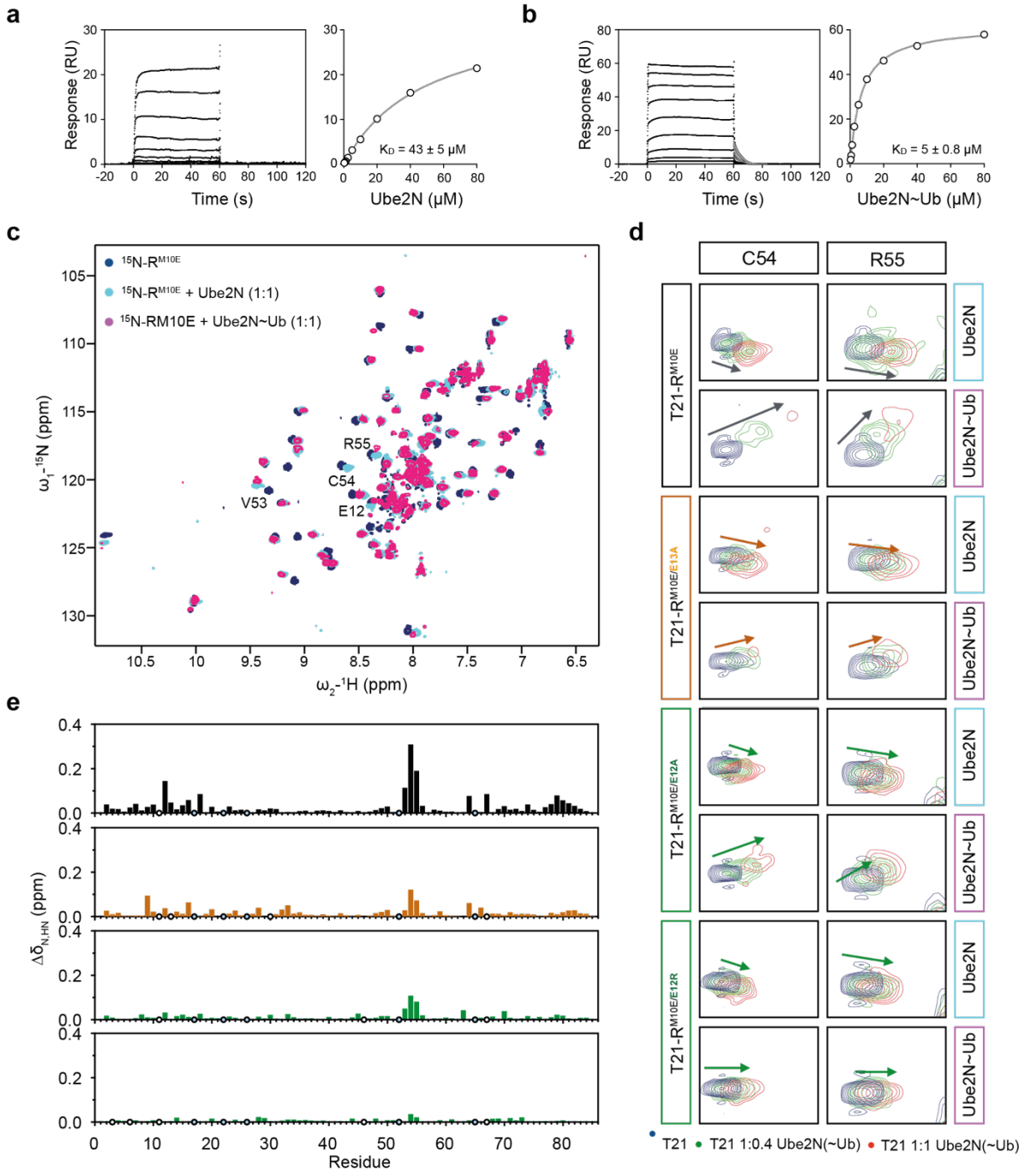


**Figure 11 The tandem glutamates E12 and E13 cooperatively promote formation of the closed Ube2N~Ub conformation.** SPR sensograms and binding plots for immobilized GST-T21-R titrated against **a** Ube2N and **b** Ube2N~Ub. The dissociation of Ube2N~Ub could be fitted (grey) with dissociation rate constant ($k_{off}$) of 0.15 $s^{-1}$. For Ube2N, dissociation was faster than the instrument response with the response returning to baseline at the end of injection, suggesting $k_{off}$ was >1 $s^{-1}$. $K_D$ values represent the mean ± SD of two (Ube2N) or three (Ube2N~Ub) independent experiments. **c** $^{15}$N-HSQC spectra of labelled T21-$R^{M10E}$ in alone (blue) or in presence of Ube2N (magenta) or Ube2N~Ub (cyan) are shown. **d** The peaks of amide peaks of C54 and R55 are shown during titration with Ube2N and Ube2N~Ub. Free T21-$R^{M10E}$ (blue), T21-$R^{M10E}$ in presence of 0.4 (green) and 1 (red) molar equivalents of titrant. **e** Histograms of the dCSP (differential chemical shift perturbation) of T21-

$R^{M10E}$ mutants titrated with either Ube2N or Ube2N~Ub are shown against the sequence. Blue circles indicate proline residues, white circles missing assignments.

### 3.2.4 A tri-ionic motif determines Ube2N-specificity

Together, the X-ray and NMR data suggest that the novel tri-ionic motif drives TRIM21 catalysis, by specifically stabilizing Ube2N~Ub in the closed conformation. To test this, tri-ionic motif residues in TRIM21-RING were mutated and their impact on Ube2N~Ub discharge and free K63-linked ubiquitin chain formation with Ube2N/V2 was determined. All mutants of the tri-ionic motif show a significant reduction in both activities, as does mutation of the R55 linchpin (**Figure 12a-c**). Mutation of E12 to alanine greatly reduced, and mutation to arginine completely abolished, catalysis with Ube2N. Similarly, T21-$R^{E13A}$ showed a reduced activity, comparable to that observed for T21-$R^{E12A}$. T21-$R^{E13R}$ activity was reduced further. Consistent with the role of TRIM21 E13 in capturing ubiquitin by binding ubiquitin K11, the ability of T21-R to catalyze the formation of free ubiquitin chains was abolished when $Ub^{K11E}$ was used (**Figure 12d**). Mutation of D21 to arginine also resulted in a loss of activity (**Figure 12b,c**). These ubiquitination assays correlate strikingly well with the NMR titrations, where T21-R E12A and E13A each show a similar reduction in dCSP and E12R shows no dCSP at all (**Figure 12e**). Moreover, these biochemical results establish the tri-ionic anchor points as key residues in catalyzing ubiquitination with Ube2N.

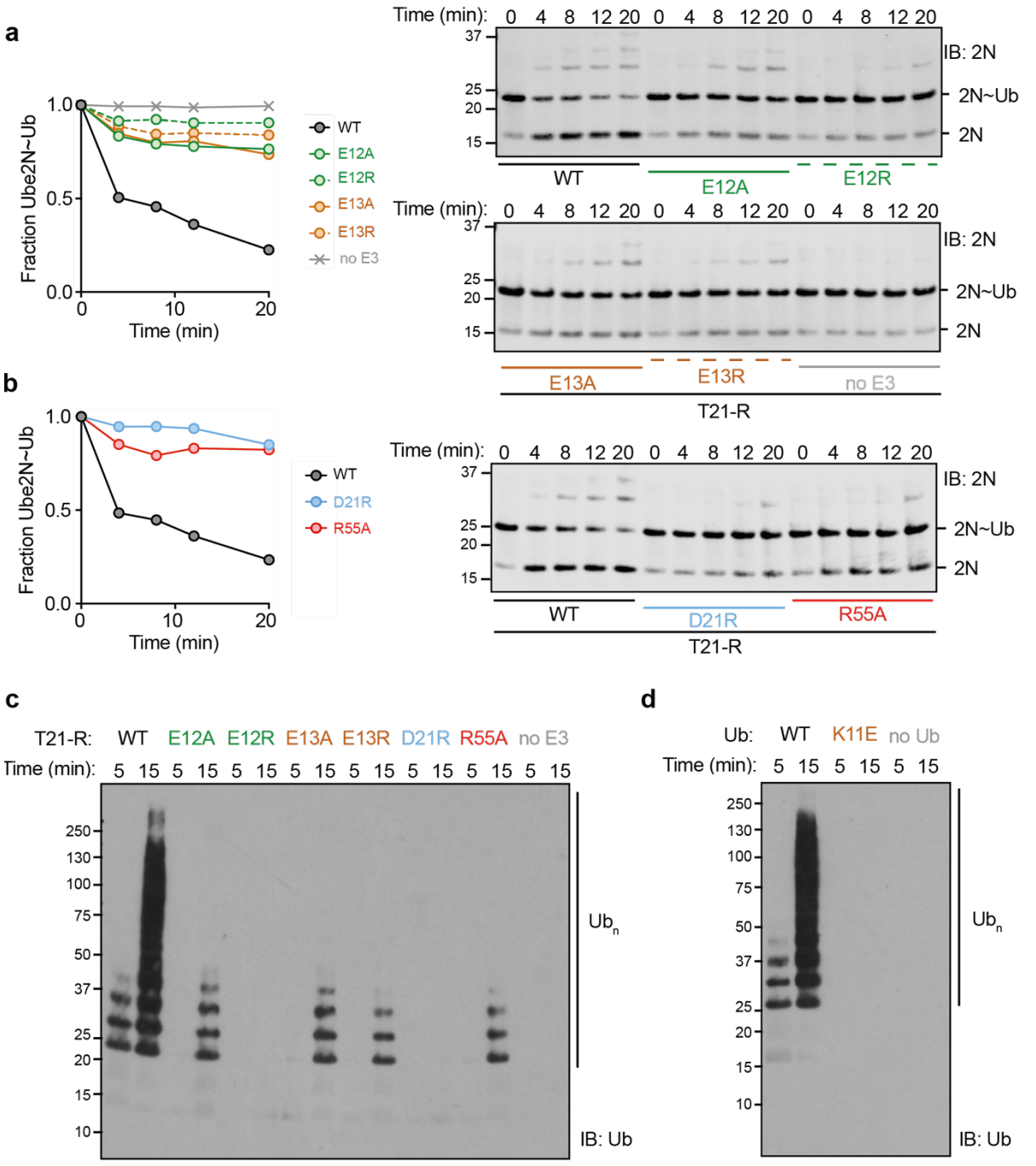


**Figure 12 The tri-ionic anchor points are essential for K63-ubiquitination in vitro.** Catalysis of ubiquitin discharge from ubiquitin conjugated Ube2N/Ube2V2 by **a** TRIM21 di-glutamate and **b** D21R, R55A mutants. Catalysis of unanchored ubiquitin chains by Ube2N/Ube2V2 of **c** T21-R mutants and **d** ubiquitin K11E.

A sequence alignment of the E2 enzymes identified in the E2 screen to interact with TRIM21 shows that the charged residue in Ube2N that is coordinated by TRIM21 E12 is not conserved (**Figure 13a**). Ube2N residue R14, which interacts with TRIM21 E12, is an acidic residue in Ube2D1 to Ube2D4, Ube2E1 and Ube2E3. This suggests that

the tri-ionic motif has specifically evolved to promote Ube2N catalysis. To test this hypothesis, I investigated how mutants of the tri-ionic motif impact Ube2D1 catalysis by TRIM21. Strikingly, none of the tri-ionic mutants (E12A/R, E13A/R, D21R) had any significant effect on activity with Ube2D1 (**Figure 13b,c**). In contrast, mutation of the linchpin residue (R55A) abolished catalysis. These results suggest that whilst the linchpin residue is required for efficient E2~Ub binding (**Figure 9b**) it does not determine specificity. This is consistent with its role in discharging ubiquitin, which is coupled to all E2s using a common mechanism. In addition, I also reversed the charges of key residues on the E2 enzymes to make Ube2N$^{R14D}$ and Ube2D1$^{D12R}$. Consistent with the ubiquitination data on tri-ionic mutants (**Figure 13a-c**) and the importance of this motif in Ube2N activity, Ube2N$^{R14D}$ displayed a strong loss of ubiquitination with T21-R (**Figure 13d**). Mutant T21-R$^{E12R}$ was unable to rescue with Ube2N$^{R14D}$, even though reversing the charges could theoretically re-form the salt bridge. This is likely because neighbouring residues are not matched to the newly swapped charged residue and cannot generate the correct local p$K_a$; indeed the p$K_a$ of a residue can be altered by charges up to 15 Å distant[129]. In contrast, Ube2D1$^{D12R}$ remained active, consistent with it not requiring the salt bridge for interaction (**Figure 13e**). Collectively, these data establish that the tri-ionic motif drives a Ube2N-specific catalytic mechanism, that is distinct from catalysis with Ube2D. Significantly, Ube2W, the only other E2 thought to be physiologically relevant for TRIM21 function[27], has an alanine at the structurally equivalent R14 position, which, unlike the aspartate in Ube2D1, would not repel binding like the aspartate in Ube2D1 (see also Chapter 5).

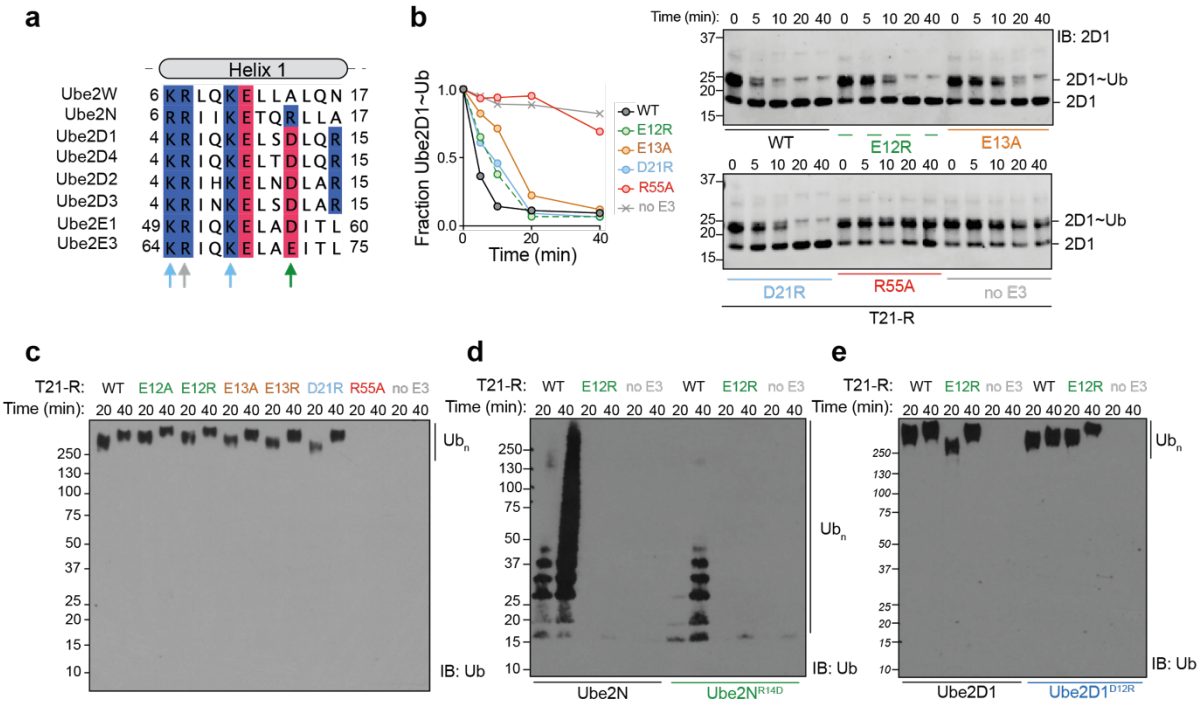


**Figure 13 Ionic anchor points enable the Ube2N-specific catalytic mechanism of TRIM21. a** Clustal omega sequence alignment of helix 1 for all positive hits of the E2 screen (**Figure 8a**). Arrows mark residues involved in RING interactions in the T21-R:Ube2N~Ub structure. Lysine and arginine residues are colored in blue, aspartate and glutamate residues in red. **b** Catalysis of ubiquitin discharge from pre-charged Ube2D1~Ub and **c** catalysis of unanchored ubiquitin chains by Ube2D1 of T21-R anchor point mutants. Catalysis of ubiquitin chains by **d** Ube2N WT and R14D mutant and **e** Ube2D1 WT and D12R mutant.

### 3.2.5 Tri-ionic mutants have impaired cellular function

The identification of an E2-specific RING mechanism provided us for the first time with an opportunity to test whether TRIM21 dependence on Ube2N for antiviral activity is due to direct recruitment of the E2 or because an additional ligase is involved. To this end, TRIM21 was ectopically expressed in *TRIM21*-knockout 293T cells under its natural promoter and tested for antibody-dependent virus neutralization, NF-κB mediated immune signalling and IKK protein depletion by Trim-Away (**Figure 14**). In agreement with our biochemical data, all mutants of the tri-ionic motif led to reduced virus neutralization to varying degrees (**Figure 14a**). Moreover, they were all deficient in immune signalling apart from E12A (**Figure 14b**), which was the most active of these mutants in virus neutralization (**Figure 14a**). All other tri-ionic motif mutants showed no immune activation. *TRIM21*$^{R55A}$ showed efficient virus neutralization and immune signalling (**Figure 14a,b**). In Trim-Away experiments[62], only *TRIM21*$^{E12A}$ was capable of efficiently depleting protein, with *TRIM21*$^{D21R}$ retaining partial depletion

activity (**Figure 14c**). All other mutants, including *TRIM21*$^{R55A}$ were deficient in protein depletion. Collectively, the biochemical and cellular data establishes the tri-ionic motif as a critical determinant of ubiquitination-dependent cellular function of TRIM21.

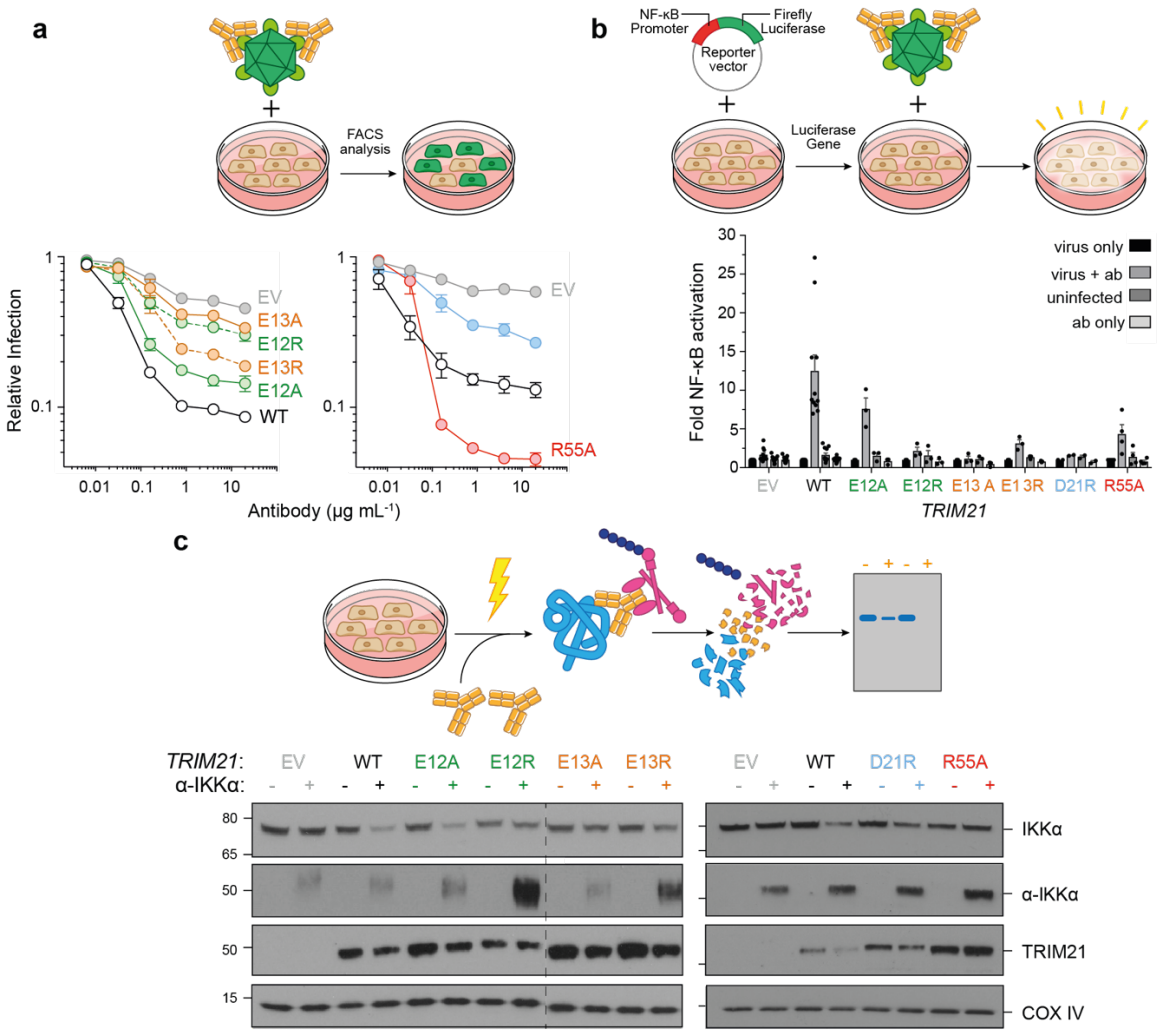


**Figure 14 The anionic anchor point motif is essential for TRIM21 function inside cells. a** Antibody (9C12)-dependent adenovirus5 (Adv5) neutralization in stably reconstituted 293T cells. Data represent the mean ± SEM from at least three biologically independent experiments. **b** Induction of NF-κB signalling in stably reconstituted 293T cells upon infection by 9C12 coated Adv5 measured using NF-κB luciferase reporter assay. Data represent the mean ± SEM from biologically independent experiments and presented as fold change over virus only. **c** Immunoblots showing Trim-Away depletion of IκB kinase alpha (IKKα) upon electroporation of 293T cells with anti- IKKα IgG (α-IKKα). Cartoon sketches explaining the cellular experiments are shown with the experimental data. EV, empty vector. The experiments shown in this Figure were performed by Dr Jingwei Zeng.

### 3.2.6 Anchor points drive Ube2N-specificity in diverse RINGs

Residues E12 and E13 belong to a di-glutamate motif that is present in many TRIM proteins[130] and has been suggested to be involved in ubiquitin transfer[84], though a mechanistic explanation for its conservation has not been given. The analysis presented here suggests that the di-glutamates are actually part of a larger conserved tri-ionic motif. The third acidic residue is also highly conserved in TRIM proteins, as either aspartate or glutamate (**Figure 15a**). This suggests that the tri-ionic mechanism of closed conformation capture observed in TRIM21 may be driving the catalytic activity of Ube2N with other TRIMs as well. To test this hypothesis, ubiquitination experiments were carried out with the retroviral restriction factor TRIM5α, which utilizes the same canonical E2 enzymes as TRIM21 and has a similar mechanism of action[124]. As the RING domains of TRIM21 and TRIM5α are highly similar, a structural model of the catalytic complex between TRIM5α-RING (T5-R) and Ube2N~Ub was built (**Figure 15b**), by superposing a T5-R:Ube2N (4TKP[90]) and the T21-R:Ube2N~Ub structure (**Figure 9**). This suggests that the tri-ionic motif in TRIM5α might drive ubiquitination activity with Ube2N. Next, free ubiquitin chain formation and Ube2N~Ub discharge assays were carried out with T5-R mutants corresponding to the mutants tested for TRIM21. T5-R$^{E11R}$ (E12 in TRIM21, which my results predict is required to form a salt bridge with Ube2N R14), had no apparent activity (**Figure 15c,d**), in line with a previous report[125]. The second predicted ionic interaction between the E2 and RING was Ube2N R6 to TRIM5α E20 (D21 in TRIM21), and this mutant (T5-R$^{E20R}$) was also catalytically inactive. Finally, a mutant of the third motif residue, T5-R$^{E12A}$ (E13 in TRIM21), did not show any catalysis, consistent with its predicted importance in stabilizing the closed conformation. These data suggest that the tri-ionic mechanism observed in TRIM21 is also used in other TRIMs.

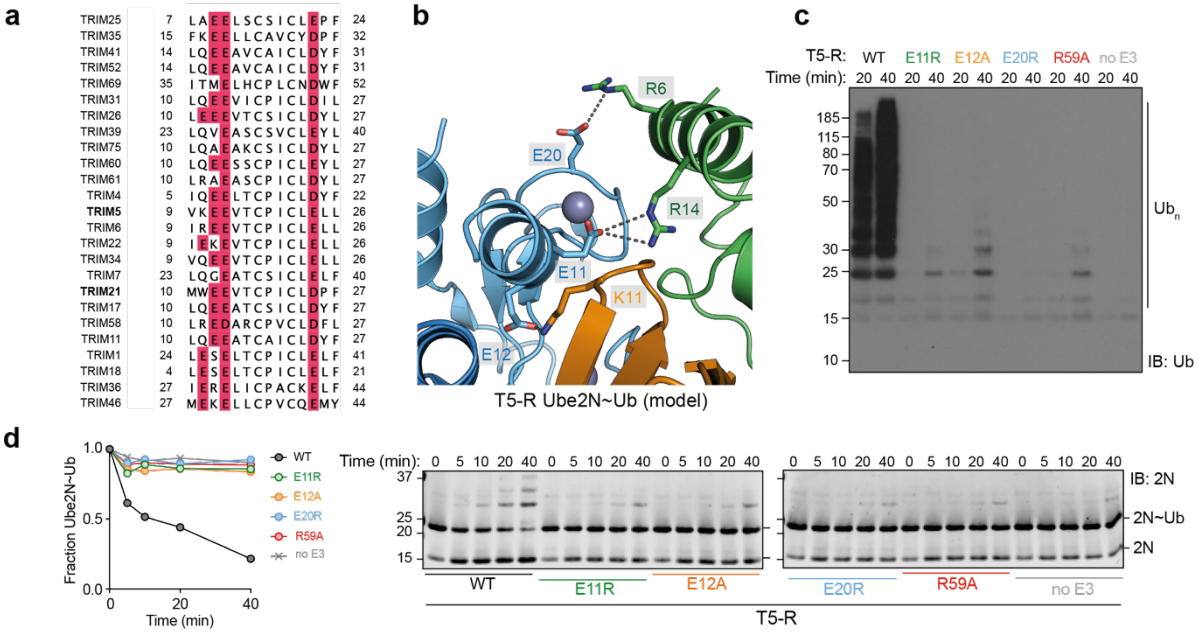


**Figure 15 The tri-ionic anchor points seen in TRIM21 are structurally and functionally conserved in TRIM5α. a** Clustal omega multiple sequence alignment of TRIM proteins. Ionic anchor points are highlighted in red. The sequences of TRIM21 and TRIM5α RING domains are highly similar (sequence identity: 47.3 %, sequence similarity: 63.4 % in pairwise sequence alignment). **b** Structural model of T5-R:Ube2N~Ub complex based on superposition of the T5-R Ube2N (4TKP)[90] and the T21-R:Ube2N~Ub structure (6S53). **c** Catalysis of unanchored ubiquitin chains by Ube2N/Ube2V2 of T5-R mutants. **d** Catalysis of ubiquitin discharge from ubiquitin conjugated Ube2N/Ube2V2 of T5-R mutants.

I further analyzed published high-resolution crystal structures of RING domains in complex with either Ube2N~Ub or Ube2N (**Figure 16**). In TRIM21, TRIM5α[90] and TRIM25[85], the tri-ionic anchor points are conserved both in sequence and structure. Consistent with results for TRIM5α and TRIM21, TRIM25 mutant E10R (E13R) renders it inactive with Ube2N[84]. Anchor points were also identified in some RING E3s outside the TRIM family, including TRAF6, LNX1, ZNRF1 and CHIP (**Figure 16**)[127,131-133]. Notably, only the RNF4:Ube2N~Ub structure lacks these interactions[101]. Of the identified RING E3s, in each case residue R6 at the N-terminal end of Ube2N helix 1, interacts with the first anchor point (D21 in TRIM21). This residue is acidic in most of the RINGs, but a Q side chain and Y carbonyl are used in LNX1 and I carbonyl is used in CHIP. At the other end of Ube2N helix 1, residue R14 is always positioned to allow a salt bridge to an acidic RING sidechain (E12 in TRIM21). The third anchor point, which contacts the ubiquitin, is found in slightly differing variations in different RINGs. LNX1 uses two aspartates (D26 and D28) to form salt bridges with K11 of ubiquitin[132], while a potential third anchor point equivalent to E13 in TRIM21 may be present in the U-box CHIP (E289, **Appendix Figure 4**). The exception is TRAF6, where ionic

interactions stabilize the dimer while an adjacent Zn-finger domain interacts with the charged ubiquitin[127]. This suggests that although tri-ionic catalysis is a prominent feature of TRIM RINGs, a similar mechanism can be found in non-TRIM RINGs.

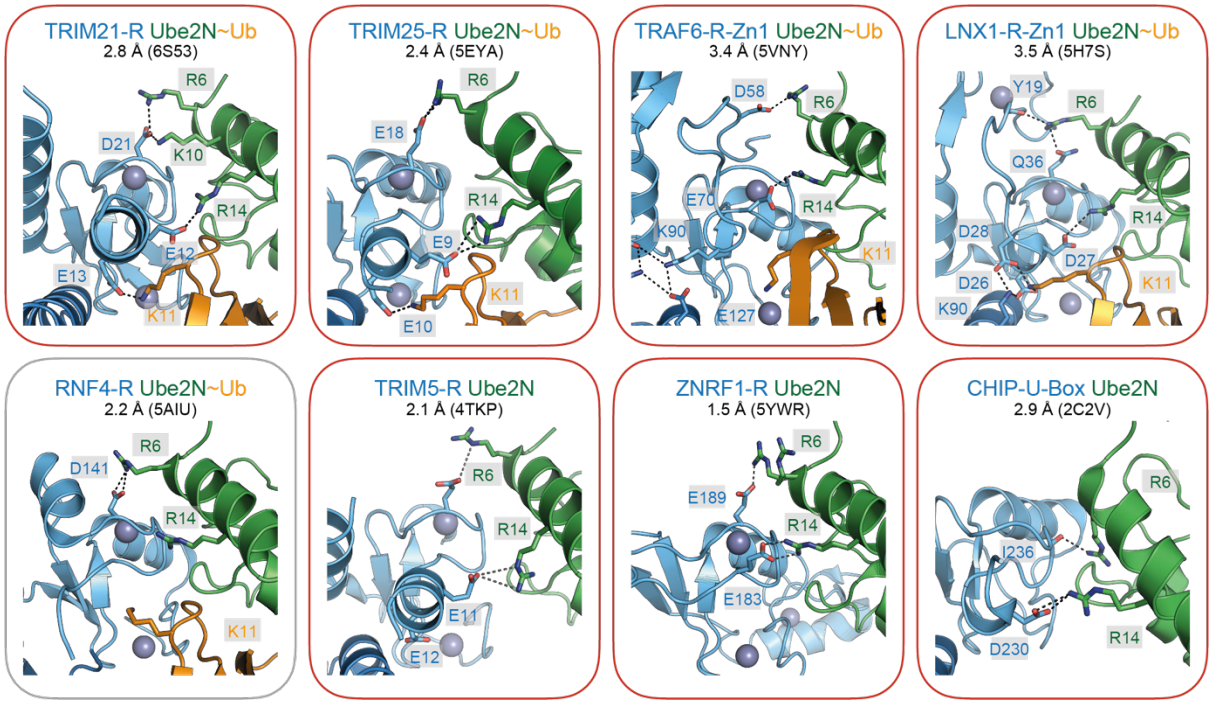


**Figure 16 The ionic anchor points are structurally conserved outside TRIM RINGs.** Close-ups of RING:Ube2N(~Ub) structures. Residues equivalent to the ionic anchor points in TRIMs are labelled. Red color of the frame indicates the presence and grey color the absence of the ionic anchor points in each structure.

## 3.3 Discussion

Mammalian cells typically possess ~40 E2s and ~600 E3s, giving ~24,000 theoretical E2:E3 pairs. Commonly used *in vitro* ubiquitination assays, together with the observed similarities between solved E2:E3 complexed structures, support the notion of significant promiscuity, yet in cells E2:E3 interactions are highly specific, delivering specialized phenotypes and functions. Determining the mechanisms behind E2:E3 specificity therefore remains a crucial and fundamental problem in ubiquitin biology. In the case of the atypical RING:E2 pair FANCL:Ube2T, a specific network of polar interactions explains their exclusivity[134], while additional modification in the form of N-terminal acetylation of the Nedd8-E2 enzyme Ube2M (Ubc12) is required for efficient interaction with the accessory E3 Dcn1[135]. However, most E2 enzymes can interact with numerous E3s, making it very difficult to identify unique features[8]. In addition,

most mechanistic studies have been performed using the promiscuous Ube2D family, thereby limiting the possibilities for generating insights into specificity. Compounding the problem of E2 substrate specificity is the fact that RING E3s are also unusual in their catalytic mechanism. They do not have a classical active site, instead promoting ubiquitin discharge from E2s by capturing a closed E2~Ub conformation[19-21], akin to a transition state. Two features have been shown to be critical – a linchpin residue (R55 in TRIM21) and RING dimerization. Crucially, because it contacts the end of the charged ubiquitin that is coupled to almost all E2s in an identical way, the linchpin does not provide any E2 specificity. In addition, a recent structure of ARC2C in complex with Ube2D2~Ub showed that the linchpin is not in itself sufficient for formation of a catalytic complex[136]. RING dimerization is also important for catalysis as inhibition of RING dimerization commonly abrogates RING activity for dimeric RINGs[20,83-85,90]. However, dimerization has not been shown to determine E2 specificity, and several active monomeric RINGs have been identified[21,137,138].

In this chapter I have proposed a general E2-specific mechanism of RING E3 catalysis, in which a tri-ionic motif provides conformation specific anchor points that capture the Ube2N~Ub closed conformation. Initially described in the context of TRIM21, I show that the same mechanism is used in TRIM5α and is structurally conserved in other TRIMs and other RING E3s (**Figure 15** and **Figure 16**). In TRIM21, this tri-ionic motif is formed by residues E12, E13 and D21. These residues provide three spatially conserved anchor points that allow an Ube2N~Ub to be wrapped around a RING E3, thereby locking the closed conformation and promoting ubiquitin discharge. D21 forms salt bridges with R6 and K10 of Ube2N at one end of the long helix at the N-terminus of Ube2N. The first glutamate of the di-glutamate repeat forms a salt bridge with R14 at the other end of the helix. Finally, the second glutamate forms a salt bridge with ubiquitin via K11 (**Figure 9e**). Importantly, in cells, mutation of anchor point residues prevents efficient TRIM21-dependent virus neutralization, immune signalling and Trim-Away (**Figure 14**). Moreover, this motif is at least as crucial as the linchpin for TRIM21 cellular function, since anchor motif mutants prevent neutralization and signalling activity, but a linchpin mutant is still active (**Figure 14**).

A crucial feature of the tri-ionic motif is that it specifically drives catalysis of Ube2N but not that of other E2 enzymes such as the promiscuous E2 Ube2D (**Figure 12**, **Figure**

**13**). While mutation of the anionic residues in both TRIM5α and TRIM21 strongly reduces ubiquitination with Ube2N in vitro it does not affect activity of TRIM21 with Ube2D1 (**Figure 13**). Classically, hydrophobic interactions and π-stacking have been described as the driving force behind E2:E3 interaction, but it is the charged nature of the interactions mediated by the tri-ionic motif that enables TRIM and some non-TRIM RINGs to promote activity with Ube2N and not Ube2D1. This is because while Ube2N has a positively charged residue positioned to interact with E12, the structurally equivalent residue in Ube2D is a negatively charged aspartate. This probably explains why an E9R TRIM25 mutation increased rather than decreased activity with Ube2D1[84]. TRIM21 cellular function is dependent upon the E2 enzymes Ube2W and Ube2N/Ube2V2, which are thought to act sequentially to build a TRIM21-anchored K63-linked ubiquitin chain[27,28]. By identifying a Ube2N-specific catalytic mechanism and introducing specific mutations that ablate it in cells, we have been able to show that the requirement for Ube2N in TRIM21 function is because of direct recruitment. A similar strategy could now be used in order to test whether direct Ube2N recruitment is necessary for the function of other RING E3s during their cellular activity.

Identification of the tri-ionic motif may also explain why monomeric TRIM21 is capable of performing catalysis. All three residues are located in one RING monomer and are critical for capture of the E2~Ub complex; specifically, mutation of E12 or E13 strongly reduced formation of the closed conformation in solution (**Figure 11**). However, while the tri-ionic motif provides a mechanism that allows the TRIM21 RING to be active as a monomer they are not sufficient to drive monomeric activity in TRIM5α[90]. This may be because TRIM21 has evolved to become a significantly more potent ligase than TRIM5α[80]. Increased RING activity may also explain the importance of B-box autoinhibition in controlling TRIM21 function. While this work has identified a Ube2N-specific mechanism, it remains an open question why TRIM21 (or indeed other RING E3s) does not seem to utilize Ube2D in cells, despite being able to. Spatio-temporal differences in protein expression and availability may contribute to functional specificity. For instance, in HeLa and U2OS cells the Ube2N concentration is 3 to 6 times higher than for Ube2D (**Appendix Figure 5**)[139,140]. It will be interesting to

determine whether there are other general mechanisms, such as that described here, that allow specific E2 recruitment by E3 ligases in other cases.

# Chapter 4 Self-ubiquitination of TRIM21

## 4.1 Introduction

Specificity in ubiquitin conjugation is determined by recruitment of the substrate to the correct E2:E3 pairs. Having established how TRIM21 specifically recruits Ube2N, my next aim was to understand how this results in a TRIM21 anchored K63-linked ubiquitin chain. However, previously published structural insights into substrate ubiquitination are limited to the transfer of one ubiquitin[141] or ubiquitin-like protein[30,31]. How specificity is achieved within the ubiquitination system remains largely elusive due to its extremely high level of complexity.

Ubiquitin chains that are linked via K63 are involved in endocytosis, DNA damage and the immune response[1]. The only E2 enzyme dedicated to K63-ubiquitination is Ube2N, which forms a heterodimer with either Ube2V2 or Ube2V1[115,142,143]. Ube2V2 binds and orients the acceptor ubiquitin, thereby generating specificity for K63 linkage[32,33,101]. While Ube2N/Ube2V2 efficiently forms free K63-linked ubiquitin chains, substrate modification requires the presence of a priming ubiquitin for elongation[29]. Such a mechanism has been established for the RING E3s TRIM21 and TRIM5α[27,124]. TRIM21 detects antibody-coated substrates by specifically recognizing the bound antibody. This activates its normally inhibited E3 ligase function, resulting in virus neutralization (**Figure 5a**) and innate immune activation via the NF-κB pathway (**Figure 6**)[28,53,80]. The envisioned pathway is the following: first, Ube2W attaches a priming ubiquitin to the TRIM21 N-terminus[27]. Next, TRIM21 specifically recruits Ube2N/Ube2V2 to produce a TRIM21-anchored K63-linked ubiquitin chain[27,113]. TRIM21 does not engage its target directly and forms the ubiquitin chain on its own N-terminus, resulting in degradation of itself, the antibody and the substrate[27,53,62]. It is unknown how this TRIM21-anchored ubiquitin chain is formed. Moreover, no ubiquitin chain formation on a substrate has been visualized until the work presented in this chapter.

### 4.1.1 Aims

In this chapter I sought to understand how RING E3-anchored ubiquitin chains are formed, thereby taking the next step from my previous findings in Chapter 3 on specific E2 recruitment[113]. I have addressed this question by solving a structure trapped in the process of RING-anchored chain elongation. Together with a kinetic analysis, this reveals how chemical activation of the acceptor ubiquitin is achieved. It also reveals a specific topology of the RING domains that is necessary for self-anchored ubiquitin chain formation. Finally, I validate the importance of this arrangement biochemically and show that it results in targeted protein degradation in a physiological setting.

## 4.2 Results

### 4.2.1 Structure showing the formation of anchored ubiquitin chains

The aim of this part of my work was to understand how a substrate-bound ubiquitin chain can be formed. In principle, ubiquitin chain elongation of TRIM proteins depends on their RING domain only. In the case of TRIM21 (and TRIM5α), the TRIM RING itself is both the enzyme and substrate for elongation, after it has undergone N-terminal mono-ubiquitination by the E2 enzyme Ube2W[27,124,125]. Therefore, I attempted to devise a crystallographic approach that might cast light on substrate-bound ubiquitination with TRIM21 RING and its chain-forming E2 heterodimer Ube2N/Ube2V2. In crystallization trials, I used N-terminally mono-ubiquitinated TRIM21 RING domain ($Ub^{G75/76A}$-$TRIM21^{1-85}$ or Ub-R), an isopeptide-linked, non-hydrolyzable ubiquitin-charged Ube2N conjugate (Ube2N~Ub) and Ube2V2. From these trials I isolated crystals of a complex with one copy each of Ub-R, Ube2N~Ub and Ube2V2 in the asymmetric unit, which I was able to solve to 2.2 Å resolution (**Appendix Figure 1**, **Appendix Table 2**). Careful examination of this structure showed that the naturally occurring TRIM21 RING homo-dimer[80] could be generated in the model by invoking crystal symmetry (**Figure 17a**). The RINGs engage Ube2N~Ub in the closed conformation[19-21] and Ube2N forms a heterodimer with Ube2V2[115,142,143]. Analyzing further interactions within the crystal lattice, it was found that the TRIM21-linked ubiquitin made additional contacts to the Ube2N/Ube2V2 of a symmetry related complex (**Figure 17b, Appendix Figure 6**), which orients the RING-bound acceptor ubiquitin so that its K63 points towards the active site, ready for

nucleophilic attack (**Figure 17b,c**). This structure thus represents a snapshot of a ubiquitin-primed RING ready for self-anchored ubiquitin chain elongation.

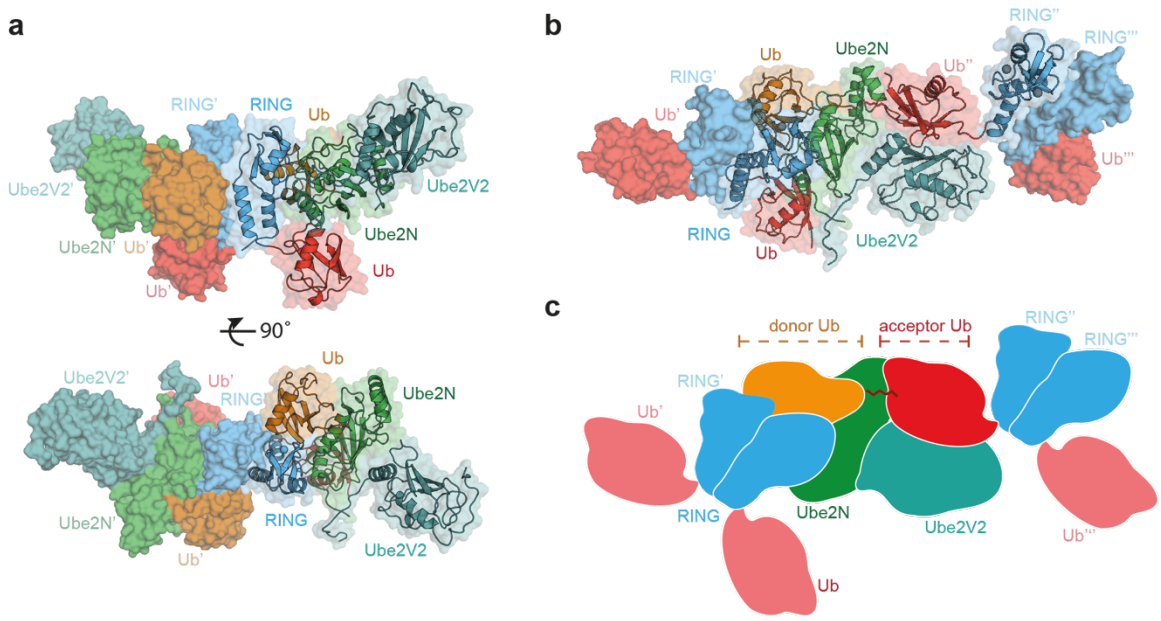


**Figure 17 Structure of initiation of RING-anchored ubiquitin chain elongation. a** Side and top view of the Ub-R:Ube2N~Ub:Ube2V2 structure (Ub-R, Ub in red, R in blue, Ube2N~Ub, Ube2N in green, Ub in orange, Ube2V2 in teal). Chains drawn as cartoon represent the asymmetric unit. **b** The canonical model of initiation of RING-anchored ubiquitin chain elongation. **c** Schematic cartoon, representing the canonical model of RING-anchored ubiquitin chain elongation shown in **b**. Symmetry mates are denoted by ' next to the label.

### 4.2.2 Chemical mechanism of ubiquitination

Having captured a 2.2 Å resolution representation of the system prior to catalysis, this enabled a detailed analysis of ubiquitin transfer. The Ube2N-charged ubiquitin can be found in the RING-promoted closed Ube2N~Ub conformation, and thus represents the donor ubiquitin (**Figure 17**). The RING-bound ubiquitin of a symmetry-related complex was captured by Ube2N/Ube2V2, positioning its nucleophilic K63 $N^{\zeta}H_3$ group 4.8 Å from the electrophilic carbonyl of the donor ubiquitin C-terminus (**Figure 18a**, **Appendix Figure 6**). Interestingly, K63 of this acceptor ubiquitin shows a direct interaction with D119 of Ube2N (**Figure 18a**). This suggests that D119 deprotonates K63 on the acceptor ubiquitin, thereby activating it for nucleophilic attack. Indeed, the corresponding residue in Ube2D (D117) has previously been suggested to be involved in positioning and/or activating an incoming acceptor lysine[19].

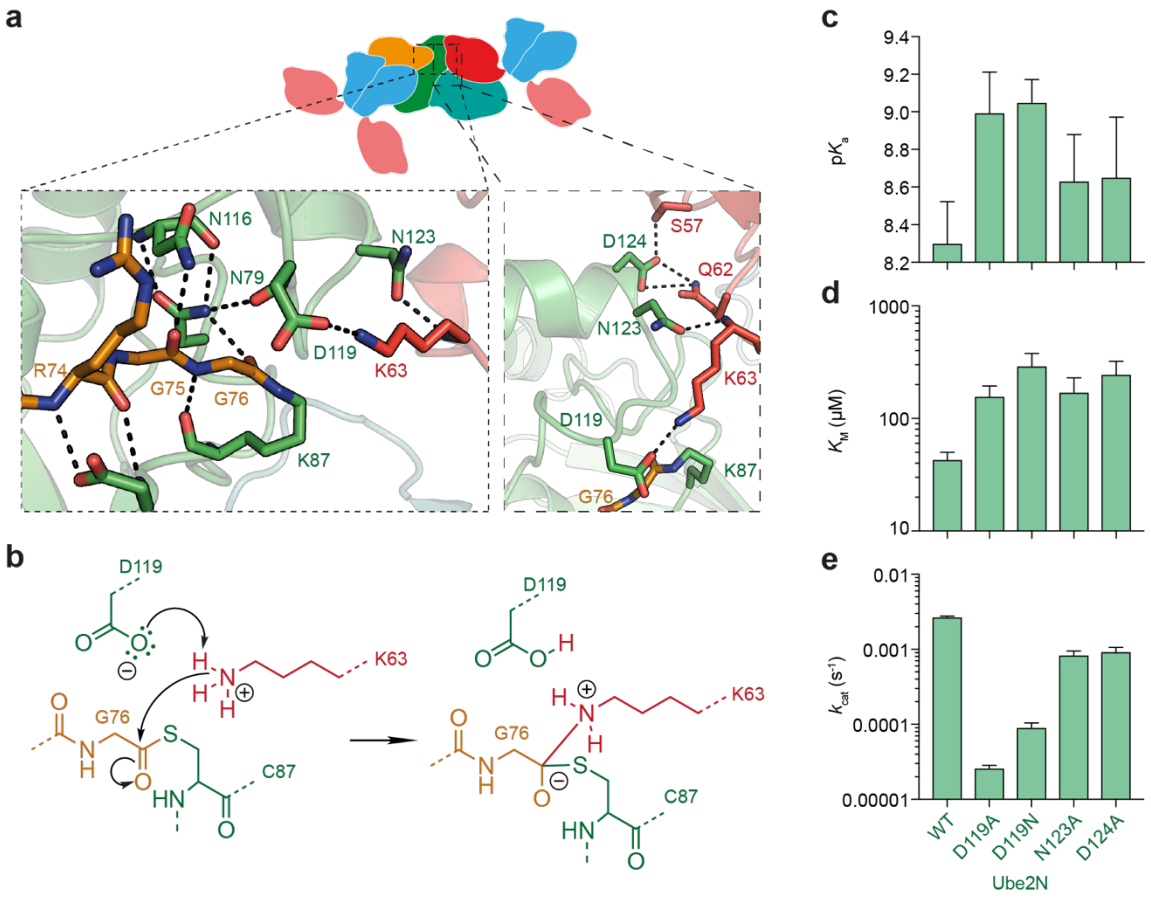


**Figure 18 Chemical mechanism of ubiquitination. a** Magnified regions of the active site of Ube2N~Ub/Ube2V2 (Ube2N in green, donor Ub in orange, acceptor Ub in red, Ube2V2 in teal). Stereo-images are shown in **Appendix Figure 7**. **b** Chemical scheme for the activation of the acceptor lysine. **c** Acid coefficients (p*K*a), **d** $K_M$ and **e** $k_{cat}$ of di-ubiquitin formation by Ube2N/V2 are presented as best fit + standard error. Fits were performed using data of n = 3 technical replicates and are shown in **Appendix Figure 7**.

To investigate the chemical mechanism of ubiquitination (**Figure 18b**), an assay to measure the kinetics of K63-linked di-ubiquitin formation was established (**Appendix Figure 7**). The acid coefficient (p$K_a$) of this reaction should solely depend on the protonation state of its nucleophile, K63. Fitting the ubiquitination velocity of reactions carried out at different pHs to an equation assuming one titratable group revealed a p$K_a$ of 8.3 for Ube2N (**Figure 18c**, **Appendix Figure 7**), comparable to what was observed for the SUMO-E2 Ube2I[144]. This is significantly lower than the p$K_a$ of 10.5 expected for a free lysine ζ-amino group[145], which would be incompatible with catalysis at physiological pH ~7.34[146]. D119 was mutated to either alanine or asparagine, as neither can act as a base but asparagine could still bind and orient K63. Both mutants increased the p$K_a$ to ~9 (**Figure 18c**). At physiological pH, Ube2N$^{D119A/N}$ modestly increased the $K_M$ by ~4 and ~7-fold, respectively (**Figure 18d**). Mutation to alanine

reduced $k_{cat}$ by 100-fold and mutation to asparagine by 30-fold (**Figure 18e**), suggesting that substrate turnover also depends on orientation of the lysine nucleophile. Yet, this catalytic rate does not drive efficient ubiquitin chain formation under physiological pH (**Appendix Figure 8**). Together, these observations establish that D119 is the base that deprotonates the incoming acceptor lysine to enable catalysis.

Interactions between ubiquitin and other proteins have been shown to depend on specific conformations of ubiquitin's $\beta_1$-$\beta_2$ loop, which can be found in either "loop-in" or "loop-out" forms[147]. These motions change the ubiquitin core structure and subsequent conformational selection enables ubiquitin to interact with many different binding partners[148]. In the present structure, the donor ubiquitin $\beta_1$-$\beta_2$ loop was found in its loop-in configuration, while the loop-out form was incompatible with formation of the closed conformation (**Figure 19a,b**). Conversely, the acceptor ubiquitin was in a loop-out configuration (**Figure 19c**), which appears to be the default state in isolated ubiquitin[147]. Donor and acceptor ubiquitin also have distinct B-factor profiles (**Figure 19d**), perhaps reflecting some other aspect of their different roles in catalysis, but could also be a reflection of crystal packing. Interestingly, the $\beta_1$-$\beta_2$ loop conformation also appears to be critical in ubiquitin-like proteins such as Nedd8, when activating cullin-RING-ligases (CRL)[141].

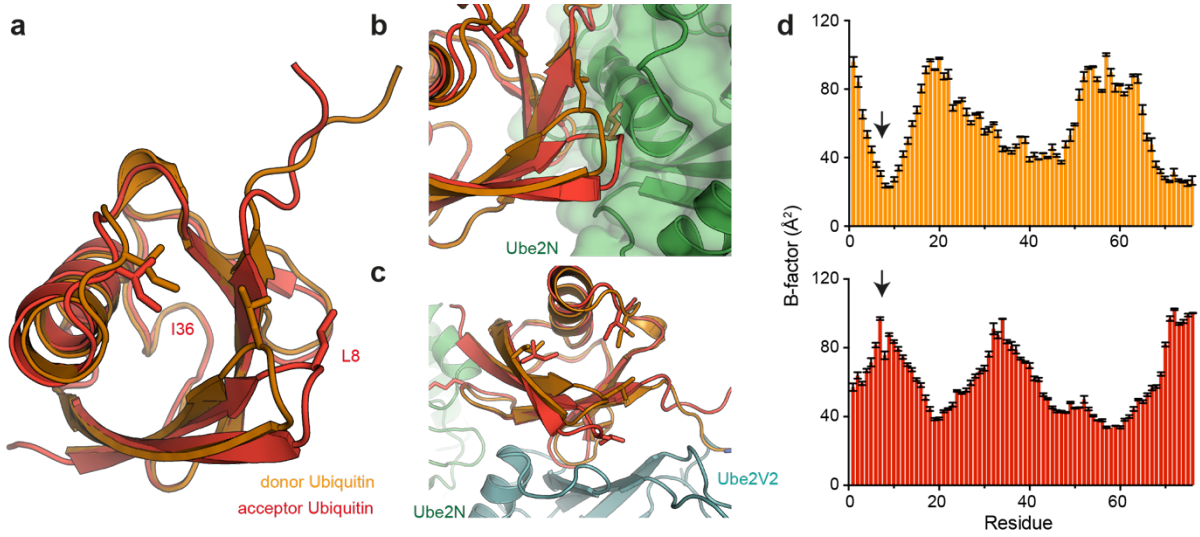


**Figure 19 Dynamic ubiquitin loop configurations. a**, **b**, **c** Structural alignments of the donor (orange) and acceptor ubiquitin (red) found in the Ub-R:Ube2N~Ub:Ube2V2 structure (7BBD, Ube2N in green and Ube2V2 in teal). Main differences can be seen in the $\beta_1$-$\beta_2$ loop carrying L8, which is either in the

loop in (donor ubiquitin, orange) or loop out configuration (acceptor ubiquitin, red). **d** Shown are B-factors (represented as mean ± SEM of N, $C^{\alpha}$, C' of the Ub-R:Ube2N~Ub:Ube2V2 structure) for donor and acceptor ubiquitin.

RING E3s act by locking the normally very dynamic E2~Ub species in a closed conformation, thereby priming it for catalysis[19-21]. Comparison with the previously determined T21-R:Ube2N~Ub structure (Chapter 3)[113] shows scarcely any difference in the position of the donor ubiquitin C-termini within the Ube2N active site (**Appendix Figure 9a**). Nonetheless, formation of the closed Ube2N~Ub conformation alone is not sufficient for catalysis, which also requires the presence of Ube2V2[142] that binds and orients the acceptor ubiquitin[32,33,101]. Further insight into how Ube2V2 positions the acceptor ubiquitin was gained by analysing a Ube2N~Ub:Ube2V2 complex that I solved at 2.5 Å resolution (**Figure 20**, **Appendix Table 2**). By again invoking crystal symmetry, this structure shows the orientation of an acceptor ubiquitin by Ube2V2, so that its K63 sidechain points towards the active site of Ube2N (**Figure 20b**), an orientation comparable with a structure of yeast Ube2N~Ub:Ube2V2 that was solved in a different crystal lattice[32]. Without a RING present, the donor ubiquitin is not in the closed conformation, and our Ube2N~Ub:Ube2V2 structure thus represents an inactive complex. Alignment to the Ub-R:Ube2N~Ub:Ube2V2 structure (**Figure 20c**, **Appendix Figure 9b-d**) reveals that Ube2N and Ube2V2 are packed more closely against each other, resulting in additional contacts between the acceptor ubiquitin and Ube2N (**Figure 18a**, **Figure 20c**) that position the nucleophile K63 much nearer to the active site (4.8 Å vs. >7.5 Å, **Figure 20c**). This is achieved because Ube2N N123 and D124 contact ubiquitin via the amide of K63 and the sidechains of S57 and Q62, respectively (**Figure 18a**). The ~3-fold reduction in $k_{cat}$ (**Figure 18e**) for the mutants $Ube2N^{N123A}$ and $Ube2N^{D124A}$ suggest that the function of these residues is to fine-tune the ubiquitination reaction by aiding orientation of the nucleophile. Taken together, these features of our structure trapped in the process of ubiquitin chain formation provide mechanistic insight into how the RING E3 promotes catalysis by simultaneously activating Ube2N~Ub discharge and allowing Ube2V2 to precisely orient the acceptor ubiquitin.

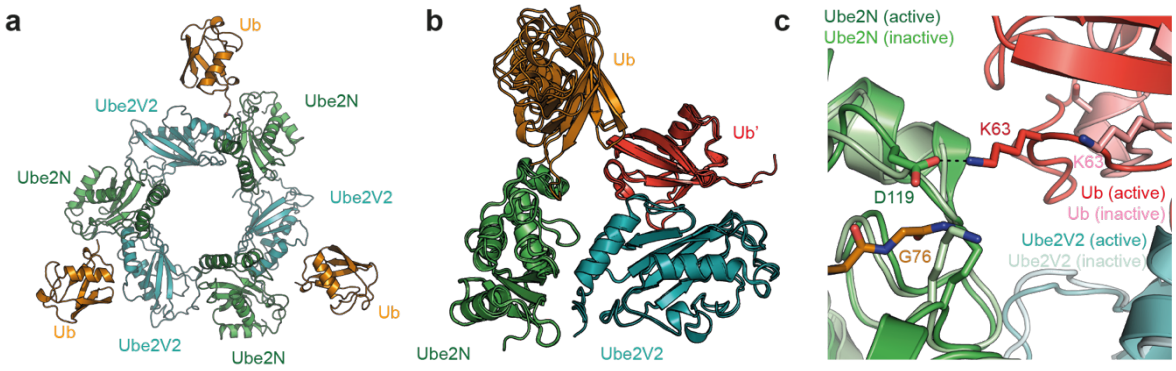


**Figure 20 X-ray structure of Ube2N~Ub:Ube2V2 in an inactive configuration. a** Asymmetric unit of Ube2N~Ub:Ube2V2 (Ube2N, green; Ub, orange; Ube2V2, teal) at 2.5 Å resolution. The three copies of Ube2N~Ub:Ube2V2 are related by translational non-crystallographic symmetry. **b** Overlay of the three copies of Ube2N~Ub:Ube2V2. The acceptor ubiquitin (red and denoted by ') was generated by invoking crystal symmetry. **c** Structure alignment (focussed on Ube2N/Ube2V2) between the structures of Ub-R:Ube2N~Ub:Ube2V2 (referred to as active) and Ube2N~Ub:Ube2V2 (referred to as inactive).

### 4.2.3 The mechanism of RING-anchored ubiquitination

Next, I sought to understand how RING-anchored ubiquitin chains are formed. In the crystal structure, one RING dimer is positioned so as to mediate the elongation of another mono-ubiquitinated RING in *trans* (**Figure 17b,c**, **Figure 21a**). Importantly, this mechanism depends only on binding of the RING-anchored acceptor ubiquitin to Ube2N/Ube2V2, as no contacts with the RING itself could be observed in the crystal structure (**Appendix Figure 6**). The relative topology of the different RING domains (enzyme and substrate) is thus mostly dictated by the catalytic interfaces, resulting in a ~9 nm separation between the enzyme and substrate RINGs (**Figure 21a**). I refer to this arrangement as the catalytic RING topology, in which a RING dimer acts as an enzyme and at least one further RING acts as the substrate for ubiquitination. This topology is not rigid, since the linkers between the acceptor ubiquitin and the RING (~3 nm apart) and the RING and the next (B-box) domain in the TRIM ligase (~3.5 nm apart) likely provide additional flexibility (**Figure 21a,b**, **Appendix Figure 6c**). In the structure it is clear that initiation of TRIM21-anchored chain elongation cannot occur in *cis*, as the priming ubiquitin cannot reach the Ube2N/Ube2V2 binding surface (**Figure 21a**). Consistent with this, I found that TRIM21 ubiquitin transfer in *trans* can occur in principle (**Appendix Figure 10**), in line with previous work on TRIM5α[125].

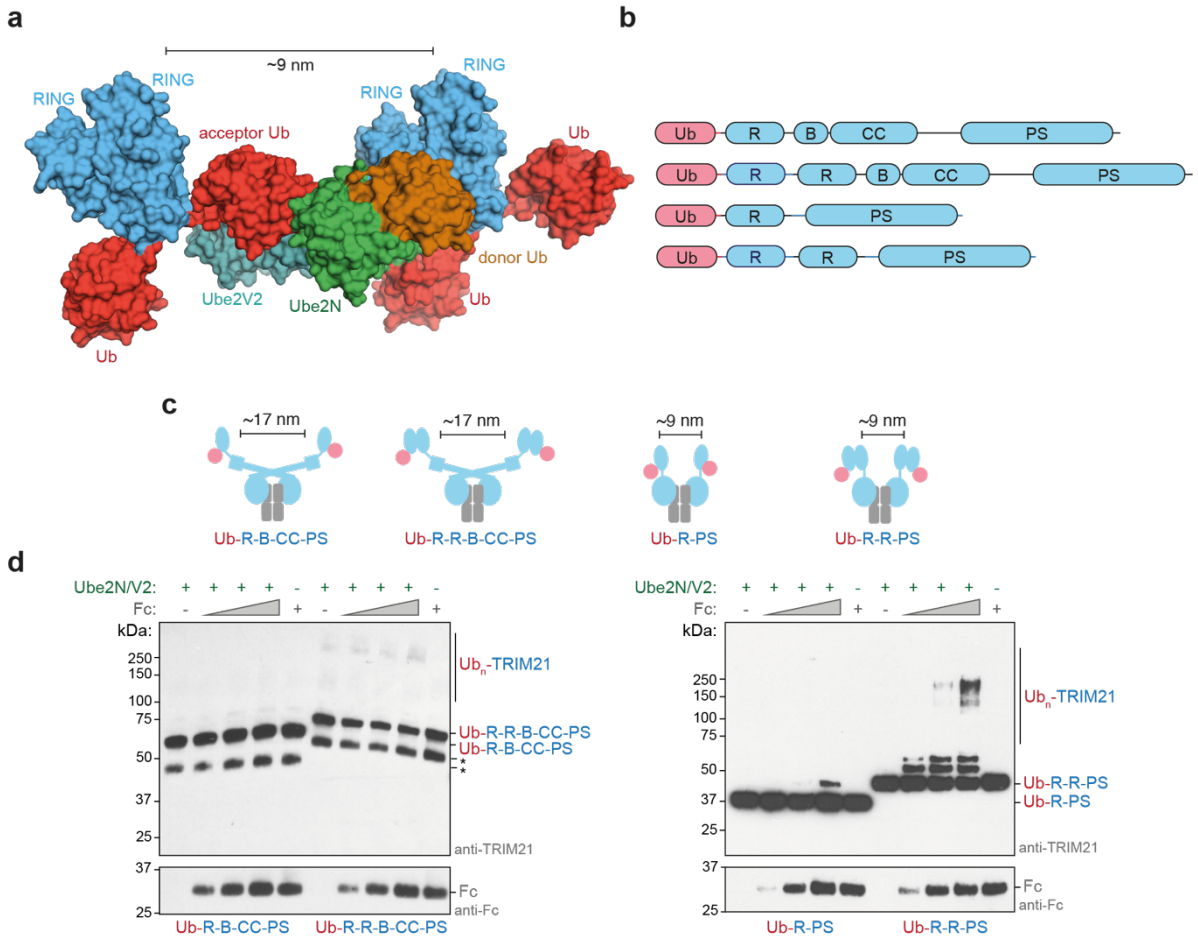


**Figure 21 The mechanism of RING-anchored ubiquitination in *trans*. a** Surface representation of the canonical model of the Ub-R:Ube2N~Ub:Ube2V2 structure (Ub-R, Ub in red, R in blue, Ube2N~Ub, Ube2N in green, Ub in orange, Ube2V2 in teal). **b** Domain architecture of TRIM21 constructs used in biochemical assays. **c** Cartoon models of substrate (Fc, gray) engagement by TRIM21 constructs (blue). The structural basis for these models is shown in **Appendix Figure 11**. **d** Substrate (Fc) induced self-ubiquitination assay of 100 nM Ub-TRIM21 constructs. Reactions were incubated for 5 min at 37 ˚C. Further data can be found in **Appendix Figure 12**. *(asterisk) indicates a TRIM21 degradation product that could not be removed during purification.

To investigate the spatial requirements of TRIM21 RING domains for self-anchored ubiquitination experimentally, I established a substrate-dependent ubiquitination assay. TRIM21 is recruited by Fc, which is an obligate dimer in solution and can be bound by two PRYSPRY (PS) domains[52] (**Appendix Figure 11**). To test for the presence of the catalytic RING topology described above, I designed a series of mono-ubiquitinated TRIM21 constructs that vary the number of RINGs available and their distance to each other when bound to Fc (**Figure 21b**, **Appendix Figure 11**). To suppress background activity, TRIM21 was used at low concentrations (100 or 50 nM) and the reaction was incubated for 5 min only. Full-length TRIM proteins form antiparallel homo-dimers via their coiled-coil domains, resulting in the separation of

the two TRIM21 RING domains by ~17 nm even when bound to Fc (**Appendix Figure 11**). According to the model proposed here, addition of Fc alone should therefore not induce the catalytic RING topology (**Figure 21c**). Consistent with this, addition of Fc did not stimulate ubiquitination of the full-length Ub-TRIM21 (Ub-RING-Box-coiled-coil-PRYSPRY or Ub-R-B-CC-PS, **Figure 21d**). Even when adding an additional RING domain to make the full-length protein a constitutive RING dimer (Ub-R-R-B-CC-PS), formation of the catalytic RING topology is excluded (**Figure 21c**) and no induction of self-ubiquitination was observed upon addition of Fc (**Figure 21d**, **Appendix Figure 12**). As a next step, I designed TRIM21 constructs lacking the B-box and coiled-coil (Ub-R-PS and Ub-R-R-PS). Fc is capable of recruiting two of these constructs, thereby locating their RINGs within ~9 nm of one another (**Figure 21c**, **Appendix Figure 11**), the distance required for the catalytic RING topology (**Figure 21a,c**). Addition of Fc to Ub-R-PS led to weak self-ubiquitination. This low level of activity likely occurs because Ub-R-PS can only provide a monomeric RING as the enzyme, while a monomeric RING on the second Ub-R-PS acts as the substrate. TRIM RING dimerization is known to greatly increase ligase activity[80,84,85,90]. Therefore these experiments were repeated using a Ub-R-R-PS construct. The prediction was that this should allow the catalytic RING topology observed in the crystal structure to form upon substrate binding, as in this case the Fc will bring two RING dimers into close proximity (**Figure 21a,c**), rather than just two monomers as before. Indeed, addition of Fc to Ub-R-R-PS resulted in efficient formation of TRIM21-anchored ubiquitin chains (**Figure 21d**). Importantly, while anchored ubiquitination occurred very efficiently, hardly any free ubiquitin chains could be observed (**Appendix Figure 12c**). Since self-ubiquitination only requires E2~Ub to be recruited by the ligase, this explains its high efficiency relative to free ubiquitin chain formation, as the latter would require recruitment of both E2~Ub and (poly-) ubiquitin. Indeed, Ub-R-R-PS worked efficiently in our substrate-induced ubiquitination assay even at reduced TRIM21 concentrations (**Appendix Figure 12d**). Thus, inducing formation of the catalytic RING topology by substrate binding enables robust and selective formation of self-anchored ubiquitin chains. Moreover, the catalytic RING topology is only achieved when the separate requirements of an active enzyme (a dimeric RING) and a correctly positioned substrate (a third RING) are fulfilled.

I next considered how long a TRIM21-anchored ubiquitin chain would have to be for *cis* ubiquitination to become sterically possible. Using the Ub-R:Ube2N~Ub:Ube2V2 structure, models were created with increasing numbers of K63-linked ubiquitin chains conjugated to the TRIM21 RING domain. These models suggested that a chain of four ubiquitin molecules would be necessary and sufficient for self-ubiquitination in *cis* (**Figure 22a**, **Appendix Figure 13**). Thus, after addition of the priming ubiquitin, three ubiquitin molecules must be added in *trans*, before the chain could be further elongated in *cis*. Consistent with this, I only observed very long TRIM21-anchored ubiquitin chains or species carrying one, two or three ubiquitin molecules in the Fc-dependent TRIM21 ubiquitination experiments (**Figure 21d**, **Appendix Figure 12c,d**). With the addition of a fourth ubiquitin, the reaction appears to progress much more quickly, as would be expected for a switch from *trans* to *cis*, rapidly consuming the tetra-ubiquitin species and converting it into a long chain. In the above experiments, self-ubiquitination only occurred when two Ub-R-R-PS constructs were co-localized by their binding to Fc to satisfy the requirements of the catalytic RING topology (**Figure 21c,d**). To confirm the switch in self-ubiquitination from *trans* to *cis* experimentally, TRIM21 R-R-PS constructs were generated in which their N-termini were fused to up to four linearly (M1) connected ubiquitin molecules. Due to their high structural similarity[149], it was assumed a linear chain would mimic a K63-linked ubiquitin chain in length and flexibility sufficiently well for the purpose of this experiment. Upon testing these new constructs, it was observed that only TRIM21 modified with tetra-ubiquitin became independent of Fc for self-ubiquitination (**Figure 22b**); all the other, shorter, constructs remained rate-limited by first having to self-ubiquitinate in *trans*, before switching to *cis*. This biochemical data is in full agreement with both the structure, which shows the initiation of RING-anchored ubiquitination in *trans*, and my model of polyubiquitinated RING elongation occurring in *cis*.

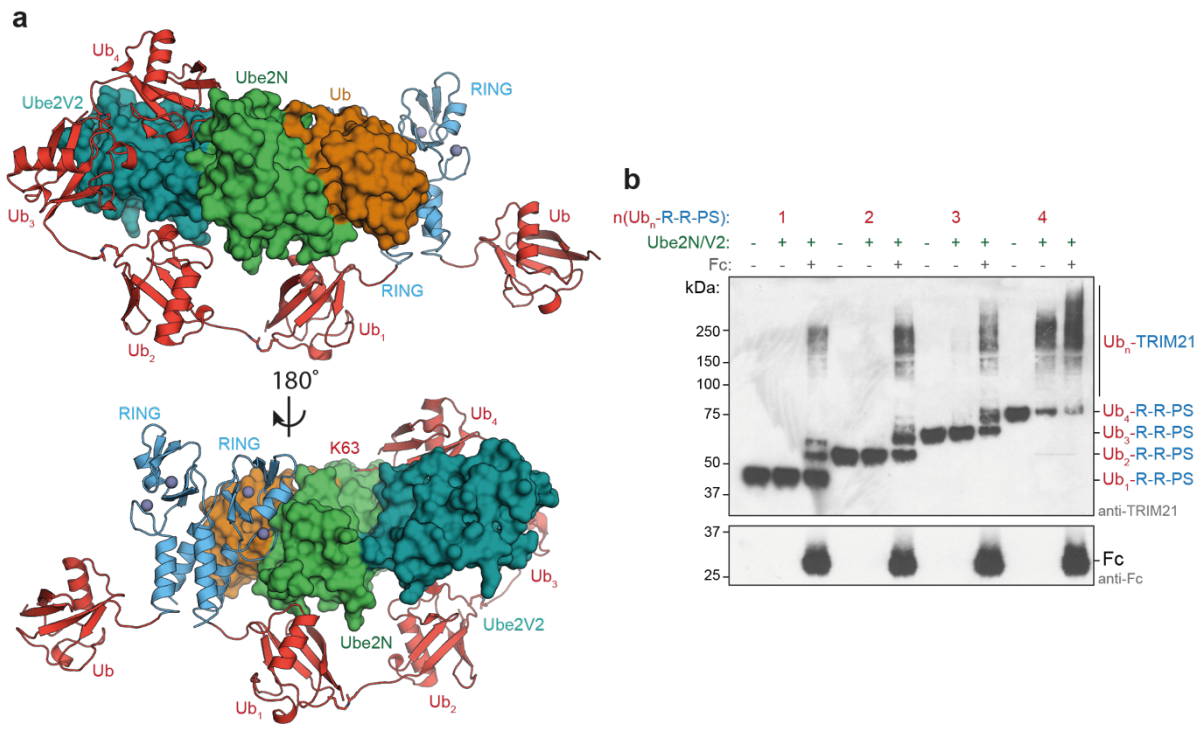


**Figure 22 The mechanism of RING-anchored ubiquitination in *cis*.** **a** For ubiquitination in *cis*, the RING-anchored (blue) ubiquitin chain (red) must be sufficiently long to reach the active site on Ube2N~Ub:Ube2V2 (Ube2N in green, Ub in orange, Ube2V2 in teal). The chain can follow two different routes, one shown here and the other in **Appendix Figure 13**. The ubiquitin chain was modelled using the Ub-R:Ube2N~Ub:Ube2V2 structure and a K63-linked $Ub_2$ structure (2JF5[149]) using PyMol. **b** Substrate (Fc) induced self-ubiquitination assay of 100 nM $Ub_n$-TRIM21 constructs (see text for interpretations). Reactions were incubated for 5 min at 37 ˚C.

Finally, I considered whether the catalytic RING topology is an arrangement specific to Ube2N or one that also works with other E2 enzymes. Thus, I tested whether addition of Fc could induce self-ubiquitination of Ub-TRIM21 in presence of Ube2D1, a highly promiscuous E2 enzyme. However, even after extended reaction times, hardly any TRIM21 modification was detected, while in contrast free ubiquitin chains could be observed (**Figure 23**). The catalytic RING topology I observe in my structure is thus specific for Ube2N/Ube2V2, explaining why this enzyme[28] and not Ube2D1 is required for TRIM21's cellular function[113]. Moreover, this may also explain why TRIM21, and other TRIMs such as TRIM5α, build K63- and not K48-linked ubiquitin chains when first activated. Their mechanism of activation, induction of the catalytic RING topology, only results in formation of self-anchored K63 chains by using Ube2N/Ube2V2. Collectively, these data identify formation of a catalytic *trans* RING topology as the driving force behind self-ubiquitination of TRIM21 with Ube2N/Ube2V2.

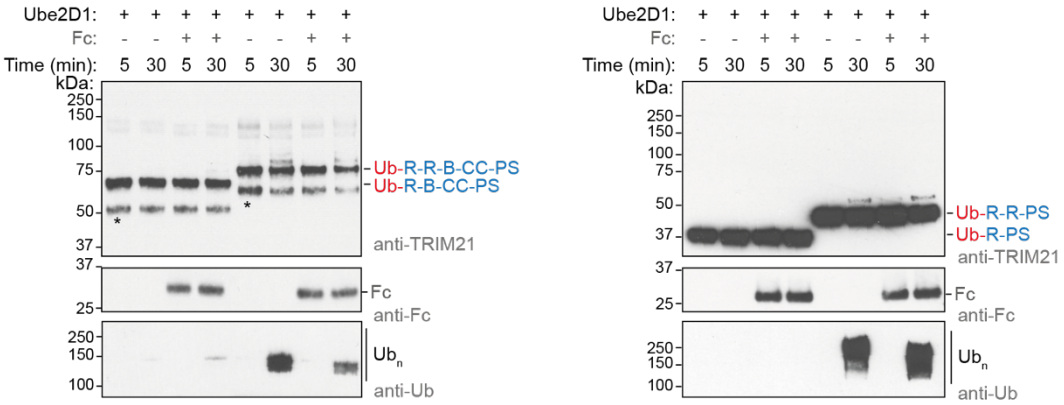


**Figure 23 Ube2D1 cannot mediate TRIM21 ubiquitination via the catalytic RING topology.** Fc-induced self-ubiquitination assay of 100 nM Ub-TRIM21 in the presence of 0.5 µM Ube2D1.

### 4.2.4 Catalytic RING topology drives targeted protein degradation

Having established the RING topology necessary for self-anchored ubiquitination in vitro, I next investigated if this same arrangement is required for TRIM21 activity in cells. I designed a similar series of TRIM21 constructs for cellular expression as above, which control for the number of RINGs available and their distance to each other when bound to Fc (**Figure 24a**). These constructs were expressed in *TRIM21* knock out RPE-1 cells together with GFP-tagged Fc, and GFP-Fc degradation was monitored as a readout for TRIM21 activity in a targeted protein degradation experiment. Consistent with the inability to form anchored chains when engaged with Fc in vitro, full-length TRIM21 did not degrade GFP-Fc in cells (**Figure 24b,c**). Degradation could not be rescued by addition of another RING to the N-terminus, presumably because in this case the RINGs are dimeric but still separated by the coiled coil, with the consequence that no 'substrate' RING is available for ubiquitination. Thus, while being necessary, RING dimerization is not sufficient for cellular TRIM21 activity. In the R-PS construct, the RINGs are within ~9 nm, and thus within the range compatible with activity as defined by the crystal structure (**Figure 21a**). Despite this, no degradation was observed (**Figure 24b,c**), likely because the RINGs can either form a single dimer, or one monomer RING would have to act as the enzyme and the other RING as the substrate. This is consistent with the inefficient self-ubiquitination of a comparable construct in the biochemical experiments (**Figure 21d**). Only R-R-PS showed efficient GFP-Fc degradation (**Figure 24b,c**). When this construct engages Fc, two RING dimers can form in close proximity, so that one RING

dimer is available to mediate the ubiquitination of the other, thus fully satisfying the requirements of the catalytic RING topology.

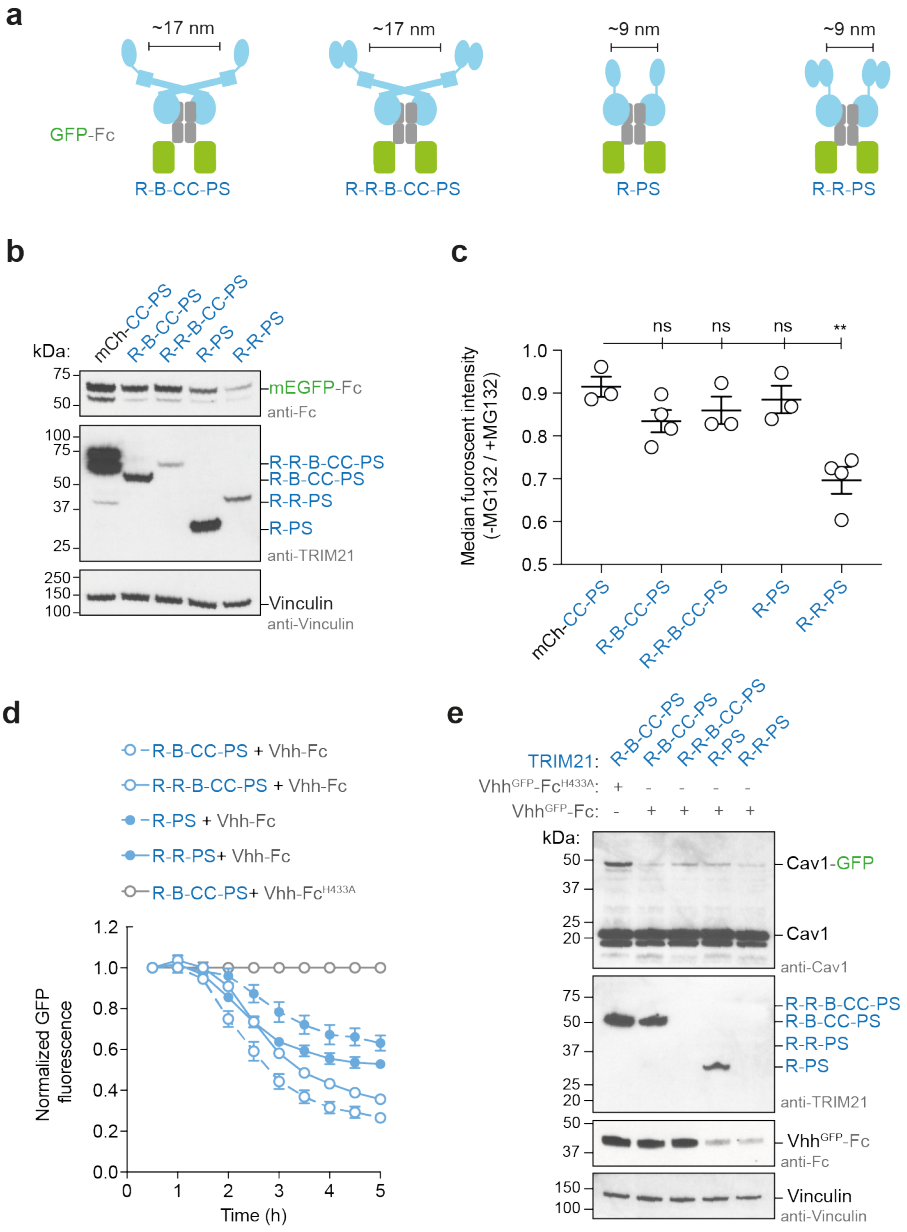


**Figure 24 Catalytic RING topology drives targeted protein degradation.** **a** Schematic cartoons showing the topology of TRIM21 (blue) on GFP-Fc (green and gray, respectively). **b**, **c** GFP-Fc degradation assay. **b** Western blot of RPE-1 *TRIM21*-knock-out cells transiently express GFP-Fc and a series of TRIM21 constructs. **c** Shown is the flow cytometry analysis of green fluorescence of RPE-1 *TRIM21*-knock-out cells transiently expressing GFP-Fc and a series of TRIM21 constructs. After electroporation, each population of cells was split in two and either treated with MG132 or DMSO. Data are presented as mean ± standard error of the mean. Each data point on the graph represents one biologically independently performed experiment. A two-tailed unpaired student T test was performed to assess the significance of fluorescence reduction relative to mCh-CC-PRYSPRY (P values: R-B-CC-PRYSPRY, 0.0797 (ns); R-R-B-CC-PRYSPRY, 0.02366 (ns); R-PRYSPRY, 0.4964 (ns); R-R-PRYSPRY, 0.0035 (**)). **d**, **e** Trim-Away of Caveolin-1-mEGFP (Cav1-GFP) in NIH 3T3 *GFP-Cav-1*-knock in cells[123]. Shown in **d** is the normalized GFP fluorescence (error bars represent ± SEM of 4

images) and in **e** the western blot after the experiment. R, RING; B, Box; CC, coiled-coil; PS, PRYSPRY; mCh, mCherry; kDa, kilo Dalton; ns, not significant

All the constructs were expressed at comparable levels and were active in classical Trim-Away targeted protein degradation assays (**Figure 24d,e**, **Appendix Figure 14**), suggesting that, as intended, the only difference is the number and relative distance of RING domains when engaged with the GFP-Fc construct. This also agrees with the biochemical data, where a similar construct shows strong self-ubiquitination upon substrate binding (**Figure 21d**). Therefore, the Fc-induced self-ubiquitination assay in vitro provides a good prediction for cellular activity. The crystal structure of the initiation of RING-anchored ubiquitin chain elongation thus precisely visualizes how this process can work in a physiological context.

### 4.2.5 Improved Trim-Away using optimized TRIM21 constructs

Having established TRIM21's requirement to form the catalytic RING topology, it was next wondered how these new insights might be used to improve targeted protein degradation by Trim-Away. Generally, a successful Trim-Away experiment requires a good antibody, sufficient TRIM21 in the cell and an oligomeric substrate[62,91,150]. Many antibodies can be purchased off the shelf, or, alternatively and more tediously, can be produced in the lab. If cells do not express sufficient TRIM21, this can be compensated by co-electroporating either DNA or RNA encoding TRIM21, or TRIM21 protein[62]. However, full-length TRIM21 is difficult to express and purification does not result in a homogenous product (**Figure 25a**). Fusion of the TRIM21 RING with a GFP-nanobody overcomes issues with purification, but is only suitable for use in experiments with degradation of GFP-fusion proteins[150]. Finally, the oligomeric nature of the substrate is a limiting factor, when using native TRIM21[150]. The TRIM21 R-PS and R-R-PS constructs introduced above were able to perform rapid Trim-Away when being expressed from mRNA (**Figure 24d,e**). Moreover, degradation of GFP-Fc by R-R-PS suggest that this construct – in contrast to native TRIM21 – is able to degrade monomeric target proteins, due to its ability to enforce the catalytic RING topology (**Figure 24b,c**). Therefore, these TRIM21 constructs might overcome some of the limitations associated with full-length TRIM21 and Trim-Away in general.

Expression and purification of R-PS or R-R-PS is technically less demanding than is that of full-length TRIM21, and results in good yields and high purity (**Figure 25b**).

These constructs also show higher activity in ubiquitination (**Figure 25c**), which is largely due the dimerization state of the RING and the lack of B-box inhibition. The TRIM21 constructs designed to test for the catalytic RING topology all actively degraded Cav1-GFP when transiently expressed (**Figure 24d,e**). All transiently expressed TRIM21 constructs except R-PS showed efficient cellular depletion of IKKα (**Figure 25d**). The lack of R-PS activity may be because loss of the coiled-coil domain reduces the ability of this construct to promote formation of the catalytic RING topology, due to a reduced search radius for the RING domains. While R-PS did not degrade IKKα and performed less well in degradation of Cav1-GFP, R-R-PS appeared to be the superior candidate. I therefore tested whether purified R-R-PS could induce degradation of endogenous Erk1 in RPE-1 *TRIM21* knock-out cells. R-R-PS showed strong Erk1 depletion within one hour, while endogenous TRIM21 in WT cells required longer for depletion (**Figure 25e**). One of the major limitations of Trim-Away is the need for oligomeric substrates[150]. However, R-R-PS also showed degradation of monomeric GFP (**Figure 25f**), due to enforcing the catalytic RING topology on the antibody. Moreover, TRIM21 R-PS and R-R-PS also showed improved Trim-Away in *Xenopus laevis* extracts, as tested by our collaborators in the Meyer lab in Konstanz (unpublished data by Rebecca Demmig and Thomas Meyer). Thus, by illuminating TRIM21's mechanism of self-ubiquitination, a novel TRIM21 construct with improved degradation kinetics, target depth and applicability was revealed.

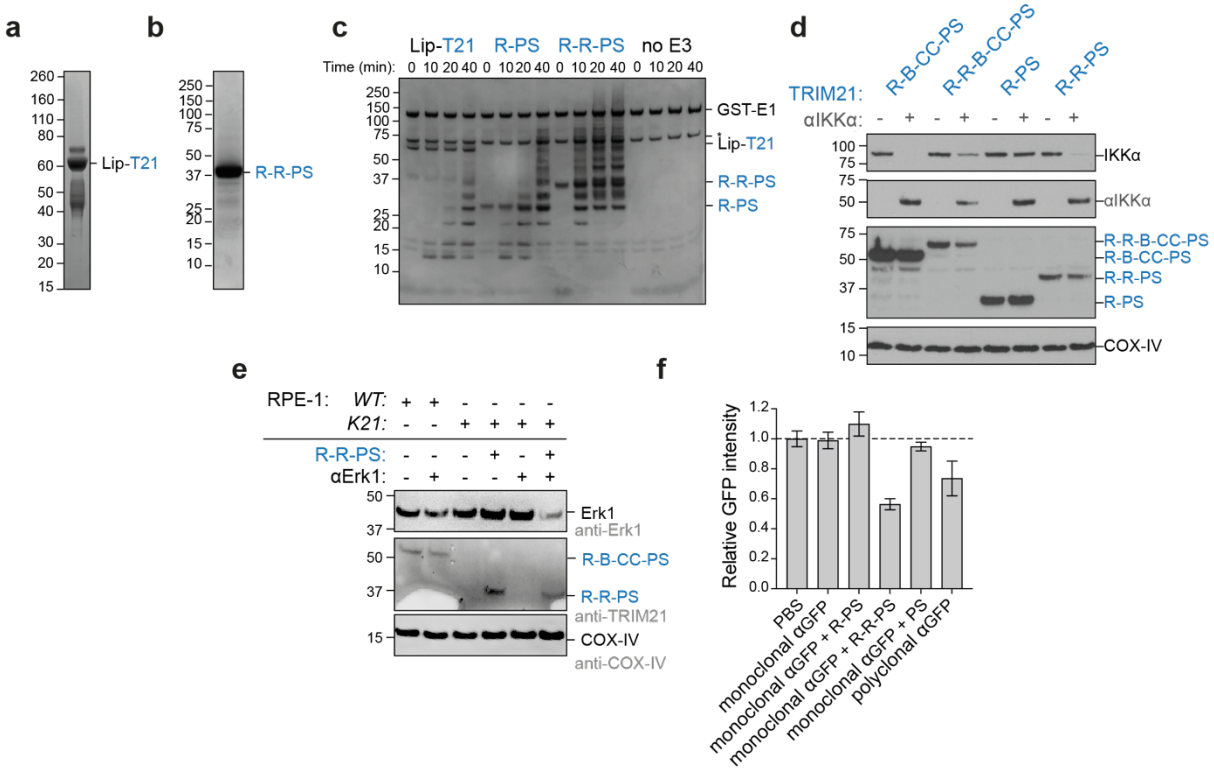


**Figure 25 Novel TRIM21 constructs for improved targeted protein degradation. a** InstantBlue-stained gel of purified Lipoyl-TRIM21 including impurities. This gel was reproduced with permission of the authors[91]. **b** InstantBlue-stained gel of TRIM21 R-R-PS. **c** Catalysis of unanchored ubiquitin chains by Ube2N/Ube2V2 of different TRIM21 constructs at 10 µM concentration. Shown is an InstantBlue gel of the reactions after 60 min. **d** Trim-Away of endogenous IKKα in RPE1 *TRIM21* knock-out cells using transiently expressed TRIM21 constructs. **e** Trim-Away of endogenous Erk1 kinase in either RPE1 WT or *TRIM21* knock-out cells using R-R-PS protein at 2.4 µM and anti-GFP antibody at 0.5 µM concentration in the electroporation reaction. Endogenous TRIM21 in RPE-1 cells would usually take 3-4 h for efficient Trim-Away of Erk1. **f** Trim-away of ectopically expressed monomeric EGFP in RPE1 cells using mono- or poly-clonal antibody against GFP (0.5 µM) and different TRIM21 constructs (2.4 µM). Shown is the relative GFP intensity after 4.5 h. Experimental data shown in panel **f** was performed by Dr Dean Clift.

# 4.3 Discussion

Protein-ubiquitination is one of the most abundant post-translational modifications, affecting essentially all cellular events. A precise understanding of its underlying mechanisms, and how selectivity is achieved, is desirable for several reasons. First, malfunction in the ubiquitin system often manifests in severe disease[14]. Second, the use of small molecules (PROTACs, molecular glues, etc.) has emerged as a promising new approach for targeted degradation of disease-causing proteins in patients[37,38,40,44-46]. Despite recent advances in the field, it remains unclear how RING E3 ligases achieve specific substrate ubiquitination and how a particular ubiquitin chain extension is formed after the priming ubiquitin has been transferred.

Here I provide a structural framework for understanding RING E3-anchored ubiquitin chain formation. I was able to capture a snapshot of this process in a crystal structure of mono-ubiquitinated TRIM21 RING (Ub-R) with the ubiquitin charged heterodimeric E2 enzyme Ube2N~Ub/Ube2V2 (**Figure 17**), showing the chemical activation of the acceptor ubiquitin, exemplified by the deprotonation of the acceptor lysine by Ube2N D119 (**Figure 18**). Most importantly, this structure reveals the domain arrangement required for the elongation reaction, in other words a catalytic RING E3 topology that enables the extension of a mono-ubiquitinated RING into a K63-linked, RING-anchored ubiquitin chain (**Figure 21**, **Figure 22**). In this arrangement, two RINGs form a dimer and act as an enzyme on a third RING domain, which is the substrate in this reaction. While rigidity is required to position all the important catalytic residues in the E2 active site optimally (**Figure 18**, **Appendix Figure 6**), formation of the substrate anchored ubiquitin chain likely requires conformational flexibility between domains that is provided by the unique topology of TRIM proteins (**Figure 21**). Substrate-induced self-ubiquitination of TRIM21 is highly efficient, even at low ligase concentration, in contrast to free-ubiquitin chain formation (**Figure 21**, **Appendix Figure 12**). This implies that physiological ubiquitin signals may not be produced as free chains but mainly on substrates, due to the higher reaction efficiency.

These data establish that the RING-anchored K63-chain is first formed in a *trans*-mechanism, where a RING dimer activates a Ube2N~Ub molecule, thereby acting as an E3 ligase. An additional mono-ubiquitinated RING acts as a substrate for ubiquitination and accepts the donor ubiquitin (**Figure 21**). Only after four ubiquitin molecules have been added to the RING in *trans*, is the chain sufficiently long for ubiquitin chain formation in *cis* (**Figure 22**). While ubiquitin chain elongation in *cis* occurs at much higher rates, the initial need for a *trans* arrangement may represent an important regulatory mechanism, suppressing activity in the absence of a target that recruits multiple TRIM21 molecules and causes the clustering necessary to generate the catalytic RING topology. Interestingly, substrate modification with linear ubiquitin chains by the RBR ligase HOIP is regulated by its partner RBR HOIL, which mono-ubiquitinates all three LUBAC components HOIP, HOIL and SHARPIN. These ubiquitin primers are then elongated in *cis* by HOIP, thereby outcompeting *trans*

ubiquitination of substrates[151]. Thus, switching between *cis* and *trans* mechanisms of ubiquitination may be a regulatory system exploited by many different types of E3 ligases.

The catalytic RING topology observed in the Ub-R:Ube2N~Ub:Ube2V2 structure predicts the requirements for TRIM21-mediated targeted protein degradation in cells (**Figure 24**). Upon substrate recognition, TRIM21 forms a K63-linked ubiquitin chain on its N-terminus[27]. Loss of this K63-linked ubiquitin chain prevents virus neutralization, immune signalling and Trim-Away[113]. The GFP-Fc degradation experiment shows that only the TRIM21 construct (R-R-PS), which can form the catalytic RING topology under these conditions, enables degradation (**Figure 24**). Interestingly, specific orientation of the E3 ligase $CRL^{VHL}$ relative to its substrate was also shown to be critical for targeted protein degradation[152]. Nevertheless, how the presence of a RING-anchored K63-chain leads to degradation of the RING and its bound substrate remains mysterious. A mechanism could be envisioned whereby this chain provides the scaffold for a branching event that allows the synthesis of degradation-competent K48-linked ubiquitin chains. Indeed, TRIM21 can be modified with both K63- and K48-linked ubiquitin chains and K48 chain formation is dependent upon, and occurs subsequent to, K63-ubiquitination[27]. Degradation of the proapoptotic regulator TXNIP for instance was shown to be mediated by K48-chains that were assembled on substrate-bound K63-chains[153]. Such K63-K48-branched ubiquitin chains have also been shown to amplify NF-κB signals[154]. A strategy of mixed, branched chains might be essential for TRIM21 to act as both an immune sensor and effector[27].

The catalytic RING topology described here is consistent with data showing that TRIM proteins can undergo higher-order assembly. In the case of TRIM5α[126], three TRIM5α RINGs are brought into close proximity when the protein is incubated with the HIV capsid[87,126,155] (**Figure 26a,b**, **Appendix Figure 15**). This positioning would fulfil the catalytic RING topology here described here, and would be consistent with the ability of TRIM5α to restrict retroviruses[156,157] and activate the innate immune response via self-anchored K63-ubiquitination[124,158]. The functional requirement for multiple TRIM molecules is also suggested by the fact that potent antibody-mediated neutralization of adenovirus by TRIM21 requires multiple antibodies bound per virus[82]. In addition,

TRIM21 was shown to be activated by substrate-induced clustering, resulting in multiple TRIM21:antibody complexes on the substrate[150]. The unique TRIM-architecture, in which the RINGs are located at either end of a coiled-coil, and the flexibility provided by the hinge region of the antibody, may be crucial in enabling TRIM21 molecules bound onto the surface of a virus to engage with each other (**Figure 26c**). To fulfil the catalytic RING topology on the virus, two RINGs need to dimerize and a third has to be within ~9 nm of the RING dimer, enabling self-anchored ubiquitination and subsequent virus neutralization (**Figure 26d**). Importantly, with this new knowledge, novel TRIM21 degrader constructs such as R-R-PS can be designed that show improved behaviour and increase the applicability of Trim-Away (**Figure 25**). Since higher-order assembly has been associated with many other K63 ubiquitin chain forming RING E3 ligases, such as TRAF6[159], RIPLET[160] and others, I propose that the mechanism presented here is thus likely to be found more widely within the realm of RING E3 ligases.

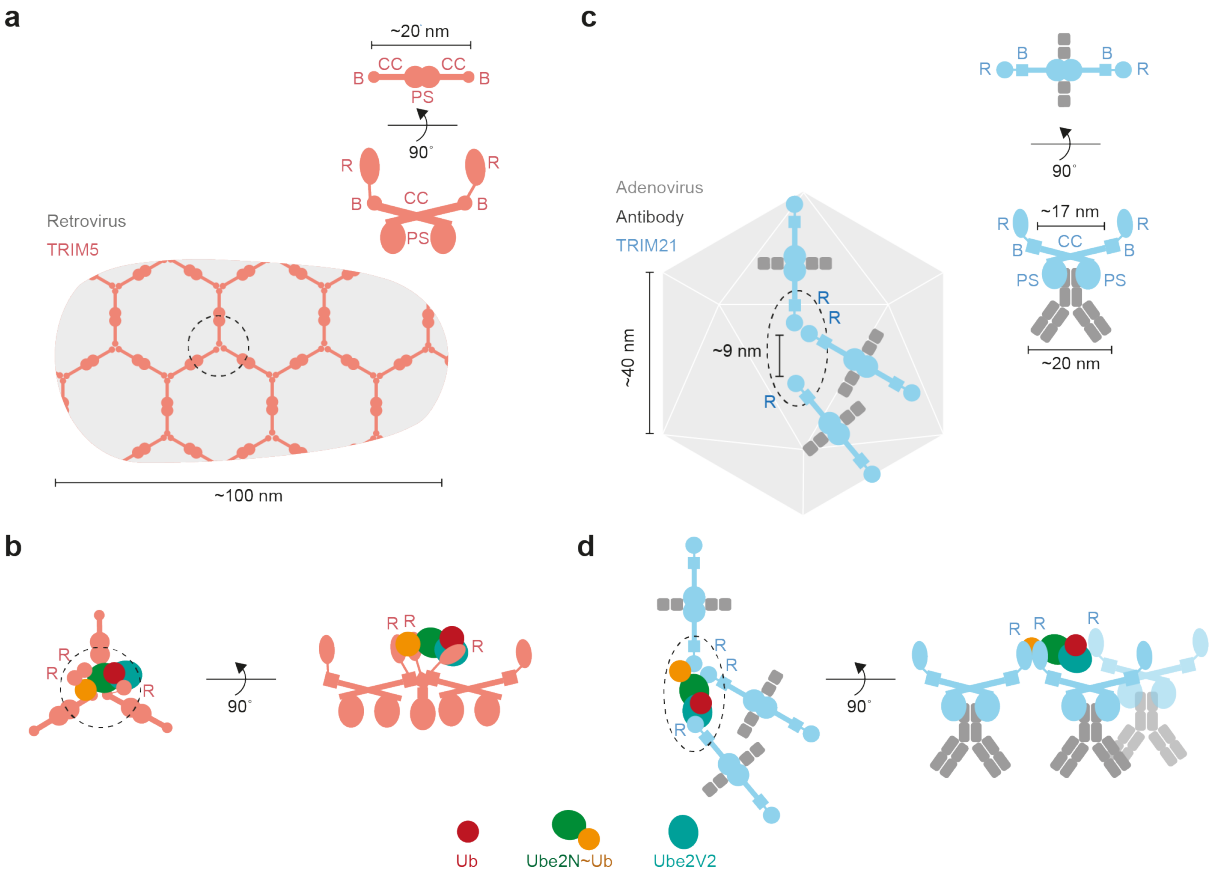


**Figure 26 TRIM protein assembly on viruses.** Cartoon models of the assembly of TRIM5α (**a**, **b**) and TRIM21 (**c**, **d**) on viral capsids. **a** Shown is the hexagonal assembly of TRIM5α on HIV-1 capsid as

imaged by cryo-electron tomography[155]. **c** Assembly of TRIM21:antibody complexes on adenovirus capsid (adenoviral measurements are based on 6B1T[161]). **b**, **d** Cartoons visualizing how the TRIM protein assembly on the viral capsid enables formation of the catalytic RING topology.

# Chapter 5 TRIM21 N-ubiquitination by Ube2W

## 5.1 Introduction

The antiviral restriction factors TRIM21 and TRIM5α both act by recognizing the capsid of an invading pathogen, either directly in the case of TRIM5α, or indirectly using antibodies as intermediaries in the case of TRIM21. Both are thought to recruit the same subset of E2 enzymes to form self-anchored K63-linked ubiquitin chains. In short, Ube2W is thought to mono-ubiquitinate the TRIM RING at the N-terminus, followed by rapid elongation with Ube2N/Ube2V2[27,28,124,158] (**Figure 27a**). By using mutants of the tri-ionic motif in TRIM21 that specifically ablate catalysis with Ube2N, it became clear than TRIM21 and Ube2N do indeed interact directly inside cells and that forming K63-linked ubiquitin chains is required for TRIM21's antiviral function (Chapter 3)[113]. Moreover, TRIM21 K63 self-ubiquitination was significantly reduced upon mutation of the tri-ionic motif[150]. Ube2W knockdown in cells inhibits TRIM21-mediated virus neutralization and immune signalling and Ube2W mono-ubiquitinated the TRIM21 N-terminus in biochemical assays[27]. However, whether TRIM21 and Ube2W actually interact in cells – and with what outcome – remains elusive.

Ube2W is the only E2 enzyme able to target protein N-termini for ubiquitination[4,5], making it an efficient initiator E2 for many RING E3s[29]. However, its mechanism of action remains unknown. Ube2W appears to target disordered protein N-termini, an activity that requires Ube2W's disordered C-terminus[117]. Ube2W is also known to form a weak homo-dimer, yet this dimerization was reported as not being important for ubiquitination[162]. Generally, the abundance of N-terminally ubiquitinated (or N-ubiquitinated) proteins inside cells is very low, and only a few target proteins were identified in a Ube2W-overexpression model[163]. How Ube2W is recruited by RING E3s and its catalytic mechanism remains largely unknown.

### 5.1.1 Aims

With Ube2W having evaded detailed study in the past, the work described in this chapter was intended to reveal whether the interactions of TRIM21 and Ube2W seen in vitro would actually occur inside cells. In addition, I sought to understand the mechanism of TRIM21 N-ubiquitination and Ube2W action in general. To tackle these objectives, a cellular biochemistry approach was combined with structural methods.

## 5.2 Results

### 5.2.1 Ube2W ubiquitinates TRIM21's N-terminus inside cells

Despite the in vitro evidence presented above, whether TRIM21 and Ube2W actually interact inside cells remains to be established. In the case of TRIM5α, an antiserum against N-ubiquitinated TRIM5α revealed that this modification does indeed occur inside cells[125]. However, such a serum could not be generated for TRIM21. Instead, I designed a new experiment to test for this modification. The basis for this experiment is that TRIM21 can be electroporated into cells alongside antibodies, as has been shown during Trim-Away[62,91]. Delivery of a TRIM21 construct with a blocked N-terminus, should block any effect N-ubiquitination via Ube2W could have (**Figure 27b**). I decided to block the N-terminus biochemically by N-acetylation – an irreversible modification that occurs inside cells. N-acetylation is performed by N-Acetyl Transferases (NATs) using the co-factor Acetyl-CoA[164]. NATs are highly sequence specific and thus a NAT with a sequence specificity for the TRIM21 N-terminus was required. The *Chaetomium thermophilum* NAT Naa50 (referred to as NAT from here on) was shown to possess high activity for such N-termini (unpublished results by Jonas Weidenhausen & Irmgard Sinning) and was provided by our collaborators from the Sinning lab in Heidelberg. While full-length TRIM21 is notoriously difficult to work with, I instead used the R-PS and R-R-PS constructs as these were shown to possess high activity both in vitro and in cells (Chapter 5)[165].

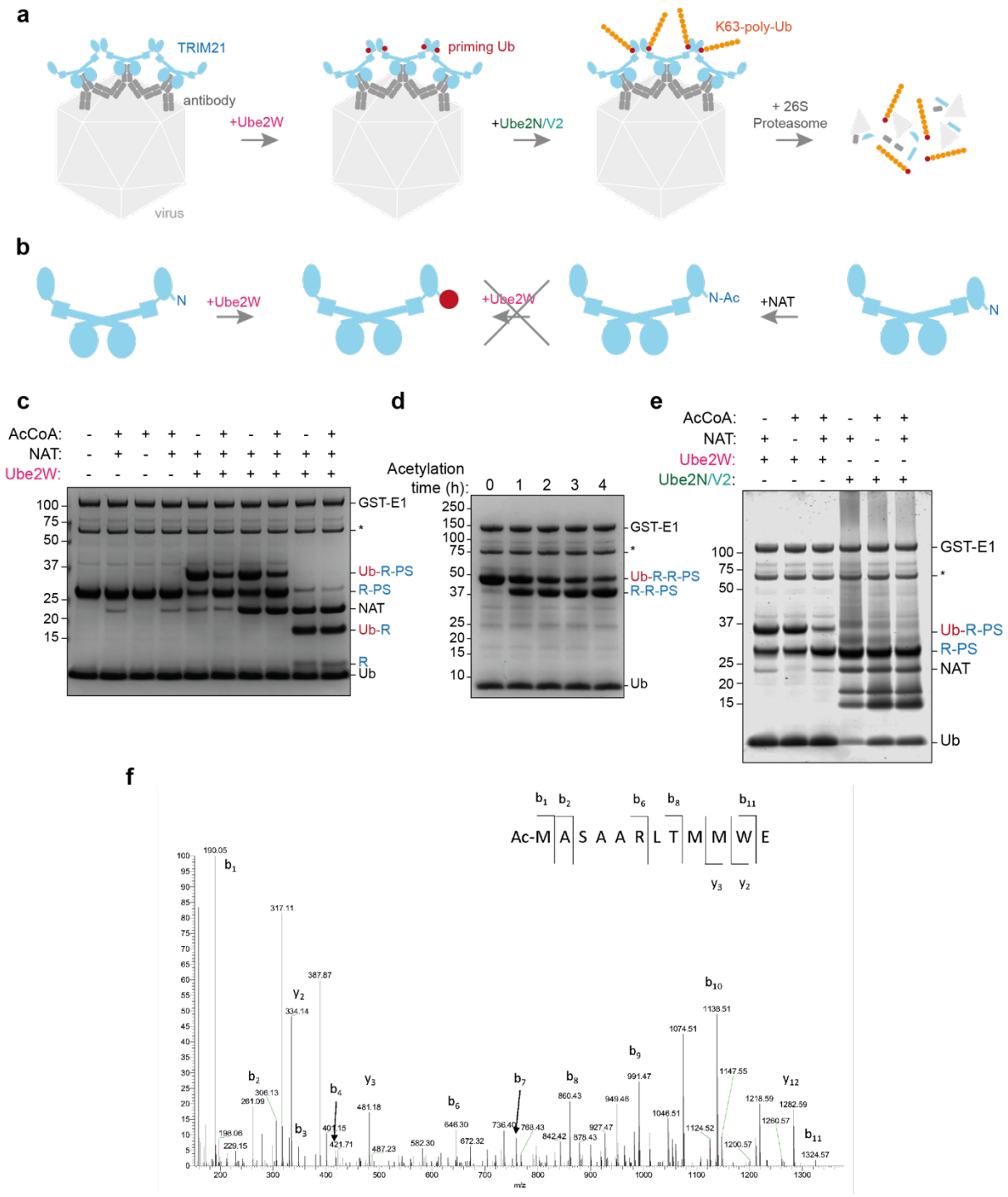


**Figure 27 TRIM21 N-acetylation blocks Ube2W-mediated N-ubiquitination in vitro. a** Cartoon depiction of a TRIM21- and antibody-coated Adenovirus and the ubiquitination events thought to occur inside cells. Ube2W is recruited to mono-ubiquitinate TRIM21, followed by extension into a K63-linked ubiquitin chain upon interaction with Ube2N/V2. These ubiquitination events result in degradation of the full complex and activation of the immune response. **b** Schematic depiction of TRIM21 N-ubiquitination by Ube2W and of TRIM21 N-acetylation by an N-Acetyl Transferase (NAT) resulting in a blocked N-terminus. **c**, **d**, **e** Shown are Instant-Blue-stained gels showing Ube2W-mediated TRIM21 mono-ubiquitination reactions. Before the ubiquitination reaction, acetylation reactions were performed (**c**, **e** for 4 h and the indicated length in **d**). **f** LC-MS/MS spectra of TRIM21 R-R-PS after 4 h acetylation

reaction show N-acetylated TRIM21 N-terminal peptides after digestion with the protease N-Asp. MS experiments presented in panel **f** were performed by Sarah S Maslen.

To test whether NAT could N-acetylate TRIM21, an acetylation reaction was performed using TRIM21, NAT and AcetylCoA. Next, this reaction mix was added into a Ube2W mono-ubiquitination reaction, to indirectly monitor blocked TRIM21 N-termini by competitive inhibition of N-ubiquitination. Indeed, acetylation reactions that contained all components showed reduced TRIM21 mono-ubiquitination both for R-PS and R-R-PS (**Figure 27c,d**). N-acetylation was highly sequence specific, as a T21-R construct that carries an additional N-terminal GSH scar was not N-acetylated (**Figure 27c**). Importantly, formation of free K63-linked ubiquitin chains was not compromised by acetylation reactions (**Figure 27e**). Finally, N-acetylation of TRIM21 could be detected via LC-MS/MS (**Figure 27f**). Thus, TRIM21's N-terminus can be blocked by acetylation, resulting in inhibition of TRIM21 N-ubiquitination by Ube2W in vitro.

The next step was to deliver this protein into cells to observe its behaviour in its natural environment. The R-R-PS construct showed reasonable levels of N-acetylation in vitro (**Figure 27d**) and was well behaved inside cells (Chapter 4, **Figure 24**)[165]. This construct is a hyperactive E3 ligase (**Figure 25c**)[165] as the two main inhibitory TRIM21 mechanisms – B-box-inhibition[80] and separations of the RINGs[79,150,165] – are not present. Inside cells, R-R-PS therefore turns itself over, which is dependent on the ubiquitin proteasome system (Chapter 4)[165]. I therefore carried out biochemical acetylation reactions with R-R-PS (**Figure 28a**). The reaction mixture was then split in two; one part was added into a Ube2W mono-ubiquitination reaction to indirectly validate the success of the N-acetylation reaction (**Figure 28b**), while the other part of the reaction was delivered into RPE-1 *TRIM21*-knock-out cells that were either treated with the proteasome inhibitor epoxomicin or DMSO. Non-acetylated TRIM21 quickly turned itself over in cells without inhibited proteasomes (**Figure 28c**). In contrast, N-acetylated TRIM21, which cannot be N-ubiquitinated by Ube2W, was stabilized. This data strongly suggests that Ube2W-mediated TRIM21 N-ubiquitination is required for TRM21 self-ubiquitination and subsequent degradation inside cells.

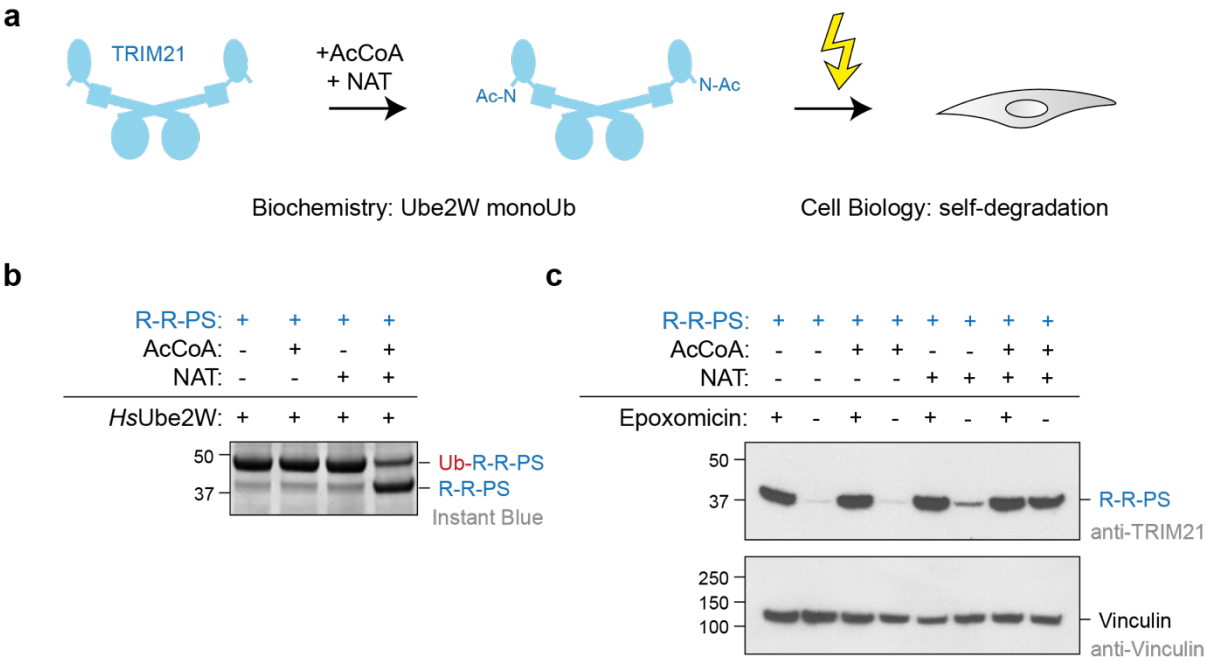


**Figure 28 TRIM21 N-ubiquitination is required for TRIM21 turnover via the ubiquitin proteasome system. a** Schematic depiction of the experimental layout. A biochemical TRIM21 acetylation reaction is performed for 4 h at 25 ˚C. **b** Success of the acetylation reaction is validated by using part of the reaction for a Ube2W-dependent N-ubiquitination reaction. **c** Another part of the same acetylation reaction is electroporated into RPE-1 *TRIM21* knock-out cells. The western blot shows cells either treated with DMSO or 10 µM epoxomicin 1 h after electroporation.

### 5.2.2 Molecular interaction between TRIM21 and Ube2W

After establishing the interaction between TRIM21 and Ube2W inside cells, the next goal was to decipher the mechanism of Ube2W action on TRIM21. Thus, T21-R together with Ube2W was subjected to crystallization trials. While T21-R did not crystallize with WT Ube2W, crystals could be obtained of a complex with a monomeric Ube2W$^{V30K/D67K/C91K}$ construct (V30K/D67K make Ube2W monomeric; the active site cysteine was also mutated to lysine) and the structure was solved to 2.25 Å resolution (**Figure 29a, Appendix Table 3**). Two copies of each Ube2W and T21-R could be found in the asymmetric unit, with the two RING domains forming a homo-dimer as described previously[80,113,165,166]. RING and Ube2W engage each other via the canonical RING:E2 interface (**Figure 29b**). To validate this interaction surface on TRIM21, NMR titrations of monomeric $^{15}$N-T21-R$^{M10E}$ with unlabelled monomeric Ube2W$^{V30K/D67K/C91K}$ were performed (**Figure 30a,c**). The CSPs observed were highly similar to those seen in the titrations performed with Ube2N and Ube2D1 (**Figure 8**, **Figure 10**), highlighting the similarities between these different E2:E3 complexes. The

structure reveals no specific interactions suggesting how TRIM21 selectively recruits Ube2W inside cells.

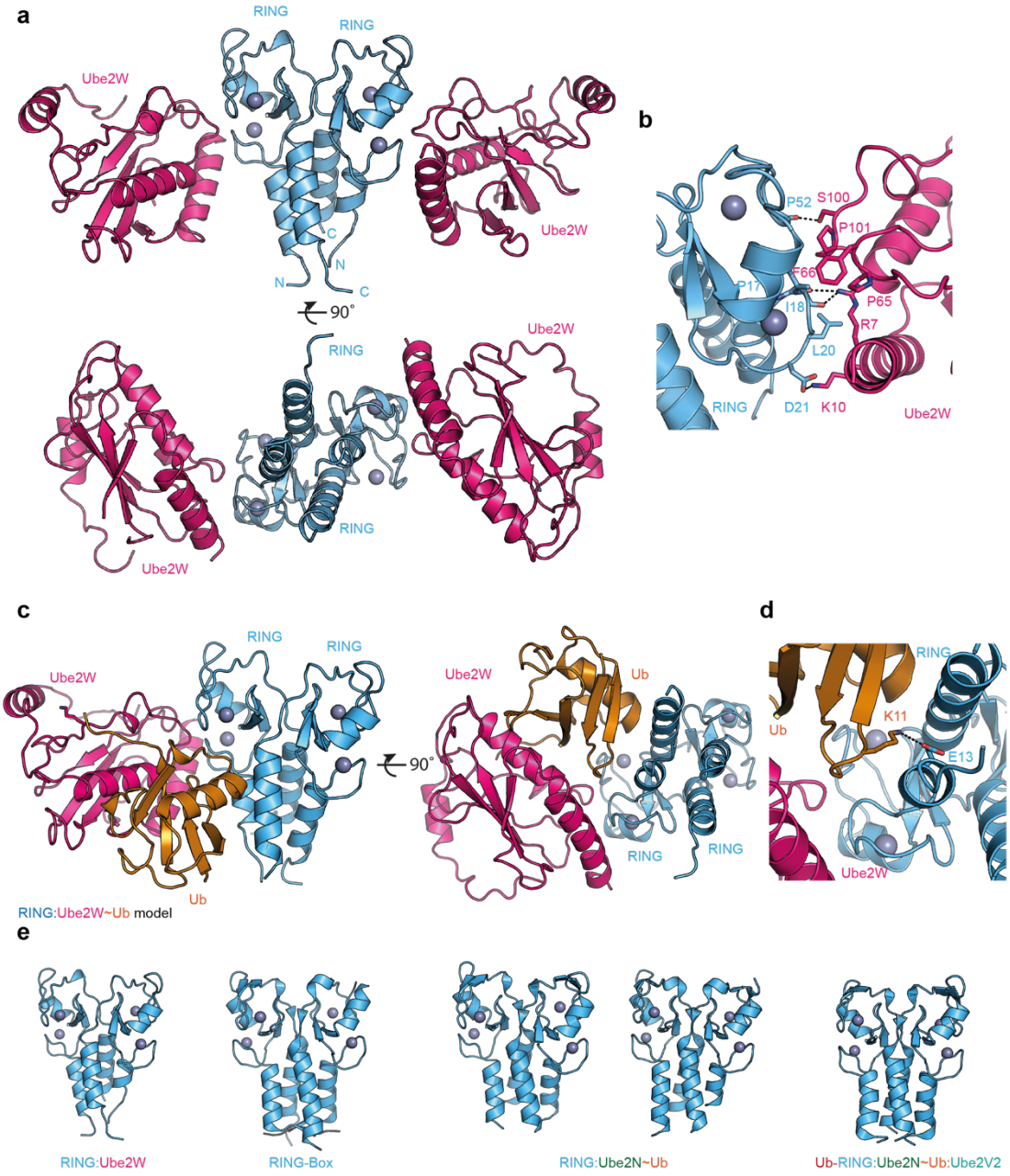


**Figure 29 Crystal structure of TRIM21 RING in complex with Ube2W a** 2.25 Å X-ray structure of T21-R (blue) in complex with Ube2W (pink). **b** Close-up of the E2:E3 interface. **c** Structural model of a T21-R:Ube2W~Ub complex based on superposition of the T21-R:Ube2W structure and the Ub-T21-R:Ube2N~Ub:Ube2V2 structure (7BBD)[165]. Ube2N~Ub was superposed onto Ube2W. **d** Close-up of the T21-R:Ube2W~Ub model showing a potential salt bridge between TRIM21 E13 and ubiquitin K11. **e** Shown are RING dimers of different TRIM21 complexes (T21-R:Ube2W, T21-R-B (5OLM)[80], T21-R:Ube2N~Ub (two RING dimers in asymmetric unit, 6S53)[113], Ub-T21:Ube2N~Ub:Ube2V2 (7BBD)[165]). $Zn^{2+}$-atoms are shown as grey spheres and polar interactions are indicated by dashed black lines. The

TRIM21 RING:Ube2W structure was crystallized and solved by Dr Claire F Dickson. The refinement was performed by Dr Claire F Dickson and I.

By superposing the T21-R:Ube2W structure with Ube2N~Ub from the previously determined Ub-T21-R:Ube2N~Ub:Ube2V2 structure (Chapter 4, **Figure 17**)[165], the activation of Ube2W~Ub was modelled (**Figure 29c**). Overall, the arrangement of a Ube2W~Ub appears to be very similar to Ube2N~Ub, when being activated by TRIM21 (**Figure 9**, **Figure 17**). In this model the donor ubiquitin is in the closed conformation, stabilized by both RING protomers. Interestingly, this model also suggests that TRIM21 E13, which is part of the tri-ionic motif, might engage ubiquitin K11 to stabilize the closed conformation (**Figure 29d**), as had been observed for Ube2N~Ub (**Figure 9**)[113]. However, this structure does not provide any particular clues as to the origin of specificity for TRIM21, nor does it explain how Ube2W can modify the TRIM21 N-terminus, which is located far away from the E2 active site. When comparing the RING in the T21-R:Ube2W structure to our apo-[80] and Ube2N~Ub[113,165] engaged structures, it becomes apparent that the N- and C-terminal helices of the RINGs are partly unfolded when bound by Ube2W (**Figure 29e**). It is entirely possible that this behaviour originates from the different crystal lattices present in these different structures. Nonetheless, this might perhaps suggest that the presence of Ube2W has the potential to destabilize the 4-helix bundle, thereby generating a disordered N-terminus for modification. However, the issue of how the donor ubiquitin is transferred from the Ube2W active site to the TRIM21 N-terminus remains open.

### 5.2.3 The tri-ionic motif is not required for recruitment and catalysis of Ube2W

Selective E2 recruitment by E3 ligases remains poorly understood and despite the existence of the T21-R:Ube2W crystal structure, no insight into specificity could be inferred. In Chapter 3, it was shown that TRIM21 specifically recruits Ube2N using the tri-ionic motif[113], which consists of TRIM21 residues E12, E13 and D21 (**Figure 9**). The T21-R:Ube2W structure shows that D21 interacts with Ube2W K10 and the model of the closed conformation suggests that E13 might form a salt bridge with ubiquitin K11 (**Figure 29d**). The most important residue in this motif was E12 in TRIM21, which formed a salt bridge to R14 of Ube2N[113]. This residue on Ube2W is alanine, implying that recruitment of Ube2W probably does not involve the tri-ionic motif. To test this

hypothesis, I performed NMR titrations of $^{15}$N-labelled TRIM21 tri-ionic mutants against Ube2W$^{V30K/D67K/C91K}$. Mutation of the tri-ionic residues E12 and E13 to alanine did not lead to a reduction in the observed CSPs (**Figure 30a-c**); only the construct carrying an E12R mutation showed slightly reduced CSPs. These data suggest that Ube2W is not being recruited via the tri-ionic motif. Next, I tested whether mutation of the tri-ionic motif would reduce TRIM21 mono-ubiquitination (**Figure 30d**). As expected, TRIM21 E12A showed activity at WT level and E12R only a slight reduction in activity. TRIM21 mutants E13A and E13R both showed a slight reduction in activity suggesting that residue E13 could indeed interact with ubiquitin K11. However, the mild reduction in activity suggests that this interaction is not as critical as was the case for Ube2N~Ub (**Figure 12**). Thus, similar to Ube2D (**Figure 13**), Ube2W does not require the tri-ionic motif for activity and it therefore remains open how Ube2W gets recruited by TRIM21 inside cells.

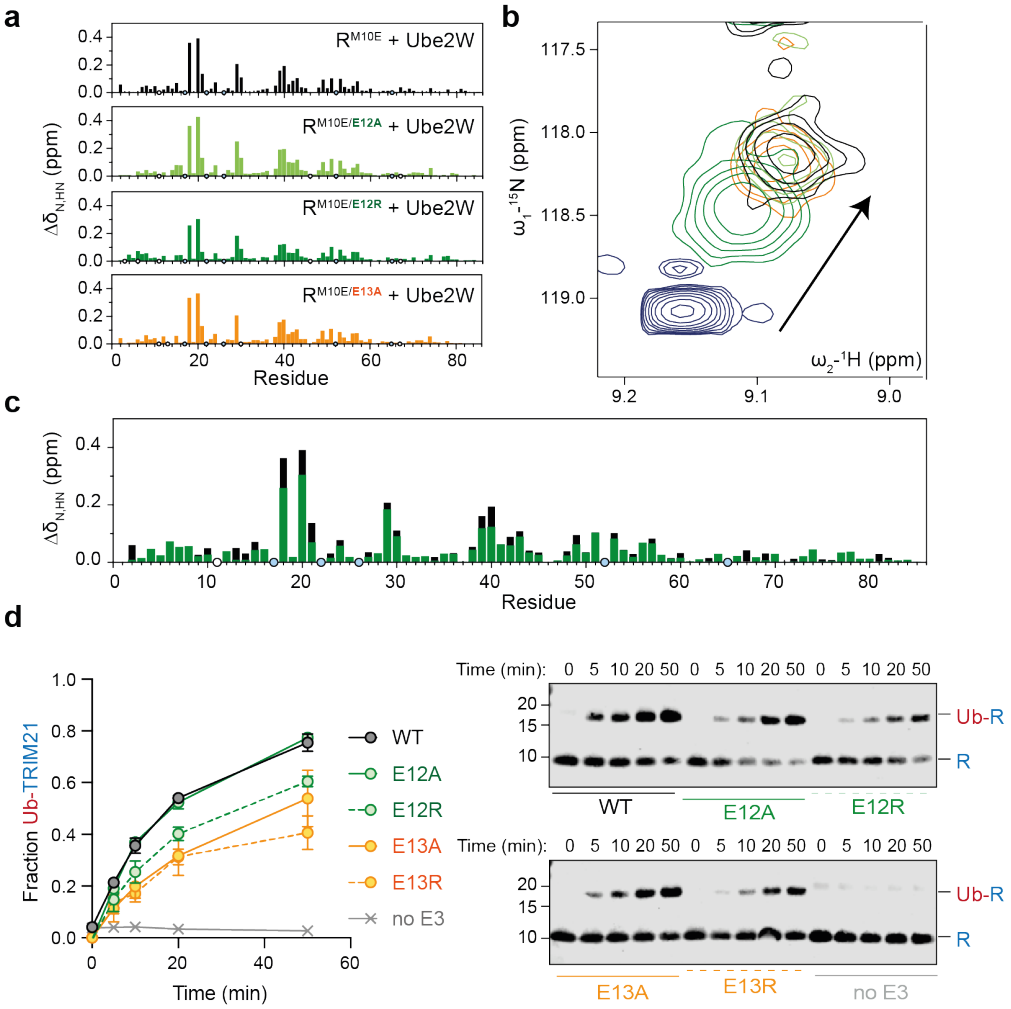


**Figure 30 Ube2W recruitment and catalysis by TRIM21 do not require the tri-ionic motif. a** Histograms of the chemical shift perturbations (CSP) is shown against the sequence of T21-R$^{M10E}$. These CSPs result from titration with Ube2W$^{V30K/D67/C91K}$ at a 1:1 molar ratio. Blue circles indicate proline residues, white circles missing assignments. **b** A part of $^{15}$N-HSQC spectral overlay of T21-R$^{M10E}$ in absence (blue) or presence of 1:1 molar equivalent of Ube2W$^{V30K/D67/C91K}$. In addition, spectra of TRIM21 mutants (E12A in light green, E12R in dark green and E13A in orange) are shown in presence of 1:1 molar equivalent of Ube2W$^{V30K/D67/C91K}$. **c** Histograms shown in a are here shown as an overlay. **d** Ube2W-mediated T21-R mono-ubiquitination assay. Shown is the time-course, where error bars represent SEM of three independently performed experiments. Shown western blots are representative for all replicates.

### 5.2.4 The catalytic RING topology drives TRIM21 N-ubiquitination

Given that the above structure of T21-R:Ube2W did not reveal the mechanism of TRIM21 N-ubiquitination, a different approach was needed. Interestingly, in cellular experiments N-terminally tagged TRIM21 shows no reduction in activity, suggesting that N-terminal mono-ubiquitination is not particularly selective with respect to the N-terminal sequence, or even the presence of additional domains, such as GFP,

mCherry or Lipoyl[62]. Indeed, Ube2W has been shown to primarily target disordered N-termini[117]. To this end, I tested whether TRIM21 constructs with different N-termini would be efficiently targeted. I compared a TRIM21 RING construct, which carried a GSH scar at the N-terminus, and a TRIM21 R-PS construct, which was designed to start without a scar at the TRIM21 N-terminus (MAS). Both constructs were ubiquitinated efficiently, showing that Ube2W cannot discriminate between these different N-termini (**Figure 31a**). Thus, it seems Ube2W mono-ubiquitinates the TRIM21 N-terminus irrespective of its sequence. However, N-ubiquitinated TRIM21 is not further ubiquitinated, as the new N-terminus of N-ubiquitinated TRIM21 is now the N-terminus of ubiquitin, which is tightly folded. Ube2W's specificity in targeting TRIM21 therefore originates from both the RING and the presence of an N-terminal unstructured region. This adds potential significance to the possibility referred to earlier that Ube2W might unfold TRIM21's N-terminus (**Figure 29e**). However, based on the R:Ube2W structure, even the unfolded TRIM21 N-terminus could not reach the E2 active site in *cis* (**Figure 29a**). Ube2W has been shown to form a homo-dimer[162], although its dimerization was reported not to compromise ubiquitination[117,162]. To validate this finding, I tested whether dimerization of either TRIM21 or Ube2W had an effect on TRIM21 ubiquitination in vitro. To achieve this, TRIM21 constructs, either carrying one or two RINGs and a PS domain were used (R-PS and R-R-PS). Both constructs were efficiently mono-ubiquitinated by Ube2W (**Figure 31b**). However, this activity was abolished when monomeric Ube2W$^{V30K/D67K}$ was used. Interestingly, no difference between R-PS and R-R-PS could be observed. RING E3s are generally activated by forming a dimer[19,20,83-85] and this is also the case for TRIM21[150,165]. The lack of difference between R-PS and R-R-PS could be either due to Ube2W not requiring a RING dimer for activity or the relatively high TRIM21 concentrations used in this assay.

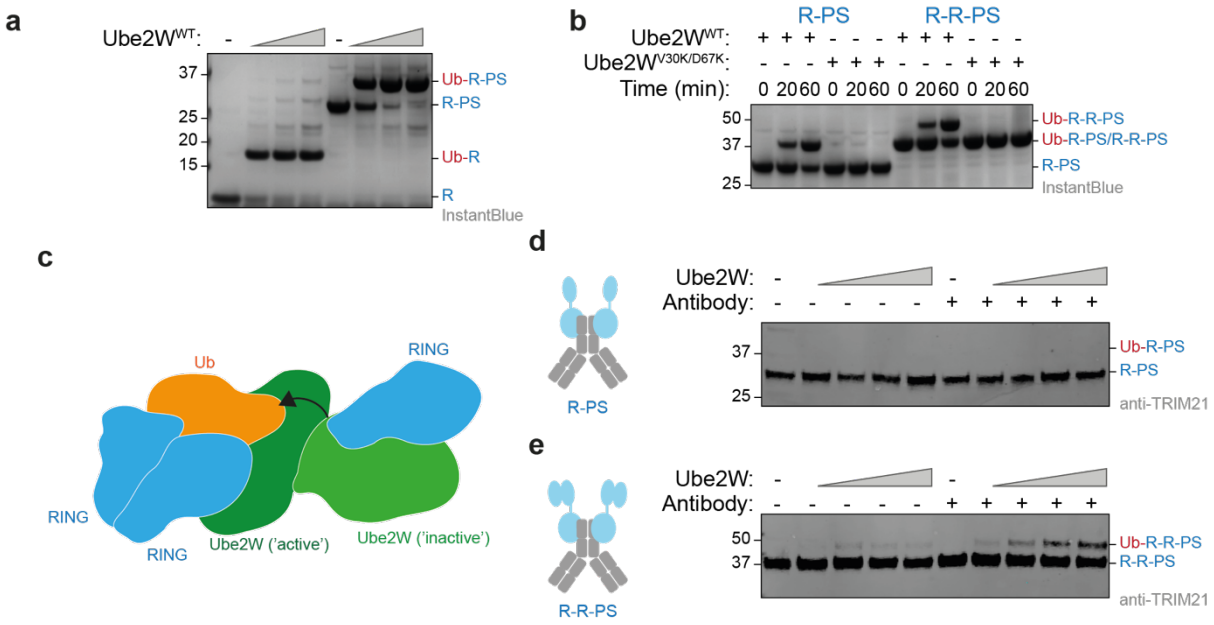


**Figure 31 Ube2W dimerization enables TRIM21 N-ubiquitination via the catalytic RING topology.** **a** Ube2W-mediated TRIM21 mono-ubiquitination assay. 10 µM of T21-R (containing a GSH scar on N-terminus) or T21-R-PS (with the native TRIM21 N-terminus (MAS)) were titrated with Ube2W (0.25, 0.5 or 1 µM) for 60 min. **b** Ube2W-mediated TRIM21 mono-ubiquitination assay using 10 µM T21-R-PS or -R-R-PS and 0.25 µM Ube2W WT or monomeric V30K/D67K. **c** Schematic model of the catalytic RING topology for N-ubiquitination of TRIM21 by a Ube2W dimer. **d**, **e** Antibody induced N-ubiquitination of 100 nM d T21-R-PS or e -R-R-PS in absence of presence of 1 molar equivalent of anti-GFP antibody. Ube2W was titrated (25, 50, 100, 200 nM). Next to the western blots in **d**, **e** are shown schematic cartoons of the respective TRIM21 constructs bound by antibody. Experiments shown in panels **b**, **d** and **e** were performed by Shannon Smyly under my supervision.

The importance of Ube2W dimerization in TRIM21 N-ubiquitination was rather surprising. However, requiring a dimeric E2 is highly reminiscent of the behaviour of heterodimeric Ube2N/Ube2V2. Ube2N is the catalytically active E2, but it needs Ube2V2 for activity. Ube2V2 is required to bind and orient the acceptor ubiquitin during K63-linked ubiquitin chain formation[32,33,101,143,165]. In Chapter 4, it was shown that Ube2N/Ube2V2 requires a so called catalytic RING topology for activity (**Figure 21**)[165]. In this arrangement, two RINGs form a dimer to act as enzyme, activating the donor ubiquitin. A third mono-ubiquitinated RING acts as the substrate, oriented by Ube2N/Ube2V2 to attack the electrophilic donor ubiquitin[165]. Requirement for a Ube2W dimer suggests a similar mechanism to that for Ube2N/Ube2V2. The catalytic RING topology for RING N-ubiquitination in *trans* (**Figure 31c**) would be mechanistically attractive, given that a *cis* mechanism is structurally impossible (**Figure 29a**) as was also the case for ubiquitin chain elongation (**Figure 20**).

To determine whether the catalytic RING topology promotes TRIM21 N-ubiquitination with Ube2W, I adjusted the Fc-induced ubiquitination experiment established in Chapter 4. Instead of using Ub-TRIM21, non-ubiquitinated TRIM21 constructs were used. In addition, Fc was replaced by using an antibody. Low concentrations of either R-PS or R-R-PS were titrated with Ube2W either in presence of absence of antibody. Overall, R-PS showed hardly any activity in the presence or absence of antibody (**Figure 31d**). The catalytic RING topology requires at least three RINGs in close proximity, which does not occur for R-PS. In contrast, activity of R-R-PS was promoted by addition of antibody (**Figure 31e**), showing that RING dimerization is critical for activity with Ube2W. More importantly, Ube2W uses a *trans* mechanism similar to Ube2N/Ube2V2 to perform TRIM21 ubiquitination.

## 5.3 Discussion

Until recently, protein ubiquitination was thought to be limited to lysine side chains. However, that view has been challenged by the finding that a subset of E2 and E3 enzymes specialize in alternative chemistries. The non-canonical E3 MYCB2 forms ester bonds to threonine side chains[7], the E2 Ube2J2 to serine side chains[6] and Ube2W to N-termini[4,5], thereby expanding the realm of ubiquitin modifications. Moreover, ubiquitin can be targeted to non-protein substrates such as ADP ribose[167], LPS on bacteria[168] or glycogen[169].

N-ubiquitination (also called linear ubiquitination) can only be performed by two enzymes: the LUBAC subunit HOIP exclusively forms linear ubiquitin chains[3] and Ube2W targets a single ubiquitin to protein N-termini[4,5]. A recent study has identified novel Ube2W targets including two DUBs[163], but further data is required to understand the exact role of N-ubiquitination in these pathways. Ube2W has been shown to perform mono-ubiquitination with many RING E3s in vitro (e.g. [29,117,162]); yet with the exception of TRIM21 and TRIM5α, cellular evidence for involvement in such pathways remains scarce. Ube2W was suggested to transfer the priming ubiquitin to the RING E3s TRIM21[27] and TRIM5α[124]. In both cases, this is followed by extension into a self-anchored K63-linked Ub chain via interaction with Ube2N/Ube2V2[27,113,124,125,150,165]. Here I show that blocking the N-terminus of a hyperactive TRIM21 construct results in loss of N-ubiquitination and concomitant self-turnover (**Figure 28**). These data provide

the first evidence that a direct physical interaction between TRIM21 and Ube2W may occur inside cells.

However, it remained unclear how TRIM21 modification is achieved by Ube2W. In line with general RING:E2 catalysis, TRIM21 RING dimerization was important for N-ubiquitination with Ube2W (**Figure 31d,e**). Rather surprisingly, Ube2W must also itself dimerize to perform N-ubiquitination of TRIM21 (**Figure 31b**). That may be because Ube2W uses a *trans* mechanism (**Figure 31c**), akin to TRIM21's other canonical E2 enzyme: Ube2N/Ube2V2 (**Figure 21**, Chapter 4)[165]. In this proposed mechanism, Ube2W forms a homo-dimer, in which the two Ube2W molecules fulfil distinct functions. A ubiquitin-carrying Ube2W protomer is activated by a TRIM21 RING dimer to transfer ubiquitin to another TRIM21 RING, which is recruited by the second Ube2W protomer within the dimer. It remains open how the Ube2W dimer is actually formed as no structures are available. NMR data for monomeric and dimeric Ube2W constructs suggested that dimerization occurred via its β-sheet, which is near to the mutation sites that prevent dimerization (V30K/D67K)[162]. Ube2V2 packs against the equivalent sheet in Ube2N[101,115,143,165], suggesting a similar binding mode. However, while Ube2V2 binds the surface of the β-sheet with its first helix, such a binding event is unlikely in the case of Ube2W as it would not enable recruitment of TRIM21 by the second Ube2W protomer, since this requires the same helix. Instead, another surface must be used that is yet unknown. Another E2 enzyme reported to dimerize to fulfil its function is the ERAD E2 Ube2G2[170]. In contrast, dimerization of Ube2S results in autoinhibition[171].

A *trans* mechanism would explain the use of Ube2W and Ube2N/Ube2V2 sequentially – TRIM21 activation on an antibody-coated virus positions its RING domains optimally for their engagement. Ube2N/Ube2V2 recruitment is the further promoted by the tri-ionic motif (**Figure 9**)[113]. Ube2N/Ube2V2 is available in concentrations ~50 times higher than Ube2W[139,140], making it more available for recruitment by its sheer abundance. Requiring the tri-ionic motif for Ube2N/Ube2V2 recruitment, in contrast to the case of Ube2W that lacks such a motif, might be due to higher competition for the respective E2 enzyme. Ube2N is the only enzyme able to form K63-linked poly-ubiquitin, which is the second most abundant ubiquitin chain type[172]. In contrast, in

absence of Ube2W overexpression, only 8 N-ubiquitinated proteins could be identified[163], suggesting less competition from orthogonal N-ubiquitination events.

Ube2W's requirement for the catalytic RING topology for RING N-ubiquitination also agrees well with the activation mechanism of TRIM5α. TRIM5α forms hexagonal lattices on retroviral capsids, thus creating vertices with three RINGs available[87,88,126,155,173]. This promotes the catalytic RING topology for K63-chain formation[165]. Overall, it appears that Ube2W recruitment by TRIM21 is mainly achieved by TRIM21 forming the catalytic RING topology. Ube2W and Ube2N thus form a perfect E2 pair as they make use of the same mechanism for substrate modification. It will be interesting to see whether other E3 ligases employ this mechanism to recruit Ube2W and Ube2N sequentially for anchored ubiquitin chain formation.

# Chapter 6 Discussion and Outlook

## 6.1 Main findings of this Thesis

In my doctoral work, my aim was to illuminate the basic principles of ubiquitination of the antiviral E3 ligase TRIM21. The motivation for this arises from two main considerations. First, most mechanistic work on E3 ligases focusses on in vitro assays and enzyme pairs that do not necessarily function together in cells. While these studies provide crucial insights into the chemical mechanisms of ubiquitination, they fail to explain the biological role that is achieved by their catalysis. Secondly, TRIM21 is a ligase with unique properties. By using antibodies as an intermediary, it targets many viral proteins as well as full viruses for degradation[53,73]. Moreover, if antibodies against cellular proteins are introduced into the cytoplasm, TRIM21 is able to degrade many different targets efficiently[62]. Two main questions emerge from this behaviour: (i) how does TRIM21 target all these different proteins for degradation and (ii) how can we modify this behaviour to re-task TRIM21 for our own purposes?

Previous work in the James lab had identified two E2 conjugating enzymes that are required for TRIM21's cellular function and that showed biochemical activity with TRIM21 in vitro[27,28]. The suggested model was that Ube2W modifies the TRIM21 N-terminus with a priming ubiquitin, which is then extended into a K63-linked ubiquitin chain upon interaction with Ube2N/Ube2V2. My first goal was to validate the proposal that these enzymes must interact directly with TRIM21 for cellular function, rather than at some other step in the pathway. Next, I wanted to understand the mechanistic basis of direct interaction, which in turn was expected to explain how TRIM21 can degrade manifold substrates.

Chapter 3 describes the first steps in my project, comprising a biochemical screen searching for E2 enzymes that could interact with TRIM21 in vitro. In this screen, TRIM21 was found to interact efficiently only with Ube2W, Ube2N and the promiscuous Ube2D family. However, as assessed by NMR chemical shift titrations, all these interactions appeared to be highly similar, thereby failing to explain how E2 specificity was achieved (**Figure 8**). Thus, I decided to focus on Ube2N, as this

enzyme was already well characterized. The crystal structure of the TRIM21 RING in complex with a stable Ube2N~Ub conjugate gave crucial insights into the mechanism of recruitment of Ube2N~Ub by TRIM21: a tri-ionic motif on TRIM21 wrapped Ube2N~Ub around the RING, thereby activating it (**Figure 9**). Mutation of this motif selectively inhibited catalysis with Ube2N, but not other E2 enzymes, such as Ube2D and Ube2W (**Figure 16**, **Figure 30**), thus demonstrating specificity for selective E2 recruitment (**Figure 12**, **Figure 13**). Inside cells, these specificity mutants had severely impaired antiviral activity and self-ubiquitination, thereby establishing the importance of a direct interaction between TRIM21 and Ube2N (**Figure 15**). Strikingly, this motif is not only found on TRIM21, but also on many other RING E3s (**Figure 15**, **Figure 16**). The work described in Chapter 3 thus established the first general E2 recruitment mechanism by RING E3s.

The next step was to try to learn how this ubiquitin chain is formed on TRIM21, work described in Chapter 4. A structure containing all the enzymes required to perform this reaction in vitro effectively caught TRIM21 in the act of modifying itself with a ubiquitin chain (**Figure 17**). Interestingly, this structure revealed an intricate arrangement involving two RING dimers, that suggested at least three RING domains are required to enable self-ubiquitination. The structure suggested that Ube2N~Ub is activated by one RING dimer and the ubiquitin transferred to a mono-ubiquitinated RING in a second RING dimer. This *trans* reaction enables self-ubiquitination of TRIM21 (**Figure 21**) and targeted protein degradation (**Figure 24**). Importantly, this topology can only be fulfilled when multiple TRIM21 molecules cluster on its target, thereby providing all of the RINGs required for activity. These new findings enabled me to design novel TRIM21 constructs for improved Trim-Away. Higher order assembly of K63-linked ubiquitin chain forming E3 ligases is not uncommon, suggesting that other ligases outside the TRIM family might share this mechanism.

Finally, I focussed on TRIM21 mono-ubiquitination by the enigmatic, and less well characterized, E2 enzyme Ube2W. Only a few hints into the role of this atypical E2 enzyme appear in the literature. To understand TRIM21's action, its connection with Ube2W is critical, as it represents the first ubiquitination event catalyzed by TRIM21. Blocking the TRIM21 N-terminus by acetylation revealed that a free N-terminus is required for ubiquitination and subsequent proteasomal degradation in cells. I

characterized the mechanism of TRIM21 N-ubiquitination and found that Ube2W must form a dimer to fulfil this function. Intriguingly, the reason for this appears to be that Ube2W and Ube2N/Ube2V2 largely share their mechanism of ubiquitin transfer with TRIM21. Within the dimer, one protomer carries ubiquitin and becomes activated by a RING dimer, while the other protomer recruits a further RING domain for modification in *trans*. This implies that Ube2W recruitment and catalysis are a consequence of TRIM21 activation by clustering on a substrate, such as an antibody-coated virus. Moreover, it fits nicely as a perfect partner enzyme for E3 ligases that form K63-linked ubiquitin chains with Ube2N, by utilizing the same general mechanism.

Overall, this Thesis describes in detail all steps of the formation of a self-anchored K63-linked ubiquitin chain on TRIM21, based on atomic structures that set the stage for understanding the cellular mechanism. By trying to understand TRIM21 biology, this work has illuminated general ubiquitination mechanisms that can be found in many different pathways. Moreover, it has led to the development of novel TRIM21 constructs with improved targeted protein degradation abilities.

## 6.2 Future directions

### 6.2.1 TRIM21 ubiquitination

The work presented in this Thesis was mainly focussed on TRIM21 forming a self-anchored K63-linked ubiquitin chain. However, it remains questionable whether this represents the only modification that occurs during TRIM21 action. Indeed, it is very likely that other ubiquitination events have to occur for TRIM21 to fulfil its full function. For instance, it is highly doubtful that K63-linked ubiquitin chains, which are not themselves known to encode degradation[10], would do so in the case of TRIM21. Moreover, recent publications suggest that many ubiquitination events involve branched ubiquitin chains including multiple different chain types rather than homotypic ubiquitin chains[153,154]. Indeed, strongly overexpressed TRIM21 was found to carry K48-linked chains if K63 chains are also present[27]. Thus, it is likely that TRIM21 initially forms a K63 chain, which is then branched into (at least) K48 poly-ubiquitin.

The current model is that TRIM21 modifies itself with a K63-linked ubiquitin chain to fulfil its antiviral function. This model is based on multiple layers of evidence, produced in different studies, including work performed in this Thesis. Depletion of Ube2N or Ube2W inhibits TRIM21 activity[27], as does preventing the direct interaction between TRIM21 and Ube2N (Chapter 3)[113]. Inhibition of Ube2N recruitment by TRIM21 or Ube2N depletion also reduces TRIM21 self-ubiquitination[27,150]. The TRIM21 N-terminus becomes a target for Ube2W initiated poly-ubiquitination and subsequent proteasomal degradation (Chapter 5). Finally, induction of TRIM21 K63-self-ubiquitination is associated with targeted protein degradation (Chapter 4)[165]. Importantly, all this evidence does not exclude the possibility of additional ubiquitination events on TRIM21, antibody or substrate. Due to difficulties in detecting cellular ubiquitination events when studying a system under native conditions, we might have missed such events in the past. It will thus be crucial to pin down whether other ubiquitination events occur during TRIM21 action, and if so what they are. The main questions to answer here are: (i) where additional ubiquitination events are involved, (ii) what role they fulfil and (iii) whether they are catalyzed by TRIM21 or via the recruitment of additional ligases.

While E3 ligases such as TRIM21 build ubiquitin signals, deubiquitinases (DUBs) erase these signals. The proteasomal DUB Rpn11 (Poh1) has been suggested to play a part in TRIM21's antiviral function[27], a role that is shared by all ubiquitinated proteins that are degraded by the 26S proteasome[174]. However, no other DUBs are known to be involved in the TRIM21 pathway. Due to TRIM21 forming K63-linked ubiquitin chains, it is likely that there is a K63-degrading DUB regulating this process, for example analogous to CYLD regulation of NF-κB signalling[175]. The more additional ubiquitin signals are involved in TRIM21's function, the more DUBs are likely to play a regulatory role. Thus, by identifying novel DUBs involved in TRIM21 action, we might gain deeper understanding of the ubiquitination events involved.

The mechanistic work described in this Thesis resulted in the development of novel TRIM21 constructs with superior abilities in Trim-Away (Chapter 4). The R-R-PS constructs degrade substrates very efficiently and quickly. They also have a shorter half-life themselves due to self-turnover. This can be seen as either an advantage or disadvantage. For instance, a Trim-Away experiment with an unstable TRIM21

construct could enable rescue experiments as these new rescue constructs would not be targeted due to TRIM21's quick self-turnover. On the other hand, highly expressed proteins might quickly be replaced after depletion, as no TRIM21 is left to sustain the protein knock-down. Thus, further engineering of these constructs towards retaining target degradation, while increasing the half-life of the construct itself, would be very beneficial. This could be done by engineering its E2 recruitment. Reducing the ability of a TRIM21 construct to engage E2 enzymes might retain activity sufficient for efficient target degradation, while being less potent in self-turnover. Another option could be the introduction of the TRIM21 B-box to reduce activity, or the TRIM5α B-box to increase it. B-boxes have been largely overlooked in past mechanistic studies and it is likely that other TRIM protein B-boxes could enable rather precise regulation of E3 ligase activation. The TRIM21 R-R-PS construct could thus be the engineered into a whole toolbox of TRIM21 proteins tailored for different applications.

### 6.2.2 E2 specificity and ubiquitin chain formation

Although the work described in this Thesis has been mainly focussed on TRIM21 (and in small parts on TRIM5α), the findings presented here have more general implications. My work on the selective Ube2N recruitment by TRIM21 represents the first general E2 specificity mechanism found for RING E3s. How the correct E2 is selected by a particular E3 is one of the most fundamental, yet overlooked, questions in ubiquitin biology. Largely this is the case because the basis for such specificity is difficult to pin down[8,25]. Compounding this problem, the first RING E3:E2 structure constituted c-CBL and Ube2L3 (UbcH7)[176], an E2:E3 pair that is not functional together[177] as Ube2L3 is not a lysine but cysteine reactive E2[178]. Indeed, structures of RING:E2 complexes look remarkably similar, each with an interface that is largely guided by the generic hydrophobic interactions and polar interactions[8,25]. In the case of the atypical E3:E2 pair FANCL and Ube2T, a specific arrangement of polar interactions provides specificity[134]. The tri-ionic motif I have identified can be found in many K63-ubiquitinating RING E3s (**Figure 15**, **Figure 16**). The underlying mechanism not only promotes recruitment, but also formation of the catalytic closed Ube2N~Ub conformation (**Figure 11**, Chapter 3)[113]. Interestingly, a recent study also found that modulating an E3's ability to promote the closed E2~Ub conformation is a

specificity driver for the ERAD E3s Hrd1 and Doa10 interacting with Ubc6 and Ubc7[179]. It should be noted that these enzymes are all localized to the ER membrane, which is likely to be the largest specificity determinator in this case.

With only a few structural specificity mechanisms known, other factors must come into play to ensure the generation of correct E2:E3 pairs. One such factor might be formation of specific higher-order structural assemblies, which could enable use of some E2s, while prohibiting others. One such topology could be the catalytic RING topology described here (Chapter 4, Chapter 5)[165], in which the cellular mechanism of the E2 enzymes Ube2N/Ube2V2 and Ube2W requires three RING domains in close proximity for catalysis to occur. By this arrangement, catalysis with Ube2W is promoted, despite the lack of a specific recruitment motif (**Figure 31**). In contrast, this arrangement does not select for Ube2D (**Figure 23**). In addition, the (sub-) cellular availability of different E2 likely plays an important role. As explained above, the ERAD E2s and E3s are all localized to the ER membrane[179]. TRIM21, Ube2W and Ube2N/Ube2V2 are all found in the cytoplasm. Their relative abundance, however, is fundamentally different. Based on quantitative MS, TRIM21 and Ube2W are present in the low nanomolar range, while Ube2N is in the micromolar concentration range[139,140]. As the only K63-linkage forming E2 enzyme, Ube2N is a rather busy enzyme, thus creating a need for a specific structural motif for efficient recruitment. In contrast, Ube2W only has a few substrates[163], potentially explaining why the catalytic RING topology might be sufficient for recruitment. The substrate, which in the case of TRIM21 and TRIM5α is required to form a catalytic E3 arrangement, therefore also encodes specificity. In mammals, Cullin-RING-ligases (CRLs) make use of Ube2D and the RBR E3 ARIH1[180,181] for initiation and Ube2R for elongation of ubiquitination[182,183]. Interestingly, the substrate plays an important role in determining which enzymes are used for transfer of the first ubiquitin[184]. Moreover, CRL ubiquitin chain elongation is performed by Ube2R, but its absence can be buffered for by Ube2G2[184]. Buffering of different E2s or E3s also increases the difficulty in linking these enzymes to specific functions. Thus, E2 selection is regulated by several layers of complexity. To further understand this under-studied area of ubiquitin biology in the future, highly interdisciplinary and quantitative methods will need to be used.

Understanding how ubiquitin is transferred to its substrate has been a long-standing question. After it had been established that RING E3s activate E2s by promoting a closed E2~Ub conformation[19-21], the question remained how this activated ubiquitin ends up on its substrate. Some early insights into this came from activation of CRLs by modification with the ubiquitin-like protein Nedd8[185]. When the Cullin-anchored RING Rbx1 engages the Nedd8-charged E2 Ube2M (Ubc12) in the closed conformation, this positions the E2 active site within a few Å of the target lysine on the Cullin[31]. Similarly, the yeast SUMO E3 Siz1 engages Ube2I~SUMO (Ubc9) in the closed conformation and simultaneously engages PCNA, to orient the PCNA acceptor lysine in close proximity to the E2 active site[30]. Two recent structures of CRLs in the process of substrate ubiquitination have provided more detailed insight into this process. Structures of CRLs with either Ube2D~Ub or ARIH~Ub capture the ligase in the process of attaching the first ubiquitin to their respective substrates[141,186]. The E2~Ub is optimally oriented for ubiquitination by multiple direct interactions: formation of the closed Ube2D~Ub conformation with the RING, interaction with the Cullin-bound Nedd8 and interaction with the substrate receptor[141]. This arrangement required strict positioning of the substrate lysine, thereby favouring disordered targets[141,186]. In contrast, a CRL with the RBR E3 ARIH1 showed a higher degree of flexibility, thereby enabling ubiquitination of globular substrates[186]. However, as of yet a structure showing the elongation of the priming ubiquitin in the context of CRLs is missing. The structure of TRIM21 in the act of elongating its priming ubiquitin into a ubiquitin chain presented in this Thesis, represents the first structure of such a process (**Figure 17**, Chapter 4)[165]. In addition, the biochemical data for mono-ubiquitination presented in Chapter 5 suggests the same mechanism for the priming step (**Figure 31**). Thus, TRIM21 requires substrate-induced assembly of multiple molecules to satisfy a specific yet dynamic topology to engage the E2 enzymes required for self-ubiquitination. This is reminiscent of the mechanistic arrangement between CRL and ARIH, as flexibility in the overall topology appears to be key for substrate modification. The yeast N-end rule E3 ligase Ubr1 (an E3 involved in targeting proteins with particular N-terminal residues for rapid degradation) has been shown in the process of both transferring the first ubiquitin to its substrate and extending this into a K48-linked chain[187]. The substrate is the N-end rule peptide degron and the initiation of

ubiquitination is highly reminiscent of the mechanisms employed by CRL with Ube2D~Ub[141], the nucleosome histone-tail modification by BRCA1/BARD1 with Ube2D[188] and the giant E3 ligase APC/C[189]. In all these cases, the substrate is a disordered peptide bound to a recognition domain of the E3 ligase, but with enough flexibility to span the distance to the E2 active site. While Nedd8 positioned Ube2D2~Ub perfectly for substrate ubiquitination[141], Ubr1 contains a helix which oriented Ubc2~Ub[187]. Interestingly, in the elongating Ubr1:Ubc2~Ub:Ub-degron structure, the E2 is rearranged to allow elongation. Moreover, additional interactions between a novel acceptor ubiquitin binding motif on Ubr1 and between acceptor ubiquitin and Ubc2 provide K48 specificity and enable Ub-degron elongation[187]. Of note, the interaction between acceptor ubiquitin and E2 in this structure is highly reminiscent of the interactions between acceptor ubiquitin and Ube2N in the TRIM21 elongation structure presented in Chapter 4 (**Figure 18**)[165]. Taken together, nearly all structural insights into substrate ubiquitination by RING E3s to date are for disordered peptide substrates rather than globular domains. However, one example that involves ubiquitination of a globular domain constitutes the Fanconi-Anaemia core complex. Here, the RING FANCL activated Ube2T, which in turn used a tri-basic motif to engage an acidic patch on its substrate FANCD2, positions the E2 active site next to the target lysine on the globular substrate[190,191]. This mechanism is structurally more constrained compared to that for disordered peptides. However, deeper insight into such mechanisms may be particularly useful for the development of novel degrader molecules.

While the past few years have been an immensely productive time in understanding the molecular basis of ubiquitination, many questions remain unanswered. The wealth of novel structural information is largely reserved to CRLs. This class of RING E3s is immensely important both due to their prominent involvement in many diseases and their therapeutic potential. However, much less is known about all the other RING E3s including the TRIM family. While this Thesis presents novel insights into TRIM21, studies presenting structural, biochemical and cellular insights into the mechanisms of other RINGs will be required to gain a deeper understanding of E3 function. Future work will both illuminate new opportunities in understanding human health and disease while improving the development of novel degrader molecules.

# Chapter 7 References


1 Komander, D. & Rape, M. The ubiquitin code. *Annu Rev Biochem* **81**, 203-229, doi:10.1146/annurev-biochem-060310-170328 (2012).

2 Swatek, K. N. & Komander, D. Ubiquitin modifications. *Cell Res* **26**, 399-422, doi:10.1038/cr.2016.39 (2016).

3 Kirisako, T. *et al.* A ubiquitin ligase complex assembles linear polyubiquitin chains. *EMBO J* **25**, 4877-4887, doi:10.1038/sj.emboj.7601360 (2006).

4 Scaglione, K. M. *et al.* The ubiquitin-conjugating enzyme (E2) Ube2w ubiquitinates the N terminus of substrates. *J Biol Chem* **288**, 18784-18788, doi:10.1074/jbc.C113.477596 (2013).

5 Tatham, M. H., Plechanovova, A., Jaffray, E. G., Salmen, H. & Hay, R. T. Ube2W conjugates ubiquitin to alpha-amino groups of protein N-termini. *Biochem J* **453**, 137-145, doi:10.1042/BJ20130244 (2013).

6 Weber, A. *et al.* Sequential Poly-ubiquitylation by Specialized Conjugating Enzymes Expands the Versatility of a Quality Control Ubiquitin Ligase. *Mol Cell* **63**, 827-839, doi:10.1016/j.molcel.2016.07.020 (2016).

7 Pao, K. C. *et al.* Activity-based E3 ligase profiling uncovers an E3 ligase with esterification activity. *Nature* **556**, 381-385, doi:10.1038/s41586-018-0026-1 (2018).

8 Stewart, M. D., Ritterhoff, T., Klevit, R. E. & Brzovic, P. S. E2 enzymes: more than just middle men. *Cell Res* **26**, 423-440, doi:10.1038/cr.2016.35 (2016).

9 Thrower, J. S., Hoffman, L., Rechsteiner, M. & Pickart, C. M. Recognition of the polyubiquitin proteolytic signal. *EMBO J* **19**, 94-102, doi:10.1093/emboj/19.1.94 (2000).

10 Nathan, J. A., Kim, H. T., Ting, L., Gygi, S. P. & Goldberg, A. L. Why do cellular proteins linked to K63-polyubiquitin chains not associate with proteasomes? *EMBO J* **32**, 552-565, doi:10.1038/emboj.2012.354 (2013).

11 Deng, L. *et al.* Activation of the IkappaB kinase complex by TRAF6 requires a dimeric ubiquitin-conjugating enzyme complex and a unique polyubiquitin chain. *Cell* **103**, 351-361, doi:10.1016/s0092-8674(00)00126-4 (2000).

12 Wang, C. *et al.* TAK1 is a ubiquitin-dependent kinase of MKK and IKK. *Nature* **412**, 346-351, doi:10.1038/35085597 (2001).

13 Xia, Z. P. *et al.* Direct activation of protein kinases by unanchored polyubiquitin chains. *Nature* **461**, 114-119, doi:10.1038/nature08247 (2009).

14 Popovic, D., Vucic, D. & Dikic, I. Ubiquitination in disease pathogenesis and treatment. *Nat Med* **20**, 1242-1253, doi:10.1038/nm.3739 (2014).

15 Li, W. *et al.* Genome-wide and functional annotation of human E3 ubiquitin ligases identifies MULAN, a mitochondrial E3 that regulates the organelle's dynamics and signaling. *PLoS One* **3**, e1487, doi:10.1371/journal.pone.0001487 (2008).

16 Deshaies, R. J. & Joazeiro, C. A. RING domain E3 ubiquitin ligases. *Annu Rev Biochem* **78**, 399-434, doi:10.1146/annurev.biochem.78.101807.093809 (2009).

17 Buetow, L. & Huang, D. T. Structural insights into the catalysis and regulation of E3 ubiquitin ligases. *Nat Rev Mol Cell Biol* **17**, 626-642, doi:10.1038/nrm.2016.91 (2016).

18 Zheng, N. & Shabek, N. Ubiquitin Ligases: Structure, Function, and Regulation. *Annu Rev Biochem* **86**, 129-157, doi:10.1146/annurev-biochem-060815-014922 (2017).

19 Plechanovova, A., Jaffray, E. G., Tatham, M. H., Naismith, J. H. & Hay, R. T. Structure of a RING E3 ligase and ubiquitin-loaded E2 primed for catalysis. *Nature* **489**, 115-120, doi:10.1038/nature11376 (2012).

20 Dou, H., Buetow, L., Sibbet, G. J., Cameron, K. & Huang, D. T. BIRC7-E2 ubiquitin conjugate structure reveals the mechanism of ubiquitin transfer by a RING dimer. *Nat Struct Mol Biol* **19**, 876-883, doi:10.1038/nsmb.2379 (2012).

21 Pruneda, J. N. *et al.* Structure of an E3:E2~Ub complex reveals an allosteric mechanism shared among RING/U-box ligases. *Mol Cell* **47**, 933-942, doi:10.1016/j.molcel.2012.07.001 (2012).

22 Walden, H. & Rittinger, K. RBR ligase-mediated ubiquitin transfer: a tale with many twists and turns. *Nat Struct Mol Biol* **25**, 440-445, doi:10.1038/s41594-018-0063-3 (2018).

23 Marin, I., Lucas, J. I., Gradilla, A. C. & Ferrus, A. Parkin and relatives: the RBR family of ubiquitin ligases. *Physiol Genomics* **17**, 253-263, doi:10.1152/physiolgenomics.00226.2003 (2004).

24 Rotin, D. & Kumar, S. Physiological functions of the HECT family of ubiquitin ligases. *Nat Rev Mol Cell Biol* **10**, 398-409, doi:10.1038/nrm2690 (2009).

25 Gundogdu, M. & Walden, H. Structural basis of generic versus specific E2-RING E3 interactions in protein ubiquitination. *Protein Sci* **28**, 1758-1770, doi:10.1002/pro.3690 (2019).

26 Williamson, A. *et al.* Identification of a physiological E2 module for the human anaphase-promoting complex. *Proc Natl Acad Sci U S A* **106**, 18213-18218, doi:10.1073/pnas.0907887106 (2009).

27 Fletcher, A. J., Mallery, D. L., Watkinson, R. E., Dickson, C. F. & James, L. C. Sequential ubiquitination and deubiquitination enzymes synchronize the dual sensor and effector functions of TRIM21. *Proc Natl Acad Sci U S A* **112**, 10014-10019, doi:10.1073/pnas.1507534112 (2015).

28 McEwan, W. A. *et al.* Intracellular antibody-bound pathogens stimulate immune signaling via the Fc receptor TRIM21. *Nat Immunol* **14**, 327-336, doi:10.1038/ni.2548 (2013).

29 Christensen, D. E., Brzovic, P. S. & Klevit, R. E. E2-BRCA1 RING interactions dictate synthesis of mono- or specific polyubiquitin chain linkages. *Nat Struct Mol Biol* **14**, 941-948, doi:10.1038/nsmb1295 (2007).

30 Streich, F. C., Jr. & Lima, C. D. Capturing a substrate in an activated RING E3/E2-SUMO complex. *Nature* **536**, 304-308, doi:10.1038/nature19071 (2016).

31 Scott, D. C. *et al.* Structure of a RING E3 trapped in action reveals ligation mechanism for the ubiquitin-like protein NEDD8. *Cell* **157**, 1671-1684, doi:10.1016/j.cell.2014.04.037 (2014).

32 Eddins, M. J., Carlile, C. M., Gomez, K. M., Pickart, C. M. & Wolberger, C. Mms2-Ubc13 covalently bound to ubiquitin reveals the structural basis of linkage-specific polyubiquitin chain formation. *Nat Struct Mol Biol* **13**, 915-920, doi:10.1038/nsmb1148 (2006).

33 McKenna, S. *et al.* An NMR-based model of the ubiquitin-bound human ubiquitin conjugation complex Mms2.Ubc13. The structural basis for lysine 63 chain catalysis. *J Biol Chem* **278**, 13151-13158, doi:10.1074/jbc.M212353200 (2003).

34 Wickliffe, K. E., Lorenz, S., Wemmer, D. E., Kuriyan, J. & Rape, M. The mechanism of linkage-specific ubiquitin chain elongation by a single-subunit E2. *Cell* **144**, 769-781, doi:10.1016/j.cell.2011.01.035 (2011).

35 Stieglitz, B. *et al.* Structural basis for ligase-specific conjugation of linear ubiquitin chains by HOIP. *Nature* **503**, 422-426, doi:10.1038/nature12638 (2013).

36 Sakamoto, K. M. *et al.* Protacs: chimeric molecules that target proteins to the Skp1-Cullin-F box complex for ubiquitination and degradation. *Proc Natl Acad Sci U S A* **98**, 8554-8559, doi:10.1073/pnas.141230798 (2001).

37 Schapira, M., Calabrese, M. F., Bullock, A. N. & Crews, C. M. Targeted protein degradation: expanding the toolbox. *Nat Rev Drug Discov* **18**, 949-963, doi:10.1038/s41573-019-0047-y (2019).

38 Verma, R., Mohl, D. & Deshaies, R. J. Harnessing the Power of Proteolysis for Targeted Protein Inactivation. *Mol Cell* **77**, 446-460, doi:10.1016/j.molcel.2020.01.010 (2020).

39 Deshaies, R. J. Multispecific drugs herald a new era of biopharmaceutical innovation. *Nature* **580**, 329-338, doi:10.1038/s41586-020-2168-1 (2020).

40 Ito, T. *et al.* Identification of a primary target of thalidomide teratogenicity. *Science* **327**, 1345-1350, doi:10.1126/science.1177319 (2010).

41 Lu, G. *et al.* The myeloma drug lenalidomide promotes the cereblon-dependent destruction of Ikaros proteins. *Science* **343**, 305-309, doi:10.1126/science.1244917 (2014).

42 Kronke, J. *et al.* Lenalidomide causes selective degradation of IKZF1 and IKZF3 in multiple myeloma cells. *Science* **343**, 301-305, doi:10.1126/science.1244851 (2014).

43 Gandhi, A. K. *et al.* Immunomodulatory agents lenalidomide and pomalidomide co-stimulate T cells by inducing degradation of T cell repressors Ikaros and Aiolos via modulation of the E3 ubiquitin ligase complex CRL4(CRBN.). *Br J Haematol* **164**, 811-821, doi:10.1111/bjh.12708 (2014).

44 Winter, G. E. *et al.* DRUG DEVELOPMENT. Phthalimide conjugation as a strategy for in vivo target protein degradation. *Science* **348**, 1376-1381, doi:10.1126/science.aab1433 (2015).

45 Bondeson, D. P. *et al.* Catalytic in vivo protein knockdown by small-molecule PROTACs. *Nat Chem Biol* **11**, 611-617, doi:10.1038/nchembio.1858 (2015).

46 Zengerle, M., Chan, K. H. & Ciulli, A. Selective Small Molecule Induced Degradation of the BET Bromodomain Protein BRD4. *ACS Chem Biol* **10**, 1770-1777, doi:10.1021/acschembio.5b00216 (2015).

47 Petroski, M. D. & Deshaies, R. J. Function and regulation of cullin-RING ubiquitin ligases. *Nat Rev Mol Cell Biol* **6**, 9-20, doi:10.1038/nrm1547 (2005).

48 Harper, J. W. & Schulman, B. A. Cullin-RING Ubiquitin Ligase Regulatory Circuits: a Quarter Century Beyond the F-box Hypothesis. *Annu Rev Biochem*, doi:10.1146/annurev-biochem-090120-013613 (2021).

49 Marin, I. Origin and diversification of TRIM ubiquitin ligases. *PLoS One* **7**, e50030, doi:10.1371/journal.pone.0050030 (2012).

50 Ozato, K., Shin, D. M., Chang, T. H. & Morse, H. C., 3rd. TRIM family proteins and their emerging roles in innate immunity. *Nat Rev Immunol* **8**, 849-860, doi:10.1038/nri2413 (2008).

51 McNab, F. W., Rajsbaum, R., Stoye, J. P. & O'Garra, A. Tripartite-motif proteins and innate immune regulation. *Curr Opin Immunol* **23**, 46-56, doi:10.1016/j.coi.2010.10.021 (2011).

52 James, L. C., Keeble, A. H., Khan, Z., Rhodes, D. A. & Trowsdale, J. Structural basis for PRYSPRY-mediated tripartite motif (TRIM) protein function. *Proc Natl Acad Sci U S A* **104**, 6200-6205, doi:10.1073/pnas.0609174104 (2007).

53 Mallery, D. L. *et al.* Antibodies mediate intracellular immunity through tripartite motif-containing 21 (TRIM21). *Proc Natl Acad Sci U S A* **107**, 19985-19990, doi:10.1073/pnas.1014074107 (2010).

54 Norris, D. A. *et al.* The role of RNP, Sm, and SS-A/Ro-specific antisera from patients with lupus erythematosus in inducing antibody-dependent cellular cytotoxicity (ADCC) of targets coated with nonhistone nuclear antigens. *Clin Immunol Immunopathol* **31**, 311-320, doi:10.1016/0090-1229(84)90084-9 (1984).

55 Oke, V. & Wahren-Herlenius, M. The immunobiology of Ro52 (TRIM21) in autoimmunity: a critical review. *J Autoimmun* **39**, 77-82, doi:10.1016/j.jaut.2012.01.014 (2012).

56 Yoshimi, R. *et al.* Gene disruption study reveals a nonredundant role for TRIM21/Ro52 in NF-kappaB-dependent cytokine expression in fibroblasts. *J Immunol* **182**, 7527-7538, doi:10.4049/jimmunol.0804121 (2009).

57 Espinosa, A. *et al.* Loss of the lupus autoantigen Ro52/Trim21 induces tissue inflammation and systemic autoimmunity by disregulating the IL-23-Th17 pathway. *J Exp Med* **206**, 1661-1671, doi:10.1084/jem.20090585 (2009).

58 Ozato, K. *et al.* Comment on "Gene disruption study reveals a nonredundant role for TRIM21/Ro52 in NF-kappa B-dependent cytokine expression in fibroblasts". *J Immunol* **183**, 7619; author reply 7720-7611, doi:10.4049/jimmunol.0990103 (2009).

59 Rhodes, D. A. & Trowsdale, J. TRIM21 is a trimeric protein that binds IgG Fc via the B30.2 domain. *Mol Immunol* **44**, 2406-2414, doi:10.1016/j.molimm.2006.10.013 (2007).

60 Keeble, A. H., Khan, Z., Forster, A. & James, L. C. TRIM21 is an IgG receptor that is structurally, thermodynamically, and kinetically conserved. *Proc Natl Acad Sci U S A* **105**, 6045-6050, doi:10.1073/pnas.0800159105 (2008).

61 Hauler, F., Mallery, D. L., McEwan, W. A., Bidgood, S. R. & James, L. C. AAA ATPase p97/VCP is essential for TRIM21-mediated virus neutralization. *Proc Natl Acad Sci U S A* **109**, 19733-19738, doi:10.1073/pnas.1210659109 (2012).

62 Clift, D. *et al.* A Method for the Acute and Rapid Degradation of Endogenous Proteins. *Cell* **171**, 1692-1706 e1618, doi:10.1016/j.cell.2017.10.033 (2017).

63 Vaysburd, M. *et al.* Intracellular antibody receptor TRIM21 prevents fatal viral infection. *Proc Natl Acad Sci U S A* **110**, 12397-12401, doi:10.1073/pnas.1301918110 (2013).

64 Caddy, S. L. *et al.* Intracellular neutralisation of rotavirus by VP6-specific IgG. *PLoS Pathog* **16**, e1008732, doi:10.1371/journal.ppat.1008732 (2020).

65 Watkinson, R. E., McEwan, W. A., Tam, J. C., Vaysburd, M. & James, L. C. TRIM21 Promotes cGAS and RIG-I Sensing of Viral Genomes during Infection by Antibody-Opsonized Virus. *PLoS Pathog* **11**, e1005253, doi:10.1371/journal.ppat.1005253 (2015).

66 Lecomte, J. *et al.* Protection from mouse hepatitis virus type 3-induced acute disease by an anti-nucleoprotein monoclonal antibody. Brief report. *Arch Virol* **97**, 123-130, doi:10.1007/BF01310740 (1987).
67 Carragher, D. M., Kaminski, D. A., Moquin, A., Hartson, L. & Randall, T. D. A novel role for non-neutralizing antibodies against nucleoprotein in facilitating resistance to influenza virus. *J Immunol* **181**, 4168-4176, doi:10.4049/jimmunol.181.6.4168 (2008).
68 LaMere, M. W. *et al.* Contributions of antinucleoprotein IgG to heterosubtypic immunity against influenza virus. *J Immunol* **186**, 4331-4339, doi:10.4049/jimmunol.1003057 (2011).
69 Nakanaga, K., Yamanouchi, K. & Fujiwara, K. Protective effect of monoclonal antibodies on lethal mouse hepatitis virus infection in mice. *J Virol* **59**, 168-171, doi:10.1128/JVI.59.1.168-171.1986 (1986).
70 Richter, K. & Oxenius, A. Non-neutralizing antibodies protect from chronic LCMV infection independently of activating FcgammaR or complement. *Eur J Immunol* **43**, 2349-2360, doi:10.1002/eji.201343566 (2013).
71 Straub, T. *et al.* Nucleoprotein-specific nonneutralizing antibodies speed up LCMV elimination independently of complement and FcgammaR. *Eur J Immunol* **43**, 2338-2348, doi:10.1002/eji.201343565 (2013).
72 Sambhara, S. *et al.* Heterosubtypic immunity against human influenza A viruses, including recently emerged avian H5 and H9 viruses, induced by FLU-ISCOM vaccine in mice requires both cytotoxic T-lymphocyte and macrophage function. *Cell Immunol* **211**, 143-153, doi:10.1006/cimm.2001.1835 (2001).
73 Caddy, S. L. *et al.* Viral nucleoprotein antibodies activate TRIM21 and induce T cell immunity. *EMBO J*, e106228, doi:10.15252/embj.2020106228 (2020).
74 Yao, T. & Cohen, R. E. A cryptic protease couples deubiquitination and degradation by the proteasome. *Nature* **419**, 403-407, doi:10.1038/nature01071 (2002).
75 Labzin, L. I. *et al.* Antibody and DNA sensing pathways converge to activate the inflammasome during primary human macrophage infection. *EMBO J* **38**, e101365, doi:10.15252/embj.2018101365 (2019).
76 Rhodes, D. A. *et al.* The 52 000 MW Ro/SS-A autoantigen in Sjogren's syndrome/systemic lupus erythematosus (Ro52) is an interferon-gamma inducible tripartite motif protein associated with membrane proximal structures. *Immunology* **106**, 246-256, doi:10.1046/j.1365-2567.2002.01417.x (2002).
77 Zeng, J., Slodkowicz, G. & James, L. C. Rare missense variants in the human cytosolic antibody receptor preserve antiviral function. *Elife* **8**, doi:10.7554/eLife.48339 (2019).
78 Reymond, A. *et al.* The tripartite motif family identifies cell compartments. *EMBO J* **20**, 2140-2151, doi:10.1093/emboj/20.9.2140 (2001).
79 Sanchez, J. G. *et al.* The tripartite motif coiled-coil is an elongated antiparallel hairpin dimer. *Proc Natl Acad Sci U S A* **111**, 2494-2499, doi:10.1073/pnas.1318962111 (2014).
80 Dickson, C. *et al.* Intracellular antibody signalling is regulated by phosphorylation of the Fc receptor TRIM21. *Elife* **7**, doi:10.7554/eLife.32660 (2018).
81 Bidgood, S. R., Tam, J. C., McEwan, W. A., Mallery, D. L. & James, L. C. Translocalized IgA mediates neutralization and stimulates innate immunity inside infected cells. *Proc Natl Acad Sci U S A* **111**, 13463-13468, doi:10.1073/pnas.1410980111 (2014).
82 McEwan, W. A. *et al.* Regulation of virus neutralization and the persistent fraction by TRIM21. *J Virol* **86**, 8482-8491, doi:10.1128/JVI.00728-12 (2012).

83 Plechanovova, A. *et al.* Mechanism of ubiquitylation by dimeric RING ligase RNF4. *Nat Struct Mol Biol* **18**, 1052-1059, doi:10.1038/nsmb.2108 (2011).

84 Koliopoulos, M. G., Esposito, D., Christodoulou, E., Taylor, I. A. & Rittinger, K. Functional role of TRIM E3 ligase oligomerization and regulation of catalytic activity. *EMBO J* **35**, 1204-1218, doi:10.15252/embj.201593741 (2016).

85 Sanchez, J. G. *et al.* Mechanism of TRIM25 Catalytic Activation in the Antiviral RIG-I Pathway. *Cell Rep* **16**, 1315-1325, doi:10.1016/j.celrep.2016.06.070 (2016).

86 Koliopoulos, M. G. *et al.* Molecular mechanism of influenza A NS1-mediated TRIM25 recognition and inhibition. *Nat Commun* **9**, 1820, doi:10.1038/s41467-018-04214-8 (2018).

87 Wagner, J. M. *et al.* Mechanism of B-box 2 domain-mediated higher-order assembly of the retroviral restriction factor TRIM5alpha. *Elife* **5**, doi:10.7554/eLife.16309 (2016).

88 Wagner, J. M. *et al.* General Model for Retroviral Capsid Pattern Recognition by TRIM5 Proteins. *J Virol* **92**, doi:10.1128/JVI.01563-17 (2018).

89 Espinosa, A. *et al.* Anti-Ro52 autoantibodies from patients with Sjogren's syndrome inhibit the Ro52 E3 ligase activity by blocking the E3/E2 interface. *J Biol Chem* **286**, 36478-36491, doi:10.1074/jbc.M111.241786 (2011).

90 Yudina, Z. *et al.* RING Dimerization Links Higher-Order Assembly of TRIM5alpha to Synthesis of K63-Linked Polyubiquitin. *Cell Rep* **12**, 788-797, doi:10.1016/j.celrep.2015.06.072 (2015).

91 Clift, D., So, C., McEwan, W. A., James, L. C. & Schuh, M. Acute and rapid degradation of endogenous proteins by Trim-Away. *Nat Protoc* **13**, 2149-2175, doi:10.1038/s41596-018-0028-3 (2018).

92 Chen, X. *et al.* Degradation of endogenous proteins and generation of a null-like phenotype in zebrafish using Trim-Away technology. *Genome Biol* **20**, 19, doi:10.1186/s13059-019-1624-4 (2019).

93 Katsinelos, T., Tuck, B. J., Mukadam, A. S. & McEwan, W. A. The Role of Antibodies and Their Receptors in Protection Against Ordered Protein Assembly in Neurodegeneration. *Front Immunol* **10**, 1139, doi:10.3389/fimmu.2019.01139 (2019).

94 McEwan, W. A. *et al.* Cytosolic Fc receptor TRIM21 inhibits seeded tau aggregation. *Proc Natl Acad Sci U S A* **114**, 574-579, doi:10.1073/pnas.1607215114 (2017).

95 Bottermann, M. *et al.* TRIM21 mediates antibody inhibition of adenovirus-based gene delivery and vaccination. *Proc Natl Acad Sci U S A* **115**, 10440-10445, doi:10.1073/pnas.1806314115 (2018).

96 Gibson, D. G. *et al.* Enzymatic assembly of DNA molecules up to several hundred kilobases. *Nat Methods* **6**, 343-345, doi:10.1038/nmeth.1318 (2009).

97 Liman, E. R., Tytgat, J. & Hess, P. Subunit stoichiometry of a mammalian K+ channel determined by construction of multimeric cDNAs. *Neuron* **9**, 861-871, doi:10.1016/0896-6273(92)90239-a (1992).

98 Zennou, V., Perez-Caballero, D., Gottlinger, H. & Bieniasz, P. D. APOBEC3G incorporation into human immunodeficiency virus type 1 particles. *J Virol* **78**, 12058-12061, doi:10.1128/JVI.78.21.12058-12061.2004 (2004).

99 Studier, F. W. Protein production by auto-induction in high density shaking cultures. *Protein Expr Purif* **41**, 207-234, doi:10.1016/j.pep.2005.01.016 (2005).

100 Pickart, C. M. & Raasi, S. in *Ubiquitin and Protein Degradation, Part B Methods in Enzymology* 21-36 (2005).

101 Branigan, E., Plechanovova, A., Jaffray, E. G., Naismith, J. H. & Hay, R. T. Structural basis for the RING-catalyzed synthesis of K63-linked ubiquitin chains. *Nat Struct Mol Biol* **22**, 597-602, doi:10.1038/nsmb.3052 (2015).

102 Bottermann, M. *et al.* Antibody-antigen kinetics constrain intracellular humoral immunity. *Sci Rep* **6**, 37457, doi:10.1038/srep37457 (2016).

103 Foss, S. *et al.* TRIM21 Immune Signaling Is More Sensitive to Antibody Affinity Than Its Neutralization Activity. *J Immunol* **196**, 3452-3459, doi:10.4049/jimmunol.1502601 (2016).

104 Fersht, A. *Enzyme Structure and Mechanism*. (WH Freeman, New York, NY, 1977).

105 Gorrec, F. The MORPHEUS protein crystallization screen. *J Appl Crystallogr* **42**, 1035-1042, doi:10.1107/S0021889809042022 (2009).

106 Kabsch, W. Xds. *Acta Crystallogr D Biol Crystallogr* **66**, 125-132, doi:10.1107/S0907444909047337 (2010).

107 Adams, P. D. *et al.* PHENIX: a comprehensive Python-based system for macromolecular structure solution. *Acta Crystallogr D Biol Crystallogr* **66**, 213-221, doi:10.1107/S0907444909052925 (2010).

108 Emsley, P. & Cowtan, K. Coot: model-building tools for molecular graphics. *Acta Crystallogr D Biol Crystallogr* **60**, 2126-2132, doi:10.1107/S0907444904019158 (2004).

109 Murshudov, G. N. *et al.* REFMAC5 for the refinement of macromolecular crystal structures. *Acta Crystallogr D Biol Crystallogr* **67**, 355-367, doi:10.1107/S0907444911001314 (2011).

110 Long, F. *et al.* AceDRG: a stereochemical description generator for ligands. *Acta Crystallogr D Struct Biol* **73**, 112-122, doi:10.1107/S2059798317000067 (2017).

111 Gorrec, F. The MORPHEUS II protein crystallization screen. *Acta Crystallogr F Struct Biol Commun* **71**, 831-837, doi:10.1107/S2053230X1500967X (2015).

112 Sammak, S. *et al.* Crystal Structures and Nuclear Magnetic Resonance Studies of the Apo Form of the c-MYC:MAX bHLHZip Complex Reveal a Helical Basic Region in the Absence of DNA. *Biochemistry* **58**, 3144-3154, doi:10.1021/acs.biochem.9b00296 (2019).

113 Kiss, L. *et al.* A tri-ionic anchor mechanism drives Ube2N-specific recruitment and K63-chain ubiquitination in TRIM ligases. *Nat Commun* **10**, 4502, doi:10.1038/s41467-019-12388-y (2019).

114 Vijay-Kumar, S., Bugg, C. E. & Cook, W. J. Structure of ubiquitin refined at 1.8 A resolution. *J Mol Biol* **194**, 531-544, doi:10.1016/0022-2836(87)90679-6 (1987).

115 Moraes, T. F. *et al.* Crystal structure of the human ubiquitin conjugating enzyme complex, hMms2-hUbc13. *Nat Struct Biol* **8**, 669-673, doi:10.1038/90373 (2001).

116 Afonine, P. V. *et al.* Towards automated crystallographic structure refinement with phenix.refine. *Acta Crystallogr D Biol Crystallogr* **68**, 352-367, doi:10.1107/S0907444912001308 (2012).

117 Vittal, V. *et al.* Intrinsic disorder drives N-terminal ubiquitination by Ube2w. *Nat Chem Biol* **11**, 83-89, doi:10.1038/nchembio.1700 (2015).

118 Solyom, Z. *et al.* BEST-TROSY experiments for time-efficient sequential resonance assignment of large disordered proteins. *J Biomol NMR* **55**, 311-321, doi:10.1007/s10858-013-9715-0 (2013).

119 Vranken, W. F. *et al.* The CCPN data model for NMR spectroscopy: development of a software pipeline. *Proteins* **59**, 687-696, doi:10.1002/prot.20449 (2005).

120 Madeira, F. *et al.* The EMBL-EBI search and sequence analysis tools APIs in 2019. *Nucleic Acids Res* **47**, W636-W641, doi:10.1093/nar/gkz268 (2019).

121 UniProt, C. UniProt: the universal protein knowledgebase in 2021. *Nucleic Acids Res* **49**, D480-D489, doi:10.1093/nar/gkaa1100 (2021).

122 Waterhouse, A. M., Procter, J. B., Martin, D. M., Clamp, M. & Barton, G. J. Jalview Version 2--a multiple sequence alignment editor and analysis workbench. *Bioinformatics* **25**, 1189-1191, doi:10.1093/bioinformatics/btp033 (2009).

123 Shvets, E., Bitsikas, V., Howard, G., Hansen, C. G. & Nichols, B. J. Dynamic caveolae exclude bulk membrane proteins and are required for sorting of excess glycosphingolipids. *Nat Commun* **6**, 6867, doi:10.1038/ncomms7867 (2015).

124 Fletcher, A. J. *et al.* TRIM5alpha requires Ube2W to anchor Lys63-linked ubiquitin chains and restrict reverse transcription. *EMBO J* **34**, 2078-2095, doi:10.15252/embj.201490361 (2015).

125 Fletcher, A. J. *et al.* Trivalent RING Assembly on Retroviral Capsids Activates TRIM5 Ubiquitination and Innate Immune Signaling. *Cell Host Microbe* **24**, 761-775 e766, doi:10.1016/j.chom.2018.10.007 (2018).

126 Ganser-Pornillos, B. K. *et al.* Hexagonal assembly of a restricting TRIM5alpha protein. *Proc Natl Acad Sci U S A* **108**, 534-539, doi:10.1073/pnas.1013426108 (2011).

127 Middleton, A. J. *et al.* The activity of TRAF RING homo- and heterodimers is regulated by zinc finger 1. *Nat Commun* **8**, 1788, doi:10.1038/s41467-017-01665-3 (2017).

128 Fu, T. M., Shen, C., Li, Q., Zhang, P. & Wu, H. Mechanism of ubiquitin transfer promoted by TRAF6. *Proc Natl Acad Sci U S A* **115**, 1783-1788, doi:10.1073/pnas.1721788115 (2018).

129 Russel, A. J. & Fersht, A. R. Rational modification of enzyme catalysis by engineering surface charge. *Nature* **328**, 496-500, doi:10.1038/328496a0 (1987).

130 Li, Y. *et al.* Structural insights into the TRIM family of ubiquitin E3 ligases. *Cell Res* **24**, 762-765, doi:10.1038/cr.2014.46 (2014).

131 Behera, A. P. *et al.* Structural insights into the nanomolar affinity of RING E3 ligase ZNRF1 for Ube2N and its functional implications. *Biochem J* **475**, 1569-1582, doi:10.1042/BCJ20170909 (2018).

132 Nayak, D. & Sivaraman, J. Structure of LNX1:Ubc13~Ubiquitin Complex Reveals the Role of Additional Motifs for the E3 Ligase Activity of LNX1. *J Mol Biol* **430**, 1173-1188, doi:10.1016/j.jmb.2018.02.016 (2018).

133 Zhang, M. *et al.* Chaperoned ubiquitylation--crystal structures of the CHIP U box E3 ubiquitin ligase and a CHIP-Ubc13-Uev1a complex. *Mol Cell* **20**, 525-538, doi:10.1016/j.molcel.2005.09.023 (2005).

134 Hodson, C., Purkiss, A., Miles, J. A. & Walden, H. Structure of the human FANCL RING-Ube2T complex reveals determinants of cognate E3-E2 selection. *Structure* **22**, 337-344, doi:10.1016/j.str.2013.12.004 (2014).

135 Scott, D. C., Monda, J. K., Bennett, E. J., Harper, J. W. & Schulman, B. A. N-Terminal Acetylation Acts as an Avidity Enhancer Within an Interconnected Multiprotein Complex. *Science* **334**, 674-678, doi:10.1126/science.1209307 (2011).

136 Wright, J. D., Mace, P. D. & Day, C. L. Secondary ubiquitin-RING docking enhances Arkadia and Ark2C E3 ligase activity. *Nat Struct Mol Biol* **23**, 45-52, doi:10.1038/nsmb.3142 (2016).

137 Buetow, L. *et al.* Activation of a primed RING E3-E2-ubiquitin complex by non-covalent ubiquitin. *Mol Cell* **58**, 297-310, doi:10.1016/j.molcel.2015.02.017 (2015).
138 Dou, H., Buetow, L., Sibbet, G. J., Cameron, K. & Huang, D. T. Essentiality of a non-RING element in priming donor ubiquitin for catalysis by a monomeric E3. *Nat Struct Mol Biol* **20**, 982-986, doi:10.1038/nsmb.2621 (2013).
139 Beck, M. *et al.* The quantitative proteome of a human cell line. *Mol Syst Biol* **7**, 549, doi:10.1038/msb.2011.82 (2011).
140 Hein, M. Y. *et al.* A human interactome in three quantitative dimensions organized by stoichiometries and abundances. *Cell* **163**, 712-723, doi:10.1016/j.cell.2015.09.053 (2015).
141 Baek, K. *et al.* NEDD8 nucleates a multivalent cullin-RING-UBE2D ubiquitin ligation assembly. *Nature* **578**, 461-466, doi:10.1038/s41586-020-2000-y (2020).
142 Hofmann, R. M. & Pickart, C. M. Noncanonical MMS2-encoded ubiquitin-conjugating enzyme functions in assembly of novel polyubiquitin chains for DNA repair. *Cell* **96**, 645-653, doi:10.1016/s0092-8674(00)80575-9 (1999).
143 VanDemark, A. P., Hofmann, R. M., Tsui, C., Pickart, C. M. & Wolberger, C. Molecular insights into polyubiquitin chain assembly: crystal structure of the Mms2/Ubc13 heterodimer. *Cell* **105**, 711-720, doi:10.1016/s0092-8674(01)00387-7 (2001).
144 Yunus, A. A. & Lima, C. D. Lysine activation and functional analysis of E2-mediated conjugation in the SUMO pathway. *Nat Struct Mol Biol* **13**, 491-499, doi:10.1038/nsmb1104 (2006).
145 Lide, D. R. *CRC handbook of chemistry and physics: a ready-reference book of chemical and phyical data*. Vol. 72 (CRC Press, 1991).
146 Llopis, J., McCaffery, J. M., Miyawaki, A., Farquhar, M. G. & Tsien, R. Y. Measurement of cytosolic, mitochondrial, and Golgi pH in single living cells with green fluorescent proteins. *Proc Natl Acad Sci U S A* **95**, 6803-6808, doi:10.1073/pnas.95.12.6803 (1998).
147 Hospenthal, M. K., Freund, S. M. & Komander, D. Assembly, analysis and architecture of atypical ubiquitin chains. *Nat Struct Mol Biol* **20**, 555-565, doi:10.1038/nsmb.2547 (2013).
148 Lange, O. F. *et al.* Recognition dynamics up to microseconds revealed from an RDC-derived ubiquitin ensemble in solution. *Science* **320**, 1471-1475, doi:10.1126/science.1157092 (2008).
149 Komander, D. *et al.* Molecular discrimination of structurally equivalent Lys 63-linked and linear polyubiquitin chains. *EMBO Rep* **10**, 466-473, doi:10.1038/embor.2009.55 (2009).
150 Zeng, J. *et al.* Target-induced clustering activates Trim-Away of pathogens and proteins. *Nat Struct Mol Biol* **28**, 278-289, doi:10.1038/s41594-021-00560-2 (2021).
151 Fuseya, Y. *et al.* The HOIL-1L ligase modulates immune signalling and cell death via monoubiquitination of LUBAC. *Nat Cell Biol* **22**, 663-673, doi:10.1038/s41556-020-0517-9 (2020).
152 Smith, B. E. *et al.* Differential PROTAC substrate specificity dictated by orientation of recruited E3 ligase. *Nat Commun* **10**, 131, doi:10.1038/s41467-018-08027-7 (2019).
153 Ohtake, F., Tsuchiya, H., Saeki, Y. & Tanaka, K. K63 ubiquitylation triggers proteasomal degradation by seeding branched ubiquitin chains. *Proc Natl Acad Sci U S A* **115**, E1401-E1408, doi:10.1073/pnas.1716673115 (2018).

154 Ohtake, F., Saeki, Y., Ishido, S., Kanno, J. & Tanaka, K. The K48-K63 Branched Ubiquitin Chain Regulates NF-kappaB Signaling. *Mol Cell* **64**, 251-266, doi:10.1016/j.molcel.2016.09.014 (2016).
155 Li, Y. L. *et al.* Primate TRIM5 proteins form hexagonal nets on HIV-1 capsids. *Elife* **5**, doi:10.7554/eLife.16269 (2016).
156 Stremlau, M. *et al.* The cytoplasmic body component TRIM5alpha restricts HIV-1 infection in Old World monkeys. *Nature* **427**, 848-853, doi:10.1038/nature02343 (2004).
157 Sayah, D. M., Sokolskaja, E., Berthoux, L. & Luban, J. Cyclophilin A retrotransposition into TRIM5 explains owl monkey resistance to HIV-1. *Nature* **430**, 569-573, doi:10.1038/nature02777 (2004).
158 Pertel, T. *et al.* TRIM5 is an innate immune sensor for the retrovirus capsid lattice. *Nature* **472**, 361-365, doi:10.1038/nature09976 (2011).
159 Napetschnig, J. & Wu, H. Molecular basis of NF-kappaB signaling. *Annu Rev Biophys* **42**, 443-468, doi:10.1146/annurev-biophys-083012-130338 (2013).
160 Cadena, C. *et al.* Ubiquitin-Dependent and -Independent Roles of E3 Ligase RIPLET in Innate Immunity. *Cell* **177**, 1187-1200 e1116, doi:10.1016/j.cell.2019.03.017 (2019).
161 Dai, X., Wu, L., Sun, R. & Zhou, Z. H. Atomic Structures of Minor Proteins VI and VII in Human Adenovirus. *J Virol* **91**, doi:10.1128/JVI.00850-17 (2017).
162 Vittal, V., Wenzel, D. M., Brzovic, P. S. & Klevit, R. E. Biochemical and structural characterization of the ubiquitin-conjugating enzyme UBE2W reveals the formation of a noncovalent homodimer. *Cell Biochem Biophys* **67**, 103-110, doi:10.1007/s12013-013-9633-5 (2013).
163 Davies, C. W. *et al.* Antibody toolkit reveals N-terminally ubiquitinated substrates of UBE2W. *Nat Commun* **12**, 4608, doi:10.1038/s41467-021-24669-6 (2021).
164 Aksnes, H., Ree, R. & Arnesen, T. Co-translational, Post-translational, and Non-catalytic Roles of N-Terminal Acetyltransferases. *Mol Cell* **73**, 1097-1114, doi:10.1016/j.molcel.2019.02.007 (2019).
165 Kiss, L., Clift, D., Renner, N., Neuhaus, D. & James, L. C. RING domains act as both substrate and enzyme in a catalytic arrangement to drive self-anchored ubiquitination. *Nat Commun* **12**, 1220, doi:10.1038/s41467-021-21443-6 (2021).
166 Anandapadamanaban, M. *et al.* E3 ubiquitin-protein ligase TRIM21-mediated lysine capture by UBE2E1 reveals substrate-targeting mode of a ubiquitin-conjugating E2. *J Biol Chem* **294**, 11404-11419, doi:10.1074/jbc.RA119.008485 (2019).
167 Chatrin, C. *et al.* Structural insights into ADP-ribosylation of ubiquitin by Deltex family E3 ubiquitin ligases. *Sci Adv* **6**, doi:10.1126/sciadv.abc0418 (2020).
168 Otten, E. G. *et al.* Ubiquitylation of lipopolysaccharide by RNF213 during bacterial infection. *Nature* **594**, 111-116, doi:10.1038/s41586-021-03566-4 (2021).
169 Kelsall, I. R. *et al.* HOIL-1-catalysed ubiquitylation of unbranched glucosaccharides and its activation by ubiquitin oligomers. *bioRxiv*, 2021.2009.2010.459791, doi:10.1101/2021.09.10.459791 (2021).
170 Liu, W. *et al.* Dimeric Ube2g2 simultaneously engages donor and acceptor ubiquitins to form Lys48-linked ubiquitin chains. *EMBO J* **33**, 46-61, doi:10.1002/embj.201385315 (2014).
171 Liess, A. K. L. *et al.* Dimerization regulates the human APC/C-associated ubiquitin-conjugating enzyme UBE2S. *Sci Signal* **13**, doi:10.1126/scisignal.aba8208 (2020).

172 Ohtake, F. *et al.* Ubiquitin acetylation inhibits polyubiquitin chain elongation. *EMBO Rep* **16**, 192-201, doi:10.15252/embr.201439152 (2015).

173 Skorupka, K. A. *et al.* Hierarchical assembly governs TRIM5alpha recognition of HIV-1 and retroviral capsids. *Sci Adv* **5**, eaaw3631, doi:10.1126/sciadv.aaw3631 (2019).

174 Verma, R. *et al.* Role of Rpn11 metalloprotease in deubiquitination and degradation by the 26S proteasome. *Science* **298**, 611-615, doi:10.1126/science.1075898 (2002).

175 Trompouki, E. *et al.* CYLD is a deubiquitinating enzyme that negatively regulates NF-kappaB activation by TNFR family members. *Nature* **424**, 793-796, doi:10.1038/nature01803 (2003).

176 Zheng, N., Wang, P., Jeffrey, P. D. & Pavletich, N. P. Structure of a c-Cbl-UbcH7 complex: RING domain function in ubiquitin-protein ligases. *Cell* **102**, 533-539, doi:10.1016/s0092-8674(00)00057-x (2000).

177 Kim, M., Tezuka, T., Tanaka, K. & Yamamoto, T. Cbl-c suppresses v-Src-induced transformation through ubiquitin-dependent protein degradation. *Oncogene* **23**, 1645-1655, doi:10.1038/sj.onc.1207298 (2004).

178 Wenzel, D. M., Lissounov, A., Brzovic, P. S. & Klevit, R. E. UBCH7 reactivity profile reveals parkin and HHARI to be RING/HECT hybrids. *Nature* **474**, 105-108, doi:10.1038/nature09966 (2011).

179 Lips, C. *et al.* Who with whom: functional coordination of E2 enzymes by RING E3 ligases during poly-ubiquitylation. *EMBO J* **39**, e104863, doi:10.15252/embj.2020104863 (2020).

180 Scott, D. C. *et al.* Two Distinct Types of E3 Ligases Work in Unison to Regulate Substrate Ubiquitylation. *Cell* **166**, 1198-1214 e1124, doi:10.1016/j.cell.2016.07.027 (2016).

181 Kelsall, I. R. *et al.* TRIAD1 and HHARI bind to and are activated by distinct neddylated Cullin-RING ligase complexes. *EMBO J* **32**, 2848-2860, doi:10.1038/emboj.2013.209 (2013).

182 Duda, D. M. *et al.* Structural insights into NEDD8 activation of cullin-RING ligases: conformational control of conjugation. *Cell* **134**, 995-1006, doi:10.1016/j.cell.2008.07.022 (2008).

183 Saha, A. & Deshaies, R. J. Multimodal activation of the ubiquitin ligase SCF by Nedd8 conjugation. *Mol Cell* **32**, 21-31, doi:10.1016/j.molcel.2008.08.021 (2008).

184 Hill, S. *et al.* Robust cullin-RING ligase function is established by a multiplicity of poly-ubiquitylation pathways. *Elife* **8**, doi:10.7554/eLife.51163 (2019).

185 Read, M. A. *et al.* Nedd8 modification of cul-1 activates SCF(beta(TrCP))-dependent ubiquitination of IkappaBalpha. *Mol Cell Biol* **20**, 2326-2333, doi:10.1128/MCB.20.7.2326-2333.2000 (2000).

186 Horn-Ghetko, D. *et al.* Ubiquitin ligation to F-box protein targets by SCF-RBR E3-E3 super-assembly. *Nature* **590**, 671-676, doi:10.1038/s41586-021-03197-9 (2021).

187 Pan, M. *et al.* Structural Insights Into the Initiation and Elongation of Ubiquitination by Ubr1. *bioRxiv*, 2021.2004.2012.439291, doi:10.1101/2021.04.12.439291 (2021).

188 Witus, S. R. *et al.* BRCA1/BARD1 site-specific ubiquitylation of nucleosomal H2A is directed by BARD1. *Nat Struct Mol Biol* **28**, 268-277, doi:10.1038/s41594-020-00556-4 (2021).

189 Chang, L., Zhang, Z., Yang, J., McLaughlin, S. H. & Barford, D. Atomic structure of the APC/C and its mechanism of protein ubiquitination. *Nature* **522**, 450-454, doi:10.1038/nature14471 (2015).

190 Chaugule, V. K. *et al.* Allosteric mechanism for site-specific ubiquitination of FANCD2. *Nat Chem Biol* **16**, 291-301, doi:10.1038/s41589-019-0426-z (2020).

191 Wang, S., Wang, R., Peralta, C., Yaseen, A. & Pavletich, N. P. Structure of the FA core ubiquitin ligase closing the ID clamp on DNA. *Nat Struct Mol Biol* **28**, 300-309, doi:10.1038/s41594-021-00568-8 (2021).

192 Goldstone, D. C. *et al.* Structural studies of postentry restriction factors reveal antiparallel dimers that enable avid binding to the HIV-1 capsid lattice. *Proc Natl Acad Sci U S A* **111**, 9609-9614, doi:10.1073/pnas.1402448111 (2014).

# Chapter 8 Appendix

**Appendix Table 1 Crystallographic data table for the TRIM21-RING:Ube2N~Ub structure in Chapter 3.** Statistics in highest resolution shell are shown in parentheses.

| | **TRIM21-RING:Ube2N~Ub (6S53)** |
|---|---|
| Wavelength | 0.97952 Å |
| Resolution range | 19.76 - 2.8 (2.9 - 2.8) |
| Space group | P 1 |
| Unit cell | 49.75 83.31 86.75 89.898 89.053 88.704 |
| Total reflections | 58804 (5933) |
| Unique reflections | 32828 (3279) |
| Multiplicity | 1.8 (1.8) |
| Completeness (%) | 95.74 (96.05) |
| Mean I/sigma(I) | 12.83 (1.69) |
| Wilson B-factor | 75.78 |
| R-merge | 0.03857 (0.3994) |
| R-meas | 0.05454 (0.5649) |
| R-pim | 0.03857 (0.3994) |
| $CC_{1/2}$ | 0.998 (0.735) |
| CC* | 1 (0.921) |
| Reflections used in refinement | 32806 (3279) |
| Reflections used for R-free | 2003 (197) |
| R-work | 0.2092 (0.3203) |
| R-free | 0.2495 (0.3655) |
| CC(work) | 0.956 (0.586) |
| CC(free) | 0.924 (0.409) |
| Number of non-hydrogen atoms | 9476 |
| macromolecules | 9454 |
| ligands | 16 |
| solvent | 6 |
| Protein residues | 1214 |
| RMS(bonds) | 0.009 |
| RMS(angles) | 1.31 |
| Ramachandran favored (%) | 96.80 |
| Ramachandran allowed (%) | 2.69 |
| Ramachandran outliers (%) | 0.51 |
| Rotamer outliers (%) | 1.56 |
| Clashscore | 4.80 |
| Average B-factor | 79.03 |
| macromolecules | 79.04 |
| ligands | 77.24 |
| solvent | 59.79 |

**Appendix Table 2 Crystallographic data table for the structures presented in Chapter 4.** Statistics in highest resolution shell are shown in parentheses.

| | **Ub-R:Ube2N~Ub:Ube2V2 (7BBD)** | **Ube2N~Ub:Ube2V2 (7BBF)** |
|---|---|---|
| Wavelength | 0.9762 | 0.9762 |
| Resolution range | 19.99 - 2.2 (2.279 - 2.2) | 47.74 - 2.542 (2.633 - 2.542) |
| Space group | C 1 2 1 | P 32 |
| Unit cell | 99.15 108.36 75.14 90 104.99 90 | 145.84 145.84 49.23 90 90 120 |
| Total reflections | 275272 (27761) | 204185 (20653) |
| Unique reflections | 38727 (3856) | 38540 (3845) |
| Multiplicity | 7.1 (7.2) | 5.3 (5.4) |
| Completeness (%) | 99.41 (99.15) | 99.89 (100.00) |
| Mean I/sigma(I) | 20.18 (2.23) | 15.81 (1.17) |
| R-merge | 0.04551 (0.9457) | 0.05449 (1.347) |
| $CC_{1/2}$ | 1 (0.932) | 0.999 (0.497) |
| Reflections used in refinement | 38720 (3857) | 38506 (3845) |
| Reflections used for R-free | 2004 (200) | 2017 (203) |
| R-work | 0.2222 (0.3245) | 0.2081 (0.3483) |
| R-free | 0.2523 (0.3285) | 0.2479 (0.4045) |
| CC(work) | 0.854 (0.362) | 0.980 (0.643) |
| CC(free) | 0.852 (0.279) | 0.964 (0.480) |
| Number of non-hydrogen atoms | 4434 | 8612 |
| macromolecules | 4147 | 8573 |
| ligands | 2 | |
| solvent | 285 | 39 |
| Protein residues | 540 | 1094 |
| RMS(bonds) | 0.002 | 0.015 |
| RMS(angles) | 0.54 | 1.41 |
| Ramachandran favored (%) | 96.98 | 96.75 |
| Ramachandran allowed (%) | 3.02 | 2.79 |
| Ramachandran outliers (%) | 0 | 0.46 |
| Rotamer outliers (%) | 0.67 | 1.51 |
| Clashscore | 3.38 | 16.05 |
| Average B-factor | 52.09 | 109 |
| macromolecules | 52.8 | 109.11 |
| ligands | 23.61 | |
| solvent | 42.01 | 85.16 |
| Number of TLS groups | 15 | 58 |

**Appendix Table 3 Crystallographic data table for the TRIM21-RING:Ube2W structure presented in Chapter 5.** Statistics in highest resolution shell are shown in parentheses. This complex was crystallized by Dr Claire F Dickson, who also solved the structure and performed the refinement, together with me. This refinement is not in its final state.

| | **TRIM21-RING:Ube2W** |
|---|---|
| Resolution range | 29.46 - 2.25 (2.33 - 2.25) |
| Space group | P 1 21 1 |
| Unit cell | 62.82 75.482 63.835 90 119.307 90 |
| Total reflections | 80113 (8259) |
| Unique reflections | 24282 (2357) |
| Multiplicity | 3.3 (3.4) |
| Completeness (%) | 95.38 (96.48) |
| Mean I/sigma(I) | 11.61 (1.14) |
| Wilson B-factor | 60.75 |
| R-merge | 0.0511 (1) |
| R-meas | 0.06125 (1.188) |
| R-pim | 0.03334 (0.6352) |
| CC1/2 | 0.999 (0.586) |
| CC* | 1 (0.86) |
| Reflections used in refinement | 23649 (2357) |
| Reflections used for R-free | 1191 (138) |
| R-work | 0.2156 (0.3534) |
| R-free | 0.2589 (0.4302) |
| CC(work) | 0.944 (0.248) |
| CC(free) | 0.910 (0.183) |
| Number of non-hydrogen atoms | 3515 |
| macromolecules | 3476 |
| ligands | 4 |
| solvent | 35 |
| Protein residues | 453 |
| RMS(bonds) | 0.011 |
| RMS(angles) | 1.41 |
| Ramachandran favored (%) | 95.69 |
| Ramachandran allowed (%) | 3.4 |
| Ramachandran outliers (%) | 0.91 |
| Rotamer outliers (%) | 0.26 |
| Clashscore | 12.89 |
| Average B-factor | 82.99 |
| macromolecules | 83.06 |
| ligands | 56.95 |
| solvent | 78.61 |

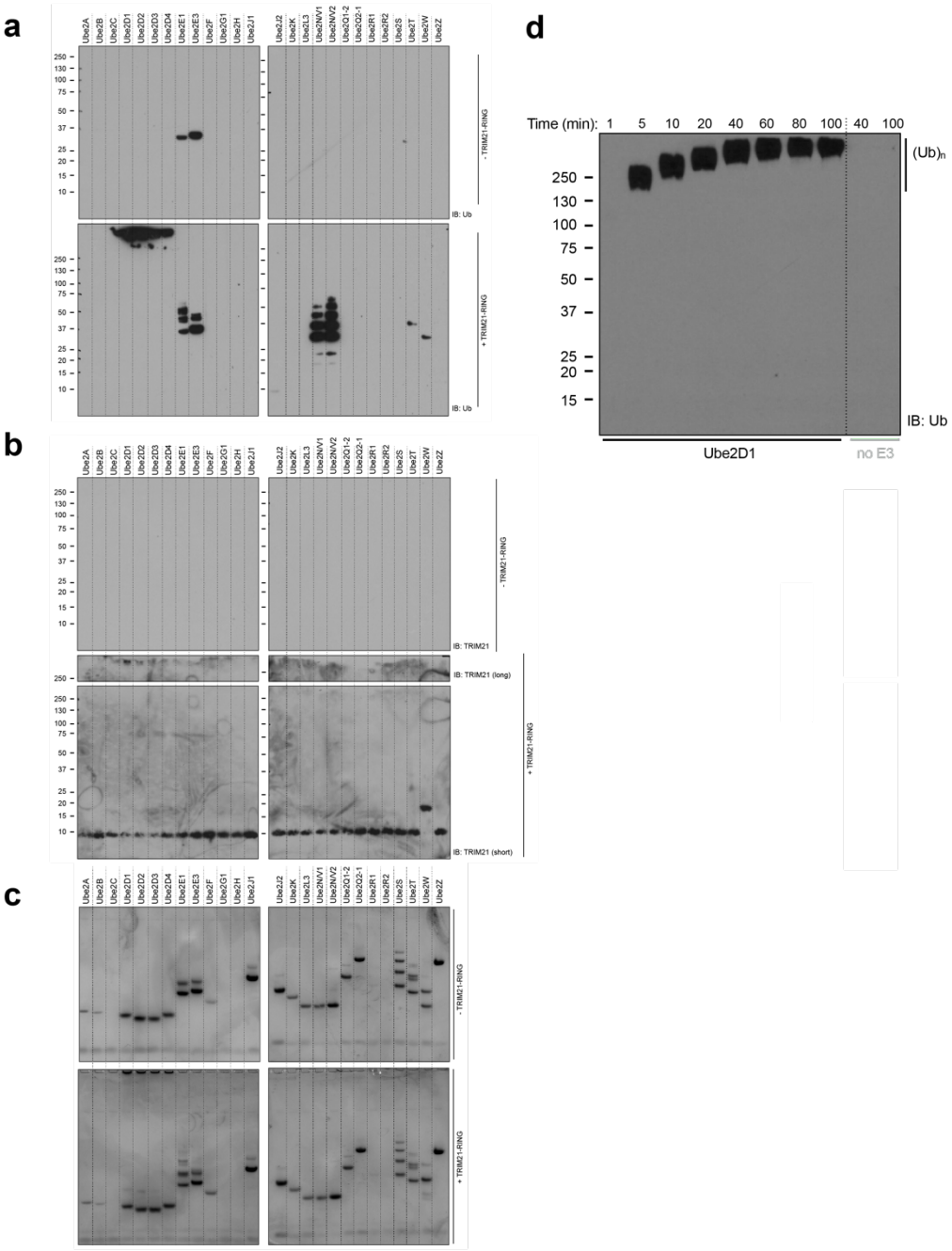


**Appendix Figure 1 E2 screen.** Full western blots and gels of the biochemical E2 screen (Boston Biochem, Cambridge, MA, USA) are shown. **a** Anti-Ub and **b** anti-T21-R western blots are shown. **c** The gels that were used for blotting and stained afterwards and are shown (without markers, as they were transferred to the membrane). The anti-T21-R western blot is shown for two different developing times, demonstrating that interaction of T21-R with Ube2D1 can result in the formation of anchored chains in addition to free ubiquitin chains. The anti-ubiquitin blot shows a band for Ube2T in presence of TRIM21. However, no difference could be detected in the gel. **d** Catalysis of Ube2D1 to confirm that the high molecular weight species seen in the E2 screen with Ube2D1-4 represent ubiquitin chains.

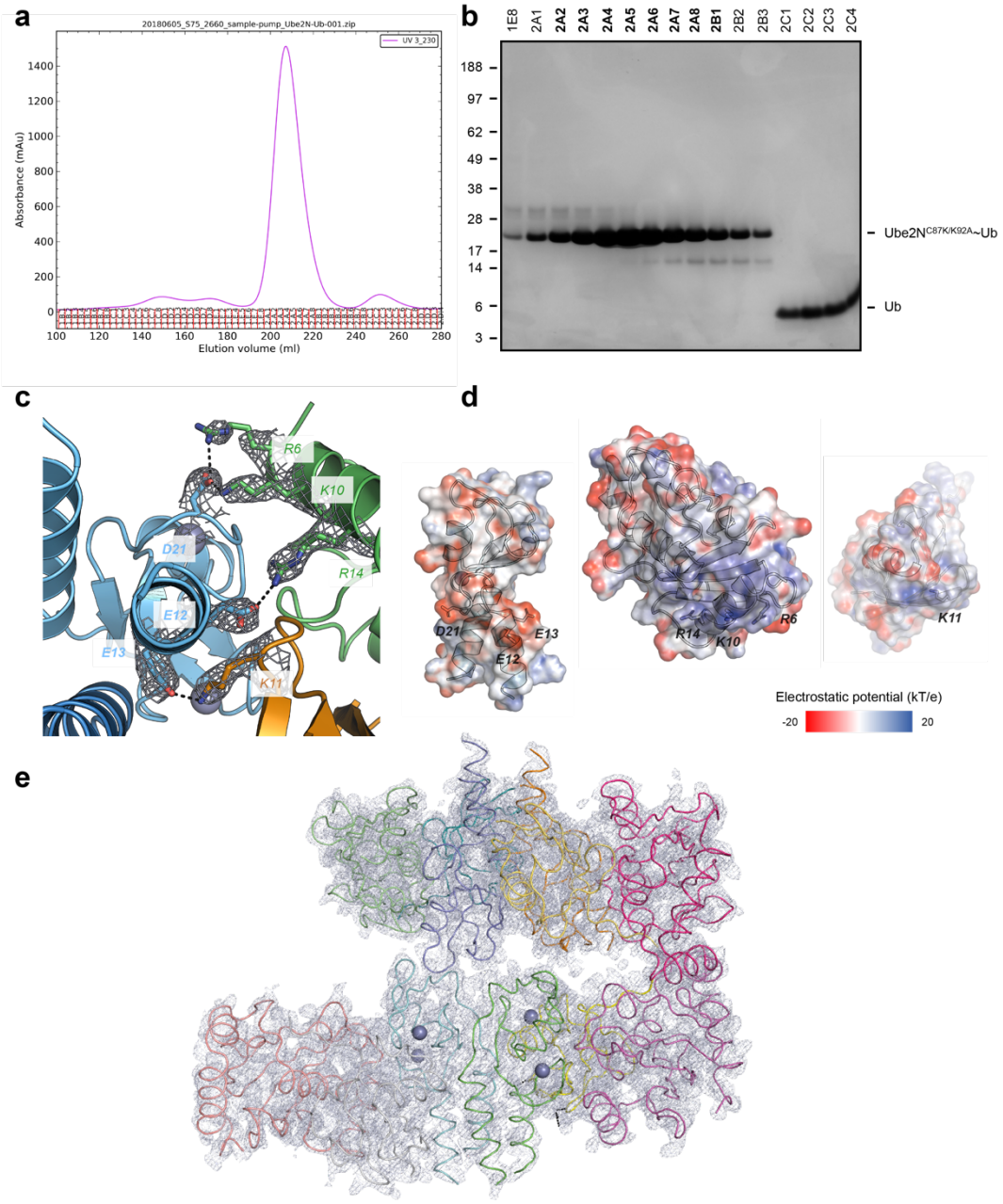


**Appendix Figure 2 X-ray structure of TRIM21-RING in complex with Ube2N~Ub**. **a** Size exclusion chromatography (Superdex75 26/60) chromatogram and **b** Instant Blue-stained LDS-PAGE gel of the purification of isopeptide-linked Ube2N$^{C87K/K92A}$~Ub, which was used for structural studies. **c** Tri-ionic motif close-up as in **Figure 9e**, showing the $2F_o$-$F_c$ density at 1.0 sigma for the residues involved. **d** Electrostatic potential surfaces from -20 (red) to +20 kV $e^{-1}$ (blue). Electrostatic potential surfaces were generated with the APBS 2.1 tool in PyMol. PQR files were generated by PDB2PQR using the Amber force field. **e** Shown is the protein in the asymmetric unit (two full complexes) as cartoon and the $2F_o$-$F_c$ density at 1.0 sigma.

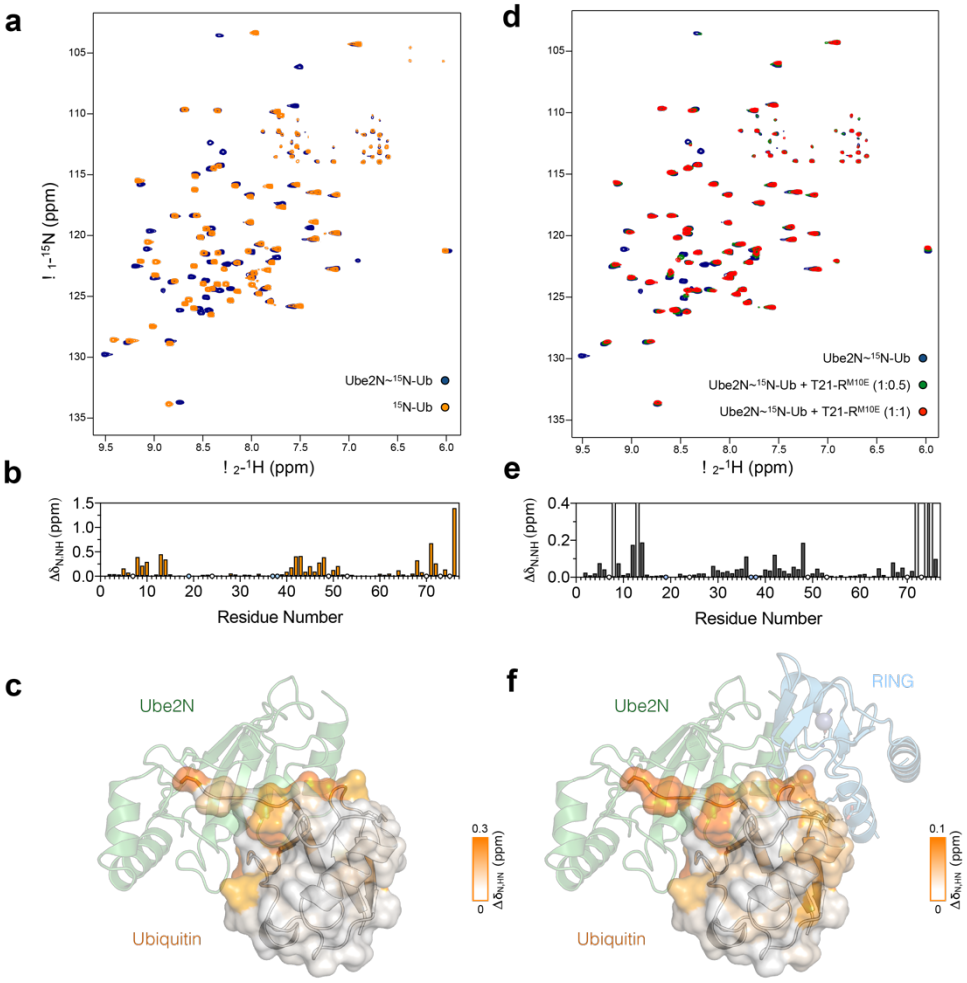


**Appendix Figure 3 Formation of the closed Ube2N~Ub conformation in solution.** Overlay of the $^{15}$N-BEST-TROSY spectra of **a** free $^{15}$N-ubiquitin (orange) and Ube2N~$^{15}$N-Ub (blue) and **d** the titration of T21-R$^{M10E}$ into Ube2N~$^{15}$N-Ub (blue, free; green, half molar equivalent; red, one molar equivalent). **b**,**e** The CSPs are plotted against the residue number. In case of the titration, the CSP are calculated between the free and one molar equivalent added titrant. Blue circles indicate proline residues, white circles missing assignments. **c**,**f** The amide CSP between **c** $^{15}$N-Ub and **f** Ube2N~$^{15}$N-Ub are mapped onto the structure in orange.

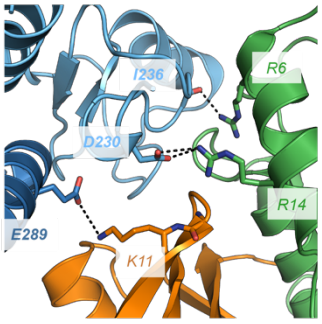


**Appendix Figure 4 Model of the CHIP$^{U\text{-}box}$:Ube2N~Ub complex.** Close-ups of CHIP$^{U\text{-}box}$:Ube2N~Ub model based on the CHIP$^{U\text{-}box}$:Ube2N/Ube2V2 structure (2C2V)[25] and the TRIM21$^{RING}$:Ube2N~Ub structure presented in Chapter 3.

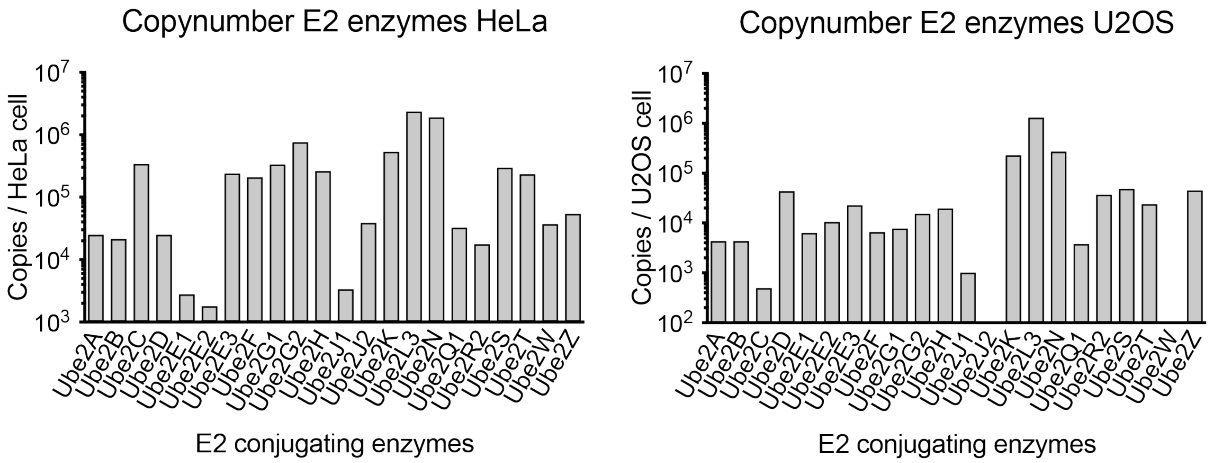


**Appendix Figure 5 Concentrations of E2 enzymes in cells.** Copies of E2 enzymes per cell are shown for HeLa and U2OS cells, as determined by mass spectrometry[139,140].

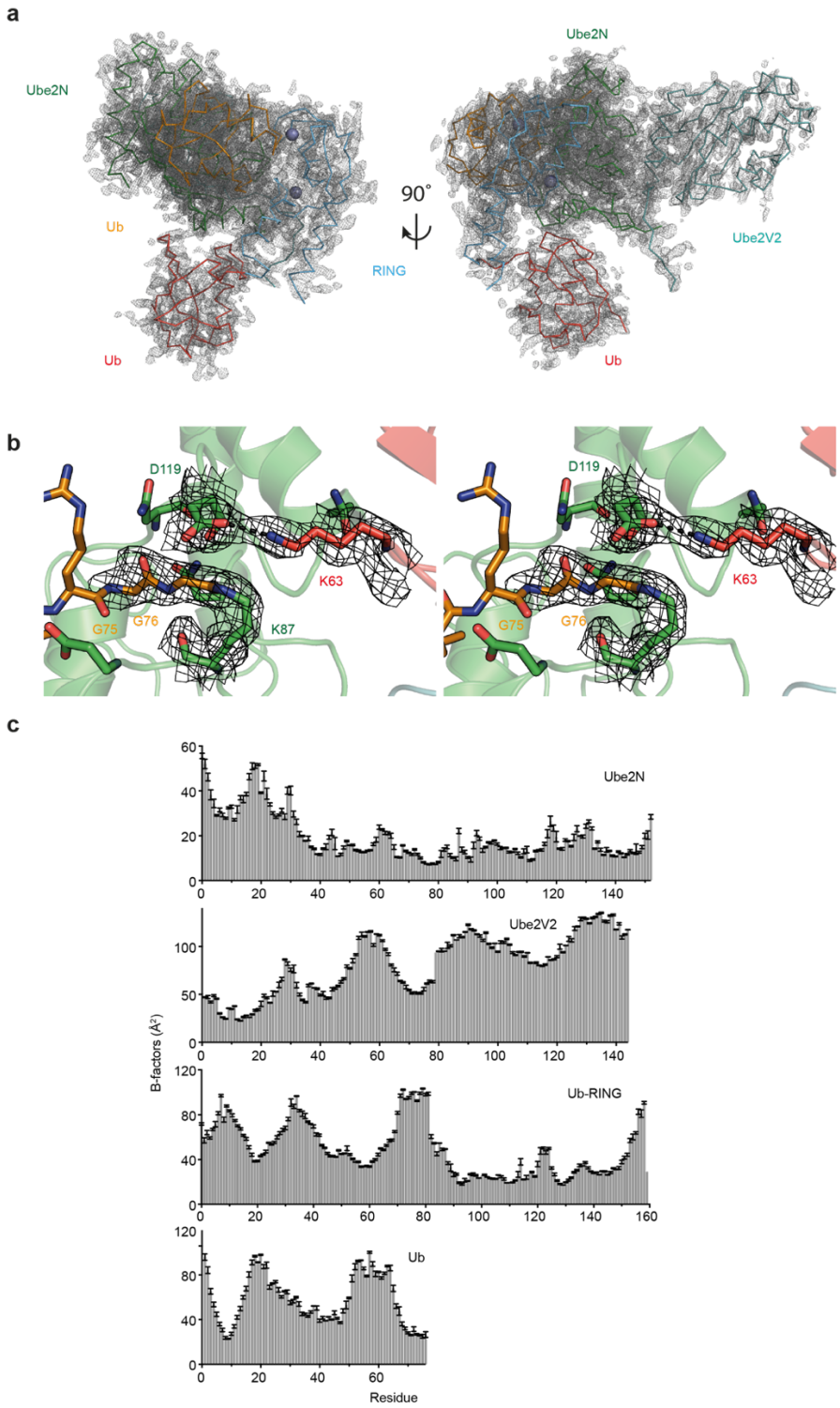


**Appendix Figure 6 Crystal structure of Ub-R:Ube2N~Ub:Ube2V2 (7BBD). a** All proteins contained in the asymmetric unit are shown as ribbon and their $2F_O$-$F_C$ density is shown at 1.0 sigma (Ub-R, Ub in red and R in blue; Ube2N~Ub, Ube2N in green and Ub in orange; Ube2V2 in teal). **b** Stereo image of the active site of Ube2N. $2F_O$-$F_C$ density is shown at 1.0 sigma for selected catalytic residues (Ube2N (green): K87, D119; donor Ubiquitin (orange): G76, G75; acceptor Ubiquitin (red): K63). **c** Shown are B-factors (represented as mean ± standard error of the mean of N, Cα, C') for all chains in the Ub-R:Ube2N~Ub:Ube2V2 structure.

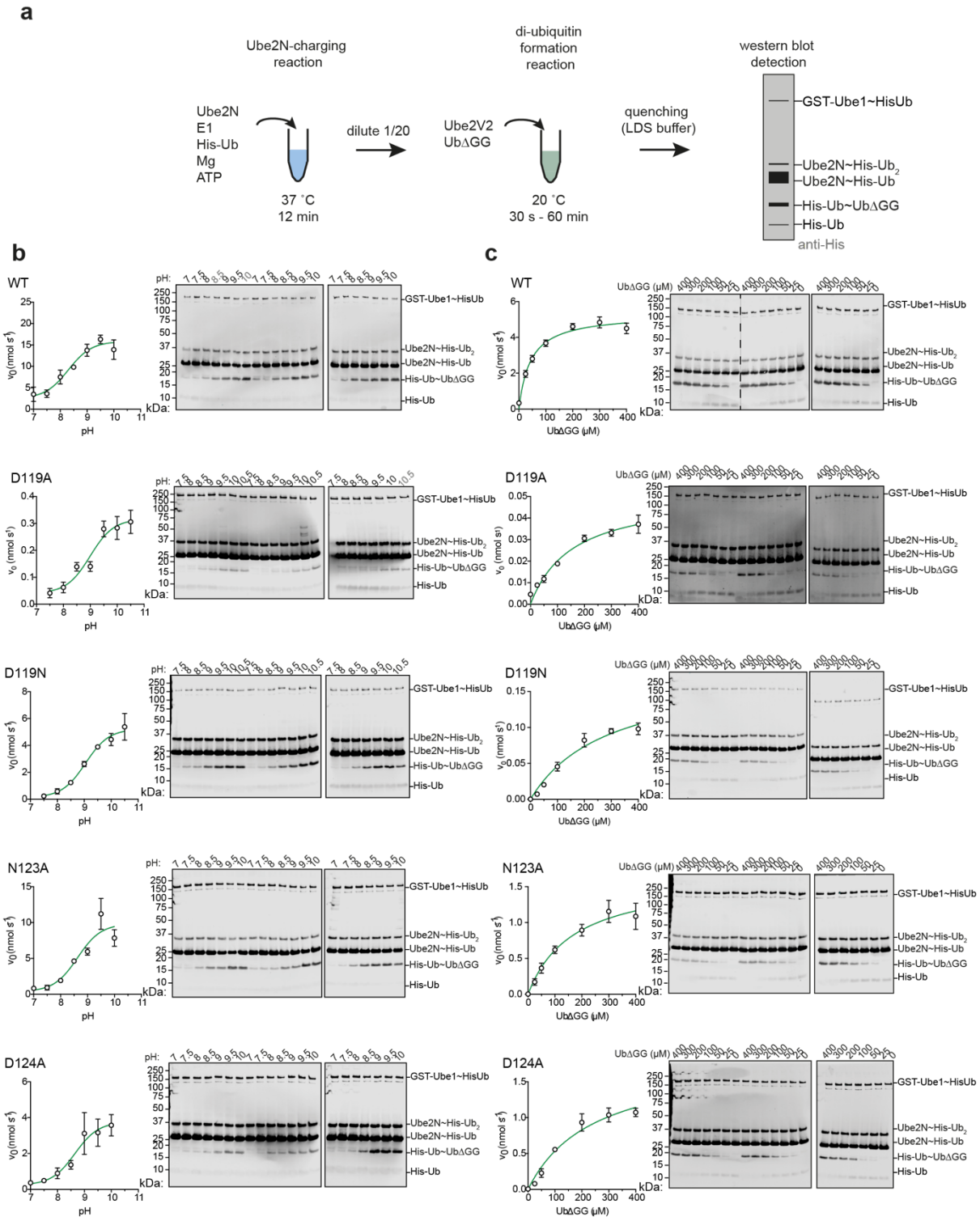


**Appendix Figure 7 Di-ubiquitination kinetics. a** Schematic cartoon of Ube2N catalyzed di-ubiquitination kinetic experiments. **b** Plots of pH dependency of kinetics and **c** Michaelis-Menten kinetics and corresponding western blots. Single measurements had to be excluded when one of the bands contained a saturated spot, making quantification impossible. These measurements have the pH/UbΔGG label in gray. Data are presented as mean ± SEM of n = 3 technical replicates.

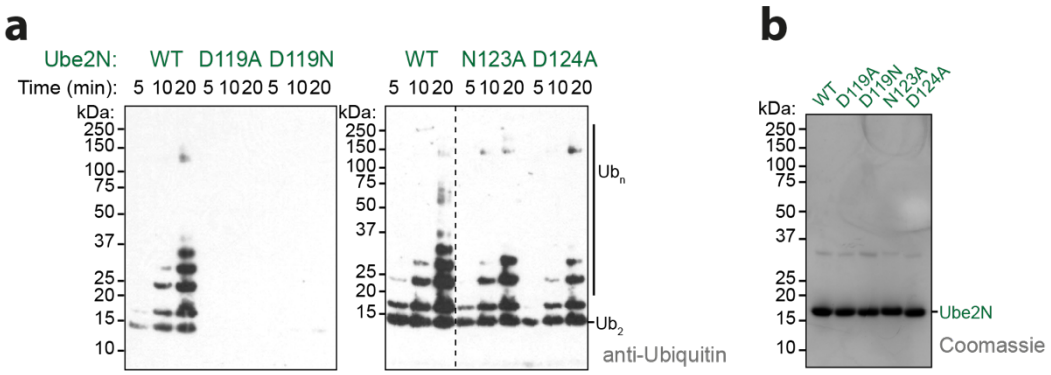


**Appendix Figure 8 Free ubiquitin chain formation of Ube2N mutants**. **a** Western blot of a free ubiquitin chain formation assay using 1 µM T21-R. Western blot is representative of n = 2 independently performed experiments. **b** Shown is an Instant Blue-stained gel of the Ube2N assay stocks.

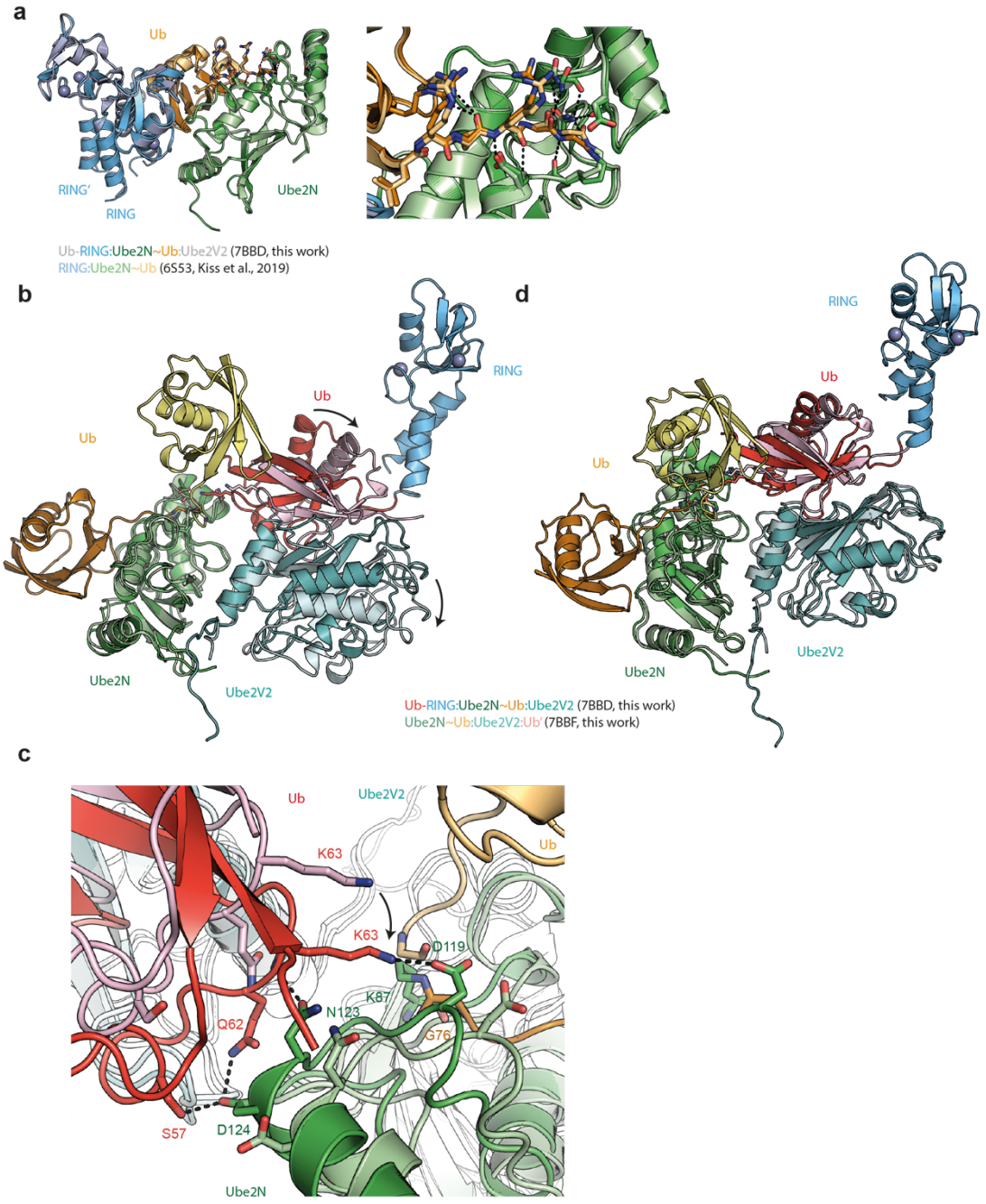


**Appendix Figure 9 Structural Alignments**. **a** Structural alignment between R:Ube2N~Ub (6S53[113]) and Ub-R:Ube2N~Ub:Ube2V2 (7BBD[165], Ub-R, Ub in red and R in blue; Ube2N~Ub, Ube2N in green and Ub in orange; Ube2V2 in teal). **b** Structural alignment between Ub-R:Ube2N~Ub:Ube2V2 and Ube2N~Ub:Ube2V2 (7BBF[165]). Alignment was performed on Ube2N/Ube2V2. **c** Close up of the alignment shown in **b**. Highlighted are interactions that are different between the two structures and that result in different orientation of the acceptor ubiquitin (red). **d** Structural alignment between Ub-R:Ube2N~Ub:Ube2V2 and Ube2N~Ub:Ube2V2. Alignment was performed on Ube2N~Ub/Ube2V2.

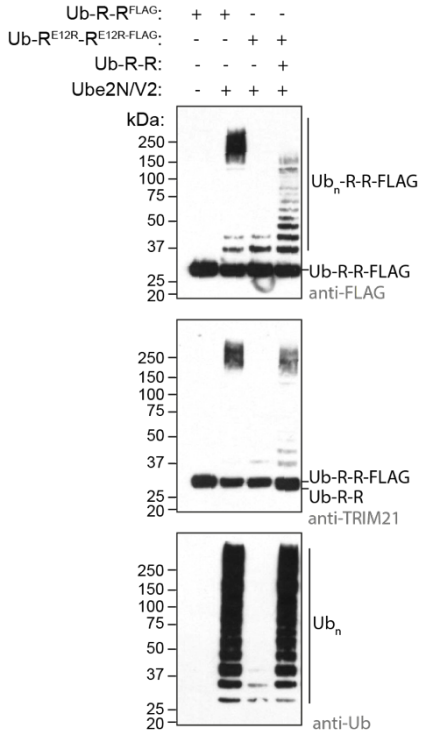


**Appendix Figure 10 TRIM21-anchored ubiquitination can occur in *trans*.** Ubiquitination was incubated for 20 min and performed as other ubiquitination assays but with 50 µM ubiquitin. All TRIM21 constructs are obligate dimers (R-R-fusions) and either tag-free or FLAG-tagged. Ubiquitination deficient Ub-R$^{E12R}$-R$^{E12R}$-FLAG can be ubiquitinated in *trans* in presence of FLAG-tag-free Ub-R-R.

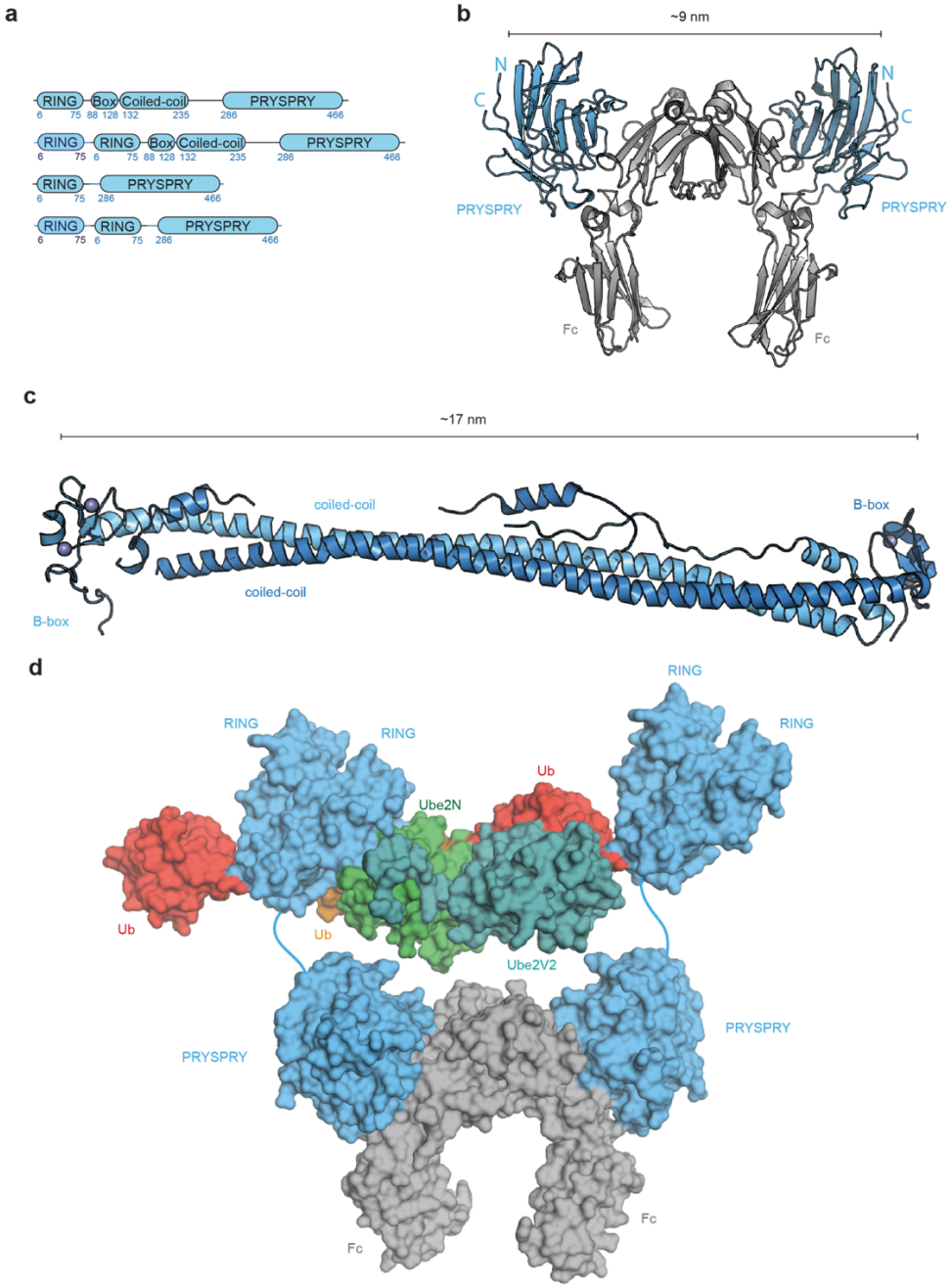


**Appendix Figure 11 Structural models for distances of different TRIM21 constructs. a** Domain architecture of TRIM21 constructs used in biochemical and cellular assays. For biochemical experiments, the N-terminus of TRIM21 was mono-ubiquitinated. **b** Structure of TRIM21 PRYSPRY (blue) in complex with Fc (gray, 2IWG[52]). The distance shown spans from the N-terminal His of one to the other. **c** Structure of TRIM5α-B-Box-coiled-coil (blue, 4TN3[192]). TRIM21 and TRIM5α coiled-coils align well by sequence and show no insertions. Thus, TRIM5α-coiled-coil is a suitable model for the corresponding region of TRIM21. The distance shown spans from the N-terminus of one B-box to the other. **d** Structural model of Ub-R-R-PRYSPRY:Fc during initiation of ubiquitin chain elongation. Our Ub-R:Ube2N~Ub:Ube2V2 (7BBD[165], Ub-R, Ub in red and R in blue; Ube2N~Ub, Ube2N in green and Ub in orange; Ube2V2 in teal) structure (as the canonical model) was superposed on the TRIM21-PRYSPRY:Fc structure. Lines indicate the linkers between RING and PRYSPRY.

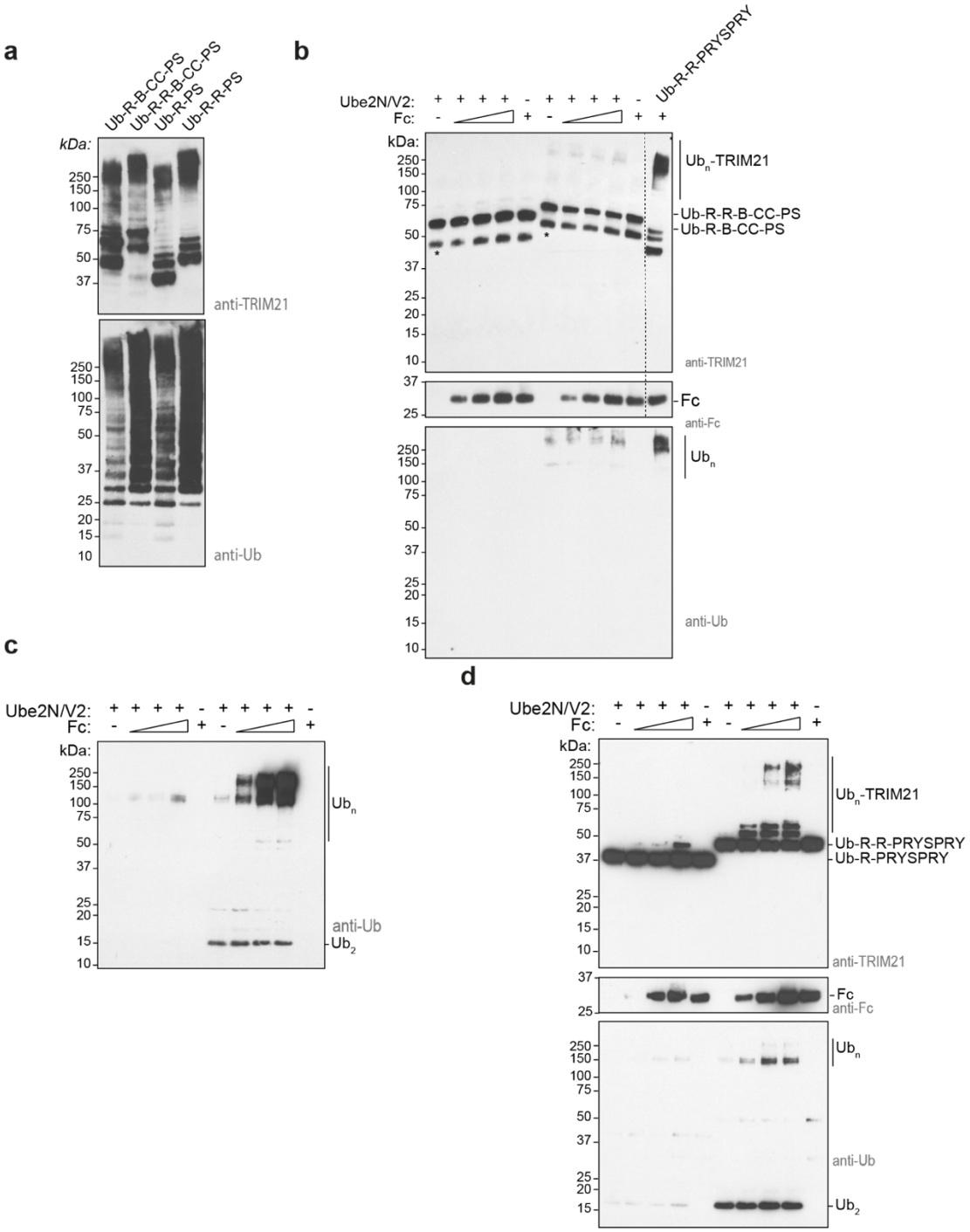


**Appendix Figure 12 Substrate binding induces catalytic RING topology. a** Ubiquitin chain formation assay of Ub-TRIM21 constructs after 40 min. **b** Substrate (Fc) induced self-ubiquitination assay of 100 nM Ub-TRIM21 constructs. Full blots and additional ubiquitin blot are shown for the data shown in **Figure 21d**. For the blot with full-length TRIM21 constructs, Ub-R-R-PS with Fc was also performed as a positive control (dashed line indicates cropping in **Figure 21b**). **c** Ubiquitin western blot for the assay shown in **Figure 21d** for Ub-R-PS and Ub-R-R-PS. **d** Substrate (Fc) induced self-ubiquitination assay of 50 nM Ub-TRIM21 constructs. Reactions were incubated for 5 min. *(asterisk) indicates a TRIM21 degradation product that could not be removed during purification.

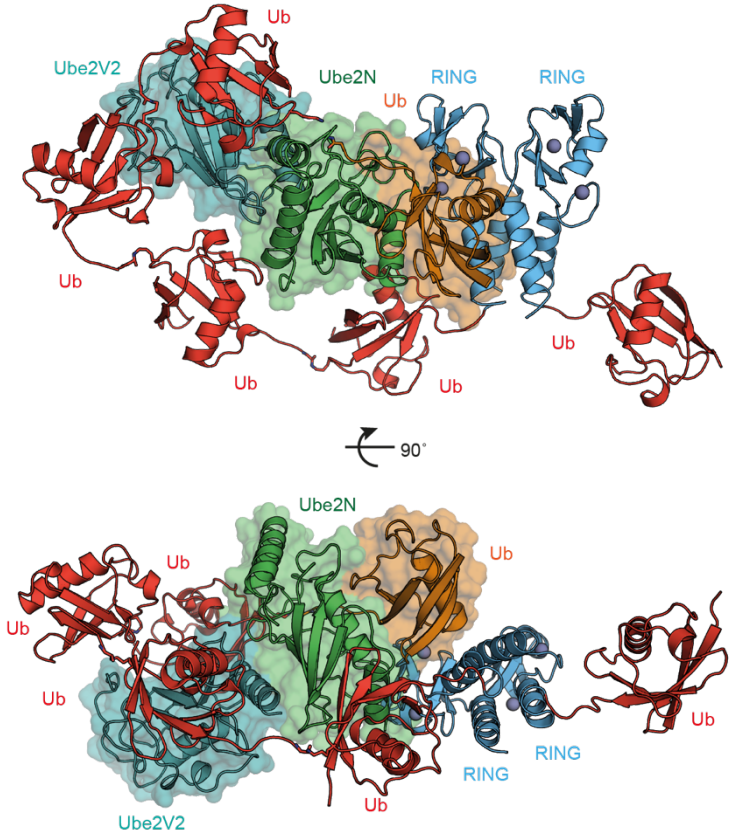


**Appendix Figure 13 Structural modelling of a *cis*-ubiquitinating TRIM21.** In order to achieve ubiquitination in *cis*, the RING-anchored (blue) ubiquitin (red) chain must be sufficiently long to reach the active site on Ube2N~Ub/Ube2V2 (Ube2N in green, Ub in orange, Ube2V2 in teal). The chain can go around two different routes and both cases were modelled in Chapter 4. The ubiquitin chain was modelled using the Ub-R:Ube2N~Ub:Ube2V2 structure (7BBD[165]) and a structure of K63-linked $Ub_2$ (2JF5[149]) using PyMol. For both cases the acceptor ubiquitin was used as orientation for the chain direction. In **Figure 22a** the priming (RING-bound) ubiquitin was moved, whereas here it was not. The two central ubiquitin molecules (i.e. numbers 2 and 3) where added by modelling. A RING-anchored ubiquitin chain length of 4 was the shortest found to be possible.

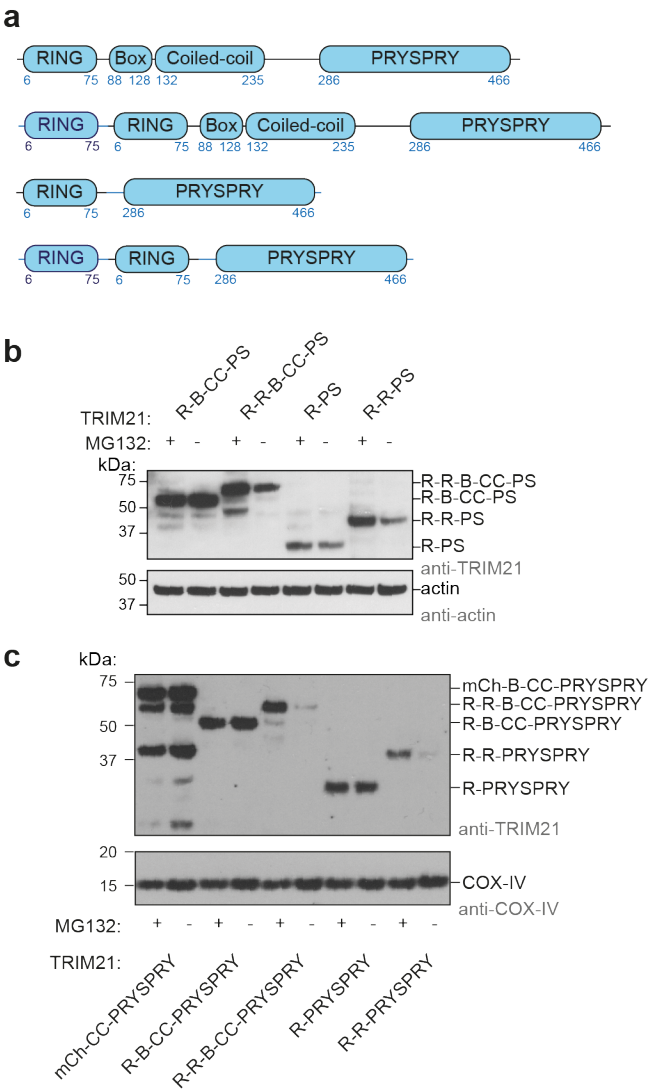


**Appendix Figure 14 Cell biological analysis of TRIM21 constructs. a** Domain architecture of TRIM21 constructs used in cellular assays. **b** Transient expression of TRIM21 constructs in *TRIM21*-knock-out RPE1 cells. After electroporation, cells were either treated with MG132 or DMSO. Constructs with constitutive RING dimers show proteasomal turnover. **c** Exemplary western blots of mEGFP-Fc degradation experiment shown in **Figure 24c**. Cells were either treated with MG132 or DMSO.

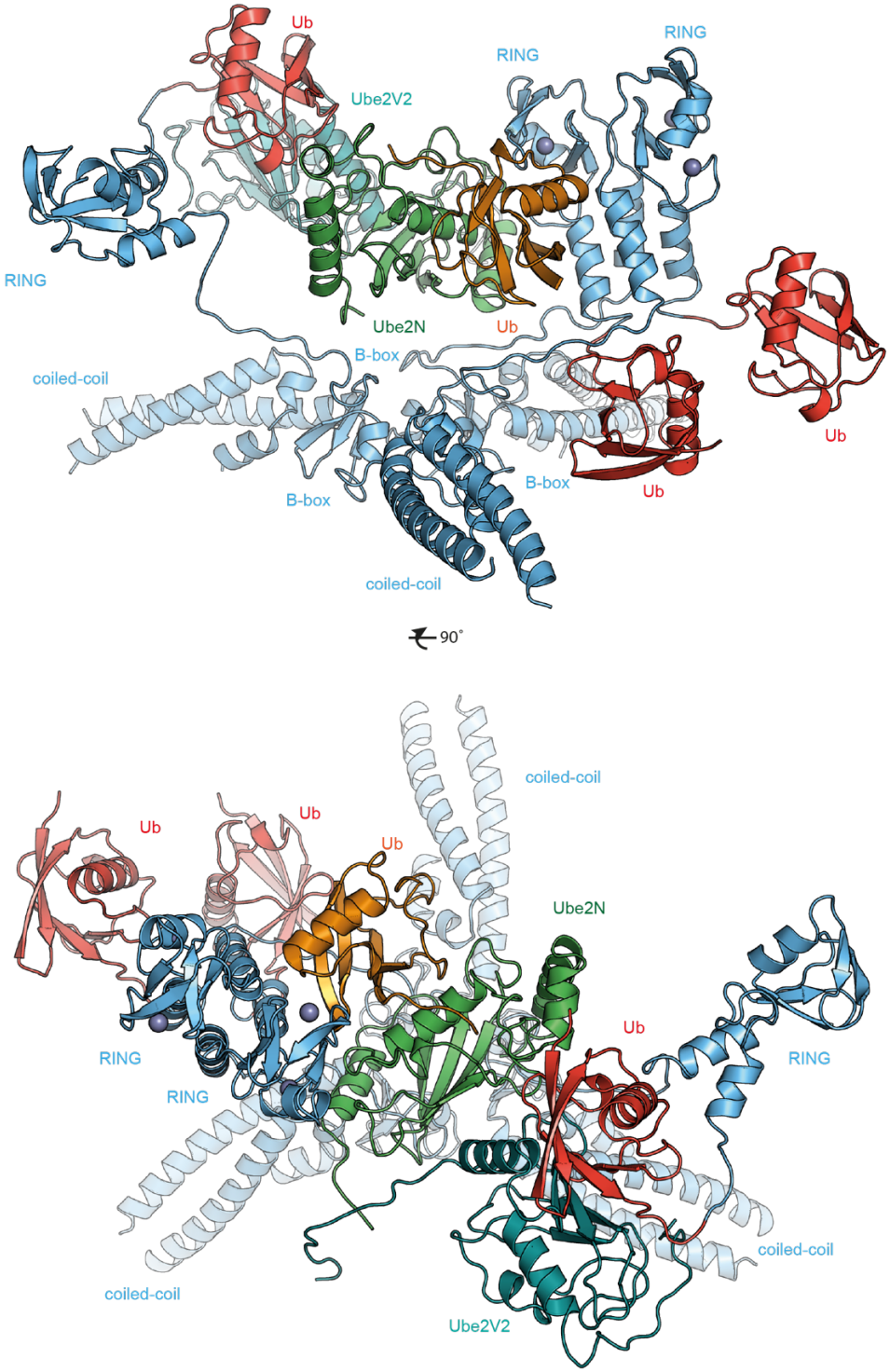


**Appendix Figure 15 Structural model of catalytic RING topology with TRIM5α.** TRIM5 catalytic RING topology model was build based on a TRIM5 trimeric B-CC$^{truncated}$ structure (blue, 5IEA[87]) and the Ub-R:Ube2N~Ub:Ube2V2 structure (7BBD[165], Ub-R, Ub in red and R in blue; Ube2N~Ub, Ube2N in green and Ub in orange; Ube2V2 in teal). The model for the catalytic RING topology was superposed on the B-CC structure. Linkers between the RING domains and B-boxes were built to connect the domains and the linker between the third RING and its Ub was modelled as being flexible, in line with our B-factor analysis (**Appendix Figure 6c**).